GAMMA RAYS, NEUTRINOS AND ANTIPROTONS FROM INTERACTIONS OF COSMIC RAYS

by

Jagdish Chandra Joshi

A Thesis submitted to the

Jawaharlal Nehru University, New Delhi

for the degree of

Doctor of Philosophy

Raman Research Institute

Bangalore 560080

INDIA

2015

Certificate

This is to certify that the thesis entitled 'Gamma Rays, Neutrinos and Antiprotons from Interactions of Cosmic Rays' submitted by Jagdish Chandra Joshi for the award of the degree of Doctor of Philosophy of Jawaharlal Nehru University is his original work. This has not been published or submitted to any other University for any other Degree or Diploma.

Prof. Ravi Subrahmanyan   **Dr. Nayantara Gupta**
Director   Thesis Supervisor

Raman Research Institute,
Bangalore 560 080
INDIA

Declaration of Authorship

I, Jagdish Chandra Joshi, declare that the work reported in this thesis titled 'Gamma Rays, Neutrinos and Antiprotons from Interactions of Cosmic Rays', is entirely original. This thesis is composed independently by me at the Raman Research Institute under the supervision of Dr. Nayantara Gupta. I further declare that the subject matter presented in this thesis has not previously formed the basis for the award of any degree, diploma, membership, associateship, fellowship or any other similar title of any university or institution.

Further, I also declare that, this thesis has been checked through the plagiarism software TURNITIN.

Dr. Nayantara Gupta   **Jagdish Chandra Joshi**

Astronomy and Astrophysics Group,
Raman Research Institute,
Bangalore 560 080
INDIA

Acknowledgements

Foremost, I would like to express my sincere gratitude to my advisor Dr. Nayantara Gupta for her continuous support during my thesis work. My collaborator in DESY, Germany Dr. Walter Winter contributed to the key results in the neutrino work. I am indebted to him for a fruitful collaboration. Besides my advisor, I would like to thank the rest of my thesis committee members: Prof. Shiv Sethi and and Dr. Arun Roy, for their encouragement and insightful comments. I am grateful to Reji Sir and Smijesh with whom I did some experimental work in laboratory plasma physics.

Thanks to Library staff for their support in providing the research papers and articles. In the Astronomy group, I had a very good time with Kanhaiya ji, Mahavir, Naveen and Nazma. Thanks to all of you for your help during my start-up days at the astro-floor. I would like to thank Vidya, who made life very easy w.r.t. all the paper work for travel and other things.

It was impossible to stay at a place for six years and don't share good moments, as a human being we don't like it. I enjoyed my trekking and travel trips in the southern part of India. Thanks to all of the friends and others with whom I travelled and explored my genuine hobby. Finally thanks to all of the people at the Astro-floor with whom I shared a good time.

This thesis is dedicated to my parents and late grandfather who motivated me to pursue with my thesis work.

Synopsis

Cosmic Rays were discovered more than one hundred years ago. They contain hadrons (protons, alpha particles, heavy nuclei) whose kinetic energy spans in the energy range of MeV to 100 EeV * and leptons (electrons, muons) whose fluxes have been measured in the energy range of GeV to TeV.

Their acceleration in distant astrophysical sources, propagation through the cosmic radiation backgrounds, interactions with radiation and matter and energy losses have been studied since their discovery. Although there has been much progress in the experimental front, we still do not know much about their origin, production, acceleration mechanisms and their interaction cross sections at energies beyond the reach of the ground based accelerators.

The gamma rays and neutrinos produced in the interactions of the cosmic rays with the radiation and matter travel directly from their sources to the detectors. They are the messengers of the underlying physical phenomena in different astrophysical sources of cosmic rays. The high energy gamma rays may interact with the ambient radiation and their flux is attenuated but the neutrinos interact very weakly. The charged particles produced in the interactions of cosmic rays are deflected by the Galactic magnetic field and finally we observe a diffuse flux of these particles.

This thesis is based on our theoretical studies to understand the following observational results (i) emission of GeV to TeV gamma rays observed by the Fermi LAT and HESS from the core of Centaurus A (ii) TeV to PeV neutrino events detected by the IceCube detector and (iii) the flux of the antiprotons and protons detected by the PAMELA experiment. In the above studies the secondary gamma rays, neutrinos and antiprotons are produced in *'the interaction of cosmic rays'*.

GeV to TeV gamma rays from the core of Centaurus A

Centaurus A (Cen A) is our nearest extragalactic radio galaxy at a distance of 3.4 Mpc. The active central region of this galaxy has been observed in electromagnetic radiations in the energy range of $10^{-5} - 10^{12}$ eV. This non thermal radiation has been modelled with synchrotron self Compton (SSC) emission upto almost 1 GeV. At higher energy the gamma ray spectrum appears as a separate component and is most likely of hadronic origin.

In this work we have assumed an inverse power law spectrum of the shock accelerated cosmic ray iron nuclei at the core of Cen A above 2.8 TeV. The daughter nuclei and the stripped nucleons are produced after the iron nuclei are photo-disintegrated in the radiation

---

*The Notation: MeV $\equiv 10^6$ eV, GeV $\equiv 10^9$ eV, TeV $\equiv 10^{12}$ eV, PeV $\equiv 10^{15}$ eV, EeV $\equiv 10^{18}$ eV

field of the core.

$$A + \gamma \rightarrow A^{\star} \rightarrow (A - 1) + \gamma' + n \ or \ p \tag{1}$$

The daughter nuclei de-excite by emitting gamma rays. The flux of the Lorentz boosted gamma rays are calculated and compared with the observed flux of gamma rays from the core of Cen A.

The cosmic ray iron nuclei of energy 2.8 TeV are photo-disintegrated by X-ray photons of energy 170 keV. The peak energy in the gamma ray spectrum from the photo-disintegration of iron nuclei by $170 \ \mathrm{KeV}$ photons is found to be at $400 \ \mathrm{MeV}$. Assuming the spectral index of the cosmic ray iron nuclei to be -2.45 above 2.8 TeV we get a good fit with the observed flux of gamma rays in the GeV to TeV energy range. The total luminosity of the iron nuclei in the energy range of 2.8 TeV to 150 EeV has been found to be $\sim 10^{47} \ \mathrm{erg/sec}$, which is higher than the Eddington luminosity ($10^{46} \ \mathrm{erg/sec}$) of Cen A.

The apparent isotropic luminosity can easily exceed $10^{46} \ \mathrm{erg/sec}$ in Cen A during high flaring states for small beaming cones. The rate of photo-disintegration is directly proportional to the density of low energy photons at the source. There is no observational data on the flux of the low energy photons in the energy range of 1 eV and 1 KeV. Higher density of low energy photons would lead to higher rate of photo-disintegration. Moreover a slight variation in the assumed value of the Doppler factor of the wind medium of the core can change the photon density drastically leading to higher rate of photo-disintegration. If the rate of photo-disintegration is higher then a lower luminosity in cosmic ray iron nuclei would be required to explain the observational results.

Our study reveals that although photo-disintegration of heavy nuclei is possible at the core of Cen A the total luminosity in cosmic rays required in this case is higher compared to the models in which the gamma rays originate from the decay of neutral photo-pions produced in $p - \gamma$ interactions.

TeV to PeV neutrinos from interactions of diffuse cosmic rays with ambient hydrogen atoms in our Galaxy

The neutrino detector IceCube at the south pole detected 28 TeV to PeV neutrino events in 2 years (2011-13) of observations. This is the first detection of very high energy neutrino events. More recently the number of events has increased to 37. None of these neutrino events are found to be correlated with astrophysical sources, which might also be due to the large angular uncertainties in the directionalities of these neutrino events. Since their origin is unknown people have tested different hypothesis to explore it. We have explored whether

they could have originated in the interactions of the diffuse cosmic rays with the hydrogen in the Galactic medium during their propagation in our Galaxy.

We have considered the steady state flux or the observed flux of cosmic rays to calculate the flux of secondary neutrinos. Thus our results neither depend on the unknown injection spectrum, nor on the escape time of very high energy cosmic rays from our Galaxy. The hadronic interactions lead to the production of charged and neutral pions with equal probabilities. The charged pions decay to neutrinos and the neutral pions to gamma rays. Each of the secondary gamma rays takes away 10% of the parent cosmic ray proton's energy while only 5% goes to each neutrino.

The density of the hydrogen atoms is the highest near the Galactic plane and decreases with the distance from the same. We have selected the region close to the Galactic plane to find the maximum contribution. In the most realistic case of our Galaxy, a cylindrical halo with radius 10 kpc, height 500 pc and density of hydrogen atoms 1 cm^{-3}, we have found that none of the TeV to PeV neutrino events has been produced from the interactions of cosmic rays with the ambient hydrogen atoms in our Galaxy.

Cosmic Ray Antiprotons from Nearby Cosmic Accelerators

The detection of antimatter from the cosmos has great implications to our understanding of the physics of nature. Fermi LAT has detected gamma rays from many SNRs and molecular clouds. In some of them the gamma rays are possibly produced in the interactions of cosmic ray protons with the hydrogen atoms. In molecular clouds the density of hydrogen atoms could be in the range of 100-1000 cm^{-3}. Antiprotons are also produced by the same interactions although their flux is very low. They are deflected in the Galactic magnetic field and merge with the diffuse flux of antiprotons. In this work we have discussed that the gamma ray emission from the hadronic accelerators close to us (SNRs plus associated molecular clouds) can be used to find out the contributions of the same sources to the diffuse cosmic ray antiproton flux measured near the earth. We have calculated the antiproton and proton fluxes from the nearby supernova remnants Vela jr, W28, W44, W30, Tycho and IC443 and included the effect of propagation on them.

We have found that the cosmic ray antiproton fluxes expected from the individual nearby cosmic accelerators are 1000 times less than the total antiproton flux observed by the PAMELA experiment. The proton fluxes from the same sources are found to be 100 times less than the total proton flux observed by the same experiment. Thus we conclude that most of the observed antiprotons and protons are coming from distant astrophysical sources.

List of Publications

"Testing hadronic models of gamma ray production at the core of Centaurus A"
Jagdish C. Joshi, Nayantara Gupta, Phys. Rev. D **87**, 023002 (2013)

"How many of the observed neutrino events can be described by cosmic ray interactions in the Milky Way?"
Jagdish C. Joshi, Walter Winter, Nayantara Gupta, MNRAS[†] **439**, 3414-3419 (2014)

"Cosmic Ray Antiprotons from Nearby Cosmic Accelerators"
Jagdish C. Joshi, Nayantara Gupta, Astroparticle Physics, **65**,108-110 (2015)

[†]MNRAS : Monthly Notices of Royal Astronomical Society

List of Figures

List of Tables

Contents

Chapter 1

Introduction

The early signatures of cosmic rays were found by Ginzburg & Syrovatskii (1964) in the ionization chambers where an unknown current was flowing without any ionizing source. The researchers at that time thought that this current might be from some unknown earth based sources or due to the radioactivity of radium and thorium. This guess led to the misconception that the flux of this ionizing radiation at earth would decrease with increasing distance from the earth.

F. Hess (1912) measured the flux of this radiation at different altitudes and found that the results were reversed. He noticed that the flux was increasing with altitude. These results indicated that the source of ionization was not terrestrial but from the outer space. Later, Millikan (1925, 1926) *confirmed these results and he named these particle cosmic rays*. The composition of the cosmic rays is energy dependent. These particles are mostly protons 86%, alpha particles 11% and 1% other heavy atomic nuclei. A small fraction of the cosmic rays are other subatomic particles like electrons 2%, and antiparticles 1% (Gaggero, 2012).

Auger et al. (1939) observed the cosmic ray air showers produced by the interactions of energetic cosmic rays with the air molecules in the earth's atmosphere. The cosmic ray air showers are made of secondary charged and neutral particles. They estimated the energy of the primary cosmic rays approximately to be 10^{15} eV and the electric fields of long extension in cosmos were accelerating these charged particles. Later, Linsley (1963) found the first evidence of cosmic ray with energy 10^{20} eV, at the Volcano Ranch experiment in New Mexico.

The observation of these energetic particles led to theoretical investigations. Fermi (1949) gave the theory of the particle acceleration in astrophysical sources. In this paper, according to Fermi, "the origin of cosmic radiation is proposed according to which cosmic rays are originated and accelerated primarily in the interstellar space of the Galaxy by collisions against moving magnetic fields." In this theoretical formulation, the cosmic rays are

injected into the interstellar medium (ISM) and their collision with the irregular magnetic field of moving molecular cloud accelerates them. The spectrum of these accelerated particles is an inverse power law which agrees with the cosmic ray observations.

In the Fermi mechanism, the energy gain per collision is proportional to $\frac{u^2}{v^2}$, where v is the particle velocity and u is the velocity of the cloud (Grupen, 2005). *The dependence of the energy gain is quadratic in the cloud velocity and it is called the Fermi mechanism of second order.* In general, the particle velocity is much greater than cloud velocity $v >> u$, which leads to very low energy gain per collision. This process needs very long time for particle acceleration in the presence of energy losses due to collisions with the ambient gas. To overcome these energy losses, Fermi (1949) discussed about the need of an injection energy above which the acceleration takes place efficiently. The injection energy to the particles can be provided by the astrophysical shocks, where the relative energy gain is proportional to the difference of inner shock front and outer shock front velocities (Grupen, 2005). Figure 1.1 shows the collision of the charged particle with the randomly moving magnetized plasma centres. The arrow inside the plasma centres shows their random direction of velocity. These plasma centres are available in the interstellar medium of the Galaxy, where a molecular cloud of parsec size can have many magnetized scattering centres.
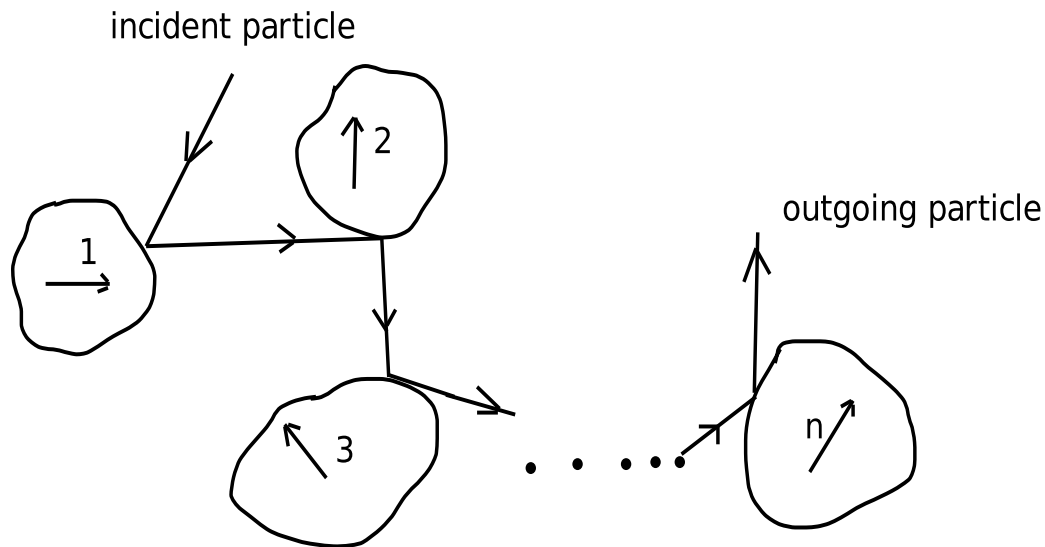
Figure 1.1: Second order Fermi mechanism of charged particle acceleration

The theory of acceleration of charged particles in astrophysical shocks was developed by Axford et al. (1977), Bell (1978a,b) and by Blandford & Ostriker (1978a), which has direct implication to astrophysical objects, for example shocks of supernovae explosion. The

acceleration of the charged particles in the shock fronts depends on the difference of inner shock front and outer shock front velocities (Grupen, 2005). Figure 1.2 shows the general morphology of the blast waves from the supernova explosion. The acceleration of charged particle occurs in between the outer and inner shock fronts. Due to this first order dependence on velocity, the acceleration in astrophysical shocks is also known as Fermi mechanism of first order. In the astrophysical shocks, the back and forth motion of charged particles across the shock front accelerates them (Bell, 1978a) if they are energetic but not necessarily relativistic (Bell, 1978b).
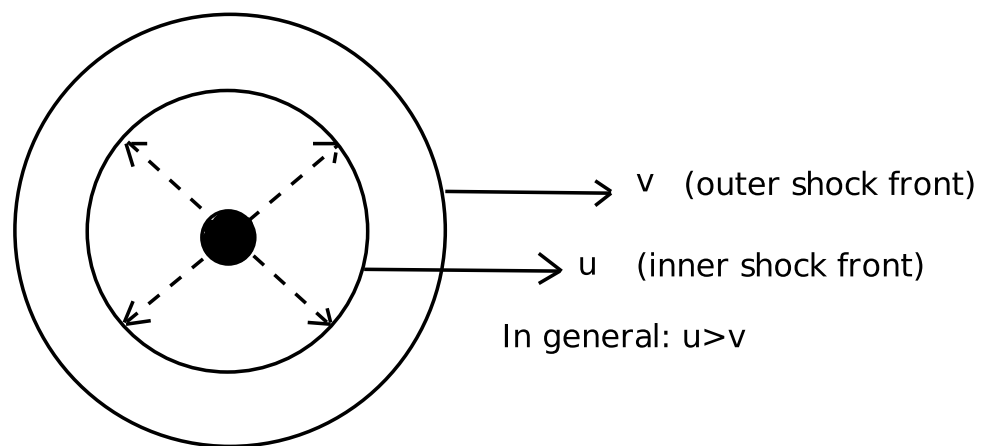
Explosion of a supernova and formation of inner and outer shock front

Figure 1.2: First order Fermi mechanism or shock acceleration of charged particles

First order Fermi shock acceleration mechanism has been used to understand the acceleration of charged particles in the interplanetary shocks by Ellison (1983), in the solar flares by Ellison & Ramaty (1984) and in the relativistic shocks by Ellison et al. (1990). The spectrum of the accelerated protons, electrons and alpha particles in the solar flare can be explained by an unique compression ratio of the infinite plane shock wave (Ellison & Ramaty, 1984). The Fermi first order acceleration mechanism in the magnetic reconnection (Drury, 2012) and in the frame work of random walk theory has been studied by Kato & Takahara (2001). In some cases of relativistic supernovae the cosmic ray can accelerate to ultra high energy (Chakraborti et al., 2011).

The Galactic cosmic rays are accelerated by the first order Fermi acceleration process in the supernova remnant shock fronts (Kotera & Olinto, 2011a; Bell, 2015). In a shock-wave, the combined effects of Fermi first and second order mechanisms can accelerate charged particles (Webb, 1983). These combined processes were discussed by Gombosi et al. (1989) for the acceleration of ions in the cometary plasma and by Kruells (1992) for the charged particle acceleration in the hot-spots of radio galaxies.

The Fermi mechanism of second order is a stochastic process where the average energy gain in the energy of the particle occurs after many collisions with the randomly moving magnetized clouds (Fermi, 1949; Davis, 1956; Parker & Tidman, 1958; Miller et al., 1990). The giant lobes of radio galaxies provide large regions for the particle confinement (Fraschetti & Melia, 2008) where the protons can be accelerated to 10^{20} eV in 10^6 years . This stochastic mechanism of particle acceleration was studied by O'Sullivan et al. (2009) in the giant lobes of Cen A where the stochastic acceleration process due to the Alfvénic turbulence can accelerate the charge particles to energies greater than 1 EeV.

There are variety of acceleration mechanisms in the astrophysical sources. The time dependent magnetic field of sunspots can accelerate charged particles upto GeV energies (Grupen, 2005). For example, in the sunspots with an extension of R, approximately 10^9 cm and the change in the magnetic field of $\frac{dB}{dt}$, approximately $2000 \, \mathrm{Gauss/day}$ can accelerate particles upto ($e\pi R^2 \frac{dB}{dt}$), 0.73 GeV (Grupen, 2005). Similarly in pulsars and in neutron stars the very high magnetic field of value approximately 10^{12} Gauss and rotational velocities of value approximately 4×10^6 m/sec can produce electric field of value 10^{15} eV/m (Grupen, 2005; Kotera & Olinto, 2011a), which accelerates the charged particles.

The various theoretical studies on the astrophysical objects like pulsars, supernova remnants, GRBs and radio galaxies have shown that these objects can accelerate cosmic rays upto the maximum energy of 1000 EeV (Gunn & Ostriker, 1969; Bell, 1992; Bell & Lucek, 1996; Torres & Anchordoqui, 2004; Lyutikov & Ouyed, 2007; Fraschetti & Melia, 2008; Neronov et al., 2009; Kotera & Olinto, 2011a). The cosmic rays in the relativistic jets of AGN with jet luminosity greater than 10^{46} erg/sec can be accelerated to 10^{19} eV (Lyutikov & Ouyed, 2007) . Neronov et al. (2009) discussed the possibility of cosmic ray acceleration in the polar cap region of the black hole magnetosphere. The acceleration occurs in the rotation induced electric field if the magnetic field is aligned along the rotation axis of the black hole (Neronov et al., 2009). The accelerated proton in the super massive black holes can produce TeV photons by the curvature or synchrotron process (Levinson, 2000).

In the last two years, an alternative of Fermi mechanism has been proposed by Ebisuzaki (2014); Ebisuzaki & Tajima (2014). Ebisuzaki (2014) has discussed ponderomotive acceleration of charged particles in the accreting black hole systems like microquasars and AGN. Ponderomotive acceleration is an electromagnetic wave-particle interaction process (Ebisuzaki & Tajima, 2014) which has the following advantage over the Fermi mechanism: *ponderomotive potential provides intense accelerating field, no particle bending cancels the synchrotron losses and due to the decay of accelerating fields the particles escape freely after their acceleration.*

The observed cosmic ray energy spectrum spans in the energy range of 1 GeV to 100's
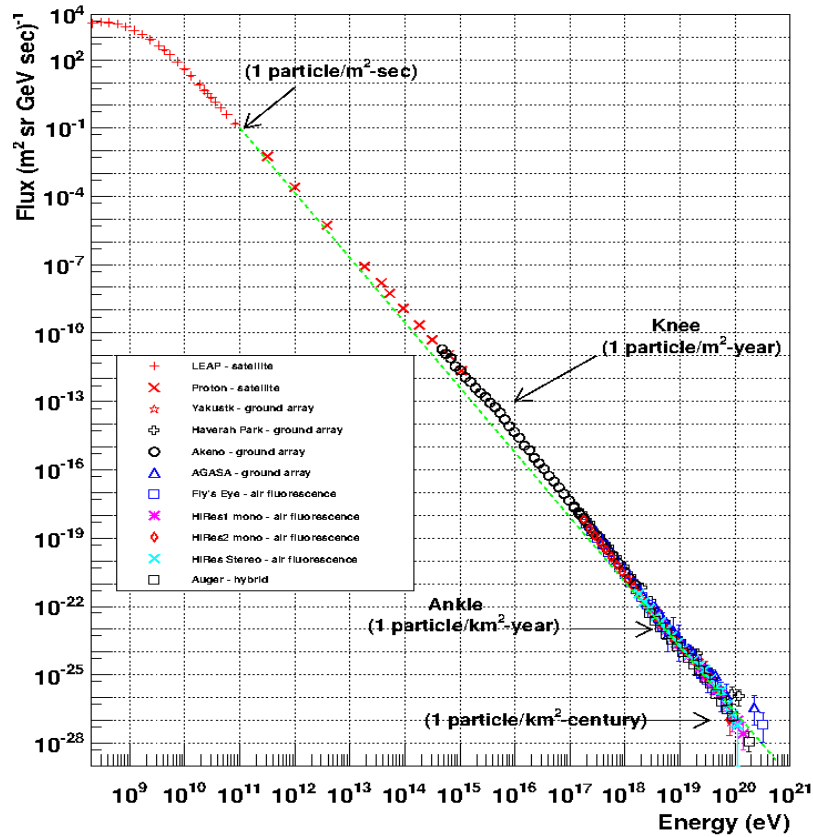
Figure 1.3: Cosmic ray spectrum observed at the earth. (figure taken from: William Hanlon @ http://www.physics.utah.edu/ whanlon/)

of EeV [*]. This spectrum in dimensions of $(eV/cm^2 \ sec \ sr)$ observed at terrestrial detectors has a power law distribution (E^s) with spectral index $s = -2.7$ upto 3 PeV of cosmic ray energy, $s = -3$ from PeV to EeV and above ~ 30 EeV, $s = -2.6$ (Kotera & Olinto, 2011b). The flux of cosmic rays observed at the earth decreases with increasing energy. The cosmic ray flux at 100 MeV is 1 particle/$(cm^2 \ sec)$. Above 10 EeV it is 1 particle/$(km^2 \ year)$ and at 100 EeV decreases to 1 particle/$(km^2 \ century)$. The observed diffuse cosmic ray spectrum is shown in Figure 1.3.

Cosmic rays are isotropically distributed in the irregular magnetic field of our Galaxy. These particles collide with the gaseous medium and the radiation field of the ambient medium. In these interactions secondary neutral and charged pions are produced. The decay of these unstable particles produces high energy photons and neutrinos.

Penzias & Wilson (1965) discovered that the universe is filled with low energy photons with an average energy of 6×10^{-4} eV and average density of $550/cm^3$. This radiation

---

[*] The notation: MeV $\equiv 10^6$ eV, GeV $\equiv 10^9$ eV, TeV $\equiv 10^{12}$ eV, PeV $\equiv 10^{15}$ eV, EeV $\equiv 10^{18}$ eV

is known as the cosmic microwave background radiation (CMBR). After the discovery of CMBR, Greisen, Zatspin and Kuz'min studied the interaction of cosmic ray protons with the CMBR.

In the $p - \gamma$ interaction the threshold photon energy for pion production in the rest frame of protons is $E_\gamma^{thr} \sim m_\pi + \frac{m_\pi^2}{2m_p} = 160$ MeV where E_γ^{thr} is the threshold photon energy for pion production in the rest frame of protons, m_π is the rest mass of a pion and m_p is the rest mass of a proton.
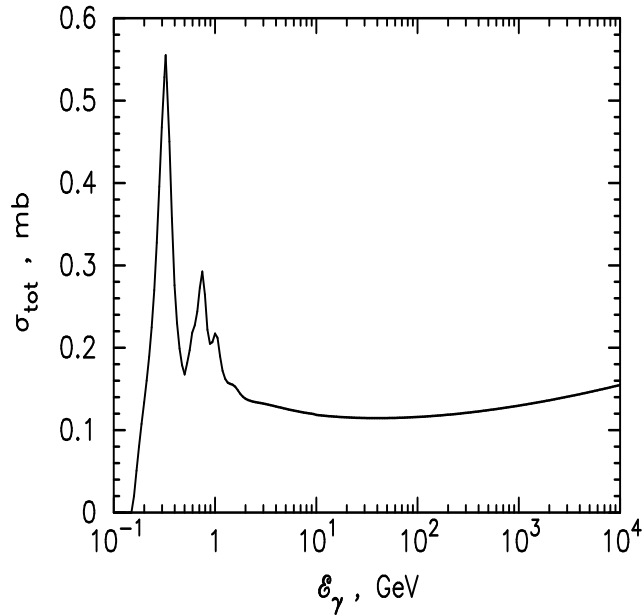
Figure 1.4: Delta resonance cross section for pion production. (figure taken from:Kelner & Aharonian (2008))

The cross section of pion production in $p - \gamma$ interaction w.r.t. energy of the photons in rest frame of the proton, is shown in Figure 1.4 (Kelner & Aharonian, 2008). In this interaction the resonance occurs at around 300 MeV. In the rest frame of the proton the CMBR photon of energy ϵ_b eV will have an energy $\epsilon_\gamma = \frac{E_p}{m_p c^2} \epsilon_b$ eV. The resonance interaction between CMBR of energy 6×10^{-4} eV and cosmic ray protons of energy approximately 6×10^{19} eV will have a cut-off signature in the cosmic ray spectrum, known as the GZK cutoff (Greisen, 1966; Zatsepin & Kuz'min, 1966).

This interaction has very important implication in cosmic ray physics, neutrino and gamma ray astronomy. In GZK interactions, secondary photons and neutrinos are produced which are called the GZK photons and GZK neutrinos. However it is challenging to detect them because of their very low flux values.

As discussed earlier, the observed cosmic ray spectrum falls steeply with increasing cosmic ray energy. To improve the statistics of the observed cosmic ray events large area detec-

tors have built. The first results on the detection of ultra high energy cosmic rays (UHECRs, cosmic rays with energy greater than EeV,) were reported by Akeno Giant Air Shower Array in Japan (AGASA), High Resolution Fly's Eye (HiRes) experiments. In the past decade Pierre Auger observatory (PAO) and Telescope array (TA) have detected cosmic rays of energy greater than EeV. These observations are very important for the identification of GZK cutoff in the cosmic ray spectrum.
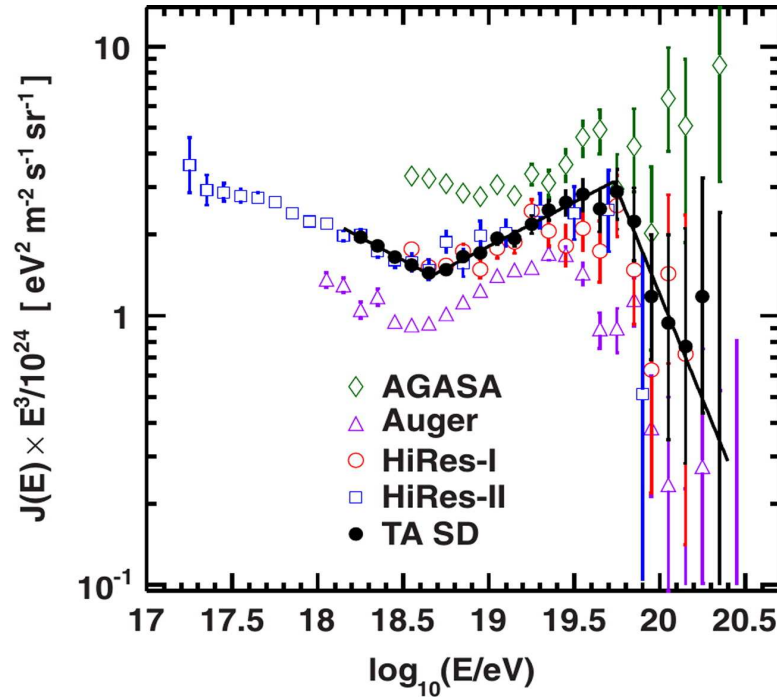
Figure 1.5: GZK features observed by different experiment. (figure taken from: Tinyakov (2014))

The AGASA observatory did not find any GZK cutoff in the cosmic ray spectrum in their 10-years (1993-2003) of observations (Takeda et al., 2003a). The other cosmic ray experiments HiRes, PAO and TA have detected a signature of GZK cut-off in their observations. The HiRes observatory detected the GZK suppression at 6×10^{19} eV after the analysis of their 6-years (1997-2006) of observational data (Abbasi et al., 2008). Similarly the TA observatory detected the GZK suppression at 5.4×10^{19} eV in their 4-years (2008-2011) of observational data (Tinyakov, 2014) and the PAO observatory detected the GZK cut off in the cosmic ray spectrum above 4×10^{19} eV in their 4-years (2004-2007) of observational data (Abraham et al., 2008). The GZK cutoff as seen by HiRes, AGASA, Pierre Auger and Telescope Array observations are shown in Figure 1.5. This GZK cut off feature is consistent with the proton composition of cosmic rays at ultra high energies for Telescope Aarray and HiRes data but the PAO data is indicative of a mixed cosmic ray composition (Tinyakov, 2014).

Pierre Auger collaboration has detected 231 cosmic ray events above 52 EeV in 10 years of observations (2004-2014) (Pierre Auger Collaboration, 2014). In the correlation study of these events with astrophysical sources, they have found that cosmic rays with energy greater than 58 EeV are correlated with Swift AGNs (Tueller et al., 2008), which lies in an angular region of $18°$, within a distance of 130 Mpc and the X-ray luminosities greater than 10^{44} erg/sec.
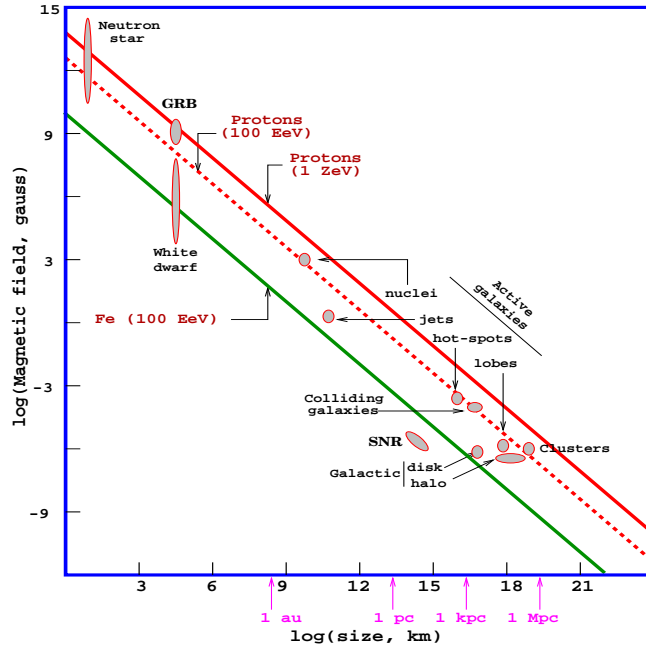
Figure 1.6: Cosmic ray accelerators in the "Hillas plot" (1 EeV $\equiv 10^{18}$ eV, 1 ZeV $\equiv 10^{21}$eV) (figure taken from: Chiarusi & Spurio (2010)

To understand the contribution to the observed cosmic ray diffuse spectrum from different astrophysical sources, Hillas (1984) introduced a plot, where the cosmic ray accelerators are plotted based on the accelerator size and the corresponding average magnetic field. In any cosmic accelerator, if the Larmor radius of the charged particle is smaller than the acceleration region R, then the maximum energy of particles can be calculated from

$$E_{\max}(\text{EeV}) \sim \beta \, Z \, B_{\mu G} \, R_{\text{kpc}}.$$

In the above expression Z is the charge of the nucleus, B is magnetic field and R is size of the source (cosmic accelerator) in which the charge particles are confined. In the Figure 1.6 "Hillas plot" shows astrophysical sources which are potential candidate for cosmic-ray acceleration.

The physics of cosmic rays can be explained from their interaction with the ambient

matter and radiation. In these interactions, the secondary particles like high energy gamma rays and neutrinos, antimatter, mainly antiprotons are produced. We now discuss about gamma ray astronomy, neutrino astronomy and the production of antiprotons in cosmic ray interactions in Section 1.1, 1.2 and 1.3 respectively.

1.1 Gamma ray Astronomy

The astrophysical or cosmic gamma rays have a very broad energy range. It spans in the energy range of MeV - 100 EeV which has been divided into 5-subintervals, as discussed by Aharonian (2004). (a) < 30 MeV, *low energy (LE)* (b) 30 MeV - 30 GeV, *high energy (HE)* (c) 30 GeV - 30 TeV, *very high energy (VHE)* (d) 30 TeV - 30 PeV, *ultra high energy (UHE)* (e) > 30 PeV, *extremely high energy (EHE)*. The various types of physical processes which can produce gamma rays in the astrophysical sources are matter-antimatter annihilation (electron-positron and proton-antiproton interactions), radioactive decay of an excited atomic nuclei, synchrotron radiation, inverse Compton effect, pion decay channels etc. These mechanisms have been discussed in details by Stecker (1971), Ramana Murthy & Wolfendale (1993) and Aharonian (2004).

The gamma ray astronomy started with the discovery of cosmic gamma rays of energy (> 100 MeV) by Clark et al. (1968) using Orbiting Solar Observatory (OSO-3) satellite. They found that the intensity of radiation was maximum towards the Galactic centre. Later Kraushaar et al. (1972) reported the detection of cosmic gamma rays (621 events) of energy ≥ 50 MeV using the same OSO-3 satellite. To understand the high energy dynamics of our solar system the gamma ray observations of solar activity started in 1972, where the gamma ray emission lines at 0.51 MeV, 2.2 MeV, 4.4 MeV, 6.1 MeV were observed (Chupp et al., 1973a,b; Forrest et al., 1973), using the OSO-7 satellite. The detection of gamma ray emission lines indicated the presence of excitetd nuclear levels (carbon and oxygen), electron-positron annihilation processes and the thermal neutron flux in solar flares (Trombka et al., 1978; Chupp et al., 1973b). In 1980's the gamma ray observations of the Galactic point sources like Crab Nebula, Vela-X pulsar and the gamma ray diffuse emission in MeV to GeV enery range were reported by the COS-B European mission (Hermsen et al., 1977; Bennett et al., 1977b,a; Kanbach et al., 1977) and by the Small Astronomy Satellite (SAS-2) NASA mission (Fichtel et al., 1975; Kniffen et al., 1977; Thompson et al., 1977a,b; Fichtel et al., 1977). The detection of the gamma rays from the point sources reveals the cosmic accelerators while the observations of the diffuse gamma rays reveal the propagation of cosmic rays in the magnetic fields.

The first detection of TeV gamma rays from Crab nebula was reported by Weekes et al.

(1989). This detection was a huge jump in the field of gamma ray astronomy. They used IACT (Imaging Atmospheric Cherenkov Technique) array for the detection of these gamma rays at the Whipple observatory. The GeV to TeV gamma rays interact with the atmospheric medium and they produce secondary relativistic charged particles. The detection of these relativistic charged particles by their Cherenkov radiation is called IACT imaging technique.

Energetic Gamma Ray Experiment Telescope (EGRET) was a gamma ray detector on the Compton Gamma Ray Observatory (CGRO) of NASA mission during 1991-2000. EGRET had an effective area of 1500 cm^2 and it could detect gamma rays in the energy range of 20 MeV to 30 GeV. Casandjian & Grenier (2008) reported 188 point sources of gamma rays by EGRET observations. They correlated these point sources with radio pulsars, pulsar wind nebulae, supernova remnants, OB associations, blazars and flat radio sources. They found that a large number of point sources (87) do not have any correlation with any known gamma ray sources. They took 1775 pulsars and 11000 radio sources for their cross correlation and they looked in three energy band above 100 MeV, 0.3 GeV, and 1 GeV. EGRET mission also detected diffuse galactic gamma ray emission for lower galactic latitudes.
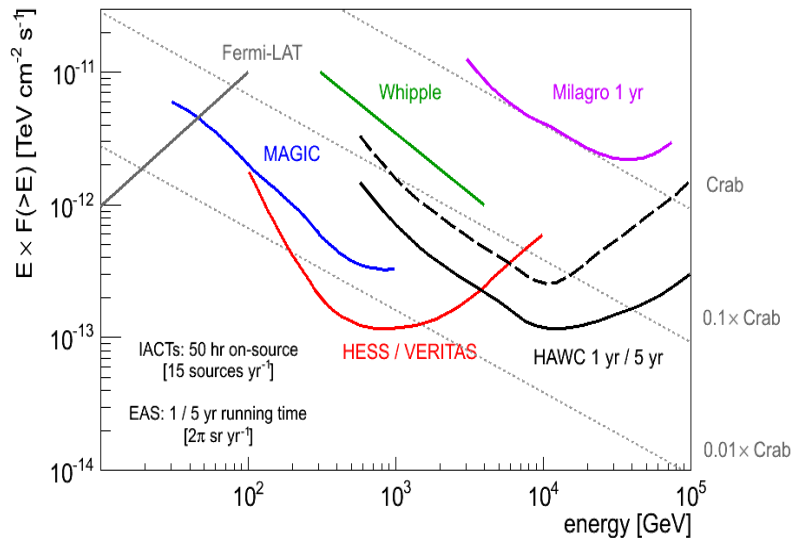
Figure 1.7: Expected gamma ray sensitivity of the instruments. (figure taken from: HAWC collaboration @ http://www.hawc-observatory.org/)

Gamma ray satellite missions operate upto 100 GeV and large area ground based gamma ray detectors operates above 100 GeV. In the current era, the active satellite missions are Swift Gamma-Ray Burst Mission, AGILE (AstroRivelatore Gamma a Immagini Leggero) and Fermi-LAT (Fermi-Large Area Telescope). AGILE detects gamma rays in the energy range of 30 MeV-50 GeV, Fermi-LAT operates in the energy range of 30 MeV-300 GeV. IACT arrays HESS (High Energy Stereoscopic System) in Namibia, MAGIC (Major Atmo-

spheric Gamma-ray Imaging Cherenkov Telescopes) in Canary Island, and VERITAS (Very Energetic Radiation Imaging Telescope Array System) in Arizona, and the HAWC (High Altitude Water Cherenkov Experiment) in Mexico are detecting GeV - TeV gamma rays (Hillas, 2013). Figure 1.7 shows the sensitivity of the ground based detectors w.r.t. the Fermi-LAT detector and the Crab flux.

1.1.1 Galactic sources

The Galactic sources of gamma rays are supernova remnants (SNRs), pulsar wind nebula (PWN), microquasars (binary systems with relativistic radio jets), gamma ray binaries and transient objects like soft gamma repeaters (SGRs). The connection between gamma rays and cosmic rays can be understood from the theoretical modelling of their observed gamma ray spectra. We have discussed below some of the Galactic sources of gamma rays.

- *Supernova Remnants:*

  Supernova remnants (SNRs) have been detected in the energy range of MeV to TeV. The acceleration of electrons, protons and nuclei in SNRs occurs by the shock acceleration process (Bell, 1978a,b; Blandford & Ostriker, 1978b; Jones & Ellison, 1991; Malkov & Drury, 2001; Caprioli et al., 2011). The multi-wavelength observations of SNRs and their theoretical modelling reveal their magnetic field, density of neutral hydrogen and physical properties like the nature of the accelerated particles Abdo et al. (2010c); Saha et al. (2014); Ackermann et al. (2013a). The gamma ray emission of SNRs upto TeV energy can be explained by both leptonic (mainly electronic contribution) and hadronic p-p interaction models.

  We consider the case of Cassiopeia A (Cas A) which is a young SNR (A.D. 1680, 330 year old), of size 2.34 pc and located at a distance of 3.4 kpc (Reed et al., 1995). The multi-wavelength observation of Cas A spans from radio-wavelength to TeV-gamma ray energies. It has been observed in radio wavelength by Baars et al. (1977), Anderson et al. (1995), Vinyaikin (2007), Helmboldt & Kassim (2009), in optical wavelength by Reed et al. (1995). The Cas A has been observed in X-rays by Allen et al. (1997), Hwang et al. (2004), Helder & Vink (2008), Maeda et al. (2009), in GeV gamma rays by Kanbach et al. (1996) (EGRET collaboration), Abdo et al. (2010c) (Fermi-LAT collaboration), in TeV gamma rays by Aharonian et al. (2001) (HEGRA collaboration), Albert et al. (2007) (MAGIC collaboration), Acciari et al. (2010) (VERITAS collaboration).

This source has been modelled by Abdo et al. (2010c), where they found that both leptonic and hadronic models can explain the gamma ray emission from this source. In the leptonic model by Abdo et al. (2010c), high energy electrons accelerated in diffusive shock acceleration transfer their energy to radio photons and converts them to gamma rays.They also discussed the hadronic p-p interaction model where the same gamma ray spectrum can be explained with hadronic model. In the hadronic model, these gamma ray emission are produced in interactions of high energy protons with the neutral hydrogen available within the source.

To explain the gamma ray observation of Cas A by leptonic models, the energy required in electrons above 10 MeV was approximately 1×10^{49} erg, while in the p-p interaction hadronic models, the energy required in protons above 10 MeV was approximately 3×10^{49} erg. The energy in electrons and protons were approximately 2% of the total explosion kinetic energy of Cas A (2×10^{51} erg/sec).

Saha et al. (2014) found that leptonic models alone can not explain the gamma ray emission from Cas A. They found that combined contribution from leptonic and hadronic (lepto-hadronic) interactions, can provide the best fit to the data.
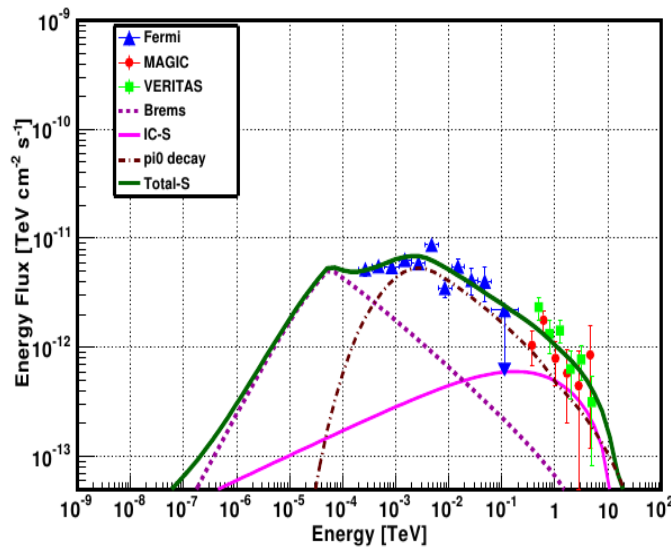
Figure 1.8: Lepto-hadronic gamma ray emission model of Cas A. (figure taken from : Saha et al. (2014))

In the lepto-hadronic case, the total energy needed in electrons above 10 MeV was approximately 4.8×10^{48} erg and in case of protons it was approximately 2.97×10^{49} erg. In Figure 1.8, the individual contribution of inverse Compton process, Bremsstrahlung and p-p interaction to the total emission have been shown (Saha et al., 2014). In some other SNRs, IC443 and W44, Ackermann et al. (2013a) (Fermi-LAT collaboration)

found that the gamma ray spectrum can be best fitted by a p-p interaction pion decay signature.

- *Pulsars and Pulsar Wind Nebulae:*

The confinement of relativistic outflow wind from pulsars produces objects known as pulsar wind nebulae (PWN). PWN are objects powered by the central compact objects (central rotating pulsars) with steady injection of energy. The rate of dissipation of rotational kinetic energy for a pulsar is $\dot{E} = \frac{4\pi^2 I \dot{P}}{P^3}$, where I is the moment of inertia of the pulsar (or the neutron star with a radius of 10 km and mass of $1.4\ M_\odot$), P is the spin period and $\dot{P} = \frac{dP}{dt}$ is the period derivative (Gaensler & Slane, 2006a). The observation of pulses from pulsars are used for the determination of P and $\dot{P}$. It has been found that pulsars with $\dot{E} \geq 4 \times 10^{36}\ \mathrm{erg/sec}$ form the pulsar wind nebula structure (Gaensler & Slane, 2006b).
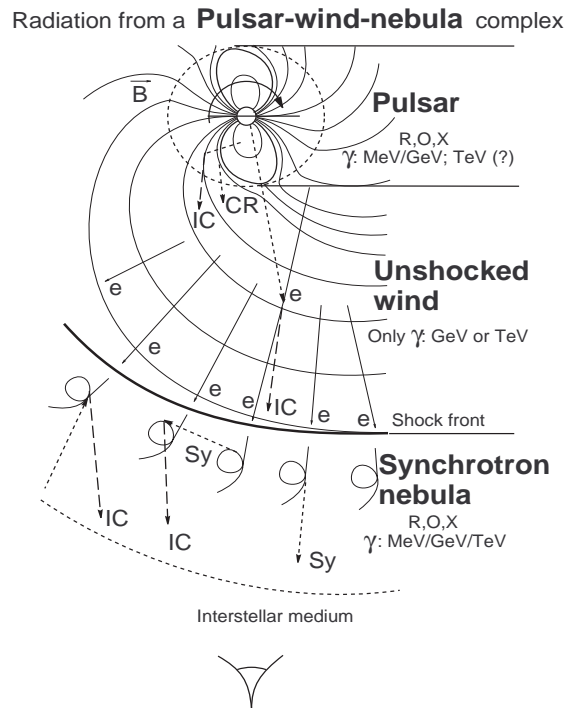
Figure 1.9: PWN and gamma ray emitting regions. (figure taken from : Aharonian & Bogovalov (2003))

The electromagnetic emission region from rotationally powered pulsars (RPP) has been shown in Figure 1.9. The innermost region very near to the poles of the pulsar produces electromagnetic radiation from radio to VHE gamma rays in the pulsed form. This region is located within the light cylinder of the pulsar. In this region,

the gamma ray production mechanism is mainly explained by two models (a) polar cap model and (b) outer gap model (Chiang & Romani, 1994; Rudak & Dyks, 1999; Baring, 2004; Yuki & Shibata, 2012). Within the unshocked wind (middle region of Figure 1.9) from where only GeV to TeV, γ-ray radiations have been observed, can be explained by the inverse Compton process. The outer most (synchrotron nebula region of Figure 1.9) region has been observed in multi-wavelength radiation from radio wavelength to TeV. The emission from this outer most region can be explained by synchrotron and inverse Compton processes.

A large fraction of electron-positron wind plasma takes away the rotational energy of the RPPs. The initial wind energy goes out in the form of Poynting flux and at the termination shock approximately all of the energy resides in the kinetic energy of the wind (Aharonian & Bogovalov, 2003). The physical mechanism for this transformation is still unknown (Aharonian, 2004). The pulsar wind finally terminates at the ISM which creates synchrotron and inverse Compton emission around the pulsars (Aharonian, 2004; Gaensler & Slane, 2006a).

- *Gamma ray Binaries:*

The emission from the binary systems in the energy range of GeV to TeV has been detected by IACTs. The gamma ray binary system is made of a neutron star of mass 1.4 $M_\odot$ associated with massive O / Be star with 10-20 $M_\odot$ (Tam et al., 2011; Dubus, 2013). Gamma ray binaries, which emits most of their power above 1 MeV, are like pulsar wind nebula in a binary system where the non thermal emission arises due to collisions between the winds from a massive star and a rotation powered pulsar (Dubus, 2013). The five confirmed gamma ray binary objects, PSR B1259-63 by Aharonian et al. (2005a), LS 5039 by Aharonian et al. (2005b), LS I +61 303 by Albert et al. (2009), HESS J0632+057 by Bongiorno et al. (2011), and 1FGL J1018.6-5856 by Fermi LAT Collaboration et al. (2012) are located within $3°$ of the galactic plane.

Recently in the HESS observations (H. E. S. S. Collaboration et al., 2015) of the source HESS J1018 - 589 A, they found the association of this source with the Fermi-LAT detected gamma ray binary 1FGL J1018.6-5856. In this HESS observations of gamma ray binary 1FGL J1018.6-5856, the light curve shows the variability in the gamma ray flux, and detection of gamma rays upto 20 TeV.

1.1.2   Extragalactic sources

In the current era of ground based GeV to TeV gamma ray detectors like HESS and VER-
ITAS, many astrophysical sources have been detected. The TeV catalog (Horan & Wakely,
2008) has listed Quasars, Radio galaxies with active central regions, AGN jets, blazars and
massive star clusters as gamma ray candidate sources. Similarly the Fermi-LAT satellite has
detected gamma ray bursts from cosmological distances. The HESS observations have de-
tected 24 extragalactic sources of TeV gamma rays (Stawarz & for the H.E.S.S.Collaboration,
2013) which includes radio galaxies Centaurus A (Cen A) and Messier 87 (M87), 20 BL Lac
type blazars, flat-spectrum radio quasar PKS 1510089, and starburst galaxy NGC 253.

   The gamma ray observations of these objects are very important to understand the com-
position of cosmic rays. The production of gamma rays in these objects can occur in the
hadronic (p-p and p-γ) pion decay models, the photo-disintegration process, the proton cur-
vature radiation, and in the leptonic models.

- *Radio Galaxy M 87:*

   In radio galaxy Messier 87 (M 87), where the relativistic jet makes an angle to the line
   of sight of the observer has been observed in multi-wavelength emission (Charlesworth
   & Spencer, 1982; Walker et al., 2012). The observation of TeV gamma rays from
   the very near region of the central black hole in M 87 reported by Aharonian et al.
   (2006). They found the emission region using the TeV variability time scale which
   was approximately two days, also shown in Figure 1.11. Figure 1.10a and Figure
   1.10b shows the HESS detected gamma ray region of the M 87 and the gamma ray
   flux values respectively.

   The luminosity of TeV gamma rays in M 87 is 3×10^{40} erg/sec and the emission
   region was very compact ($5 \times \delta R_s$), where R_s is Swarchzchild radius of M 87. The
   sources of these TeV gamma rays may be the proton curvature radiation very near to
   rotating super massive black hole (SMBH) in M 87 (Aharonian et al., 2006). This
   physical mechanism of TeV gamma ray emission from rotating SMBH is discussed
   by Levinson (2000). The variability study in the TeV gamma rays from M 87 are
   important to test their production models (Aharonian et al., 2006).

   We will discuss about GeV to TeV gamma ray emission from Cen A in our second
   chapter.
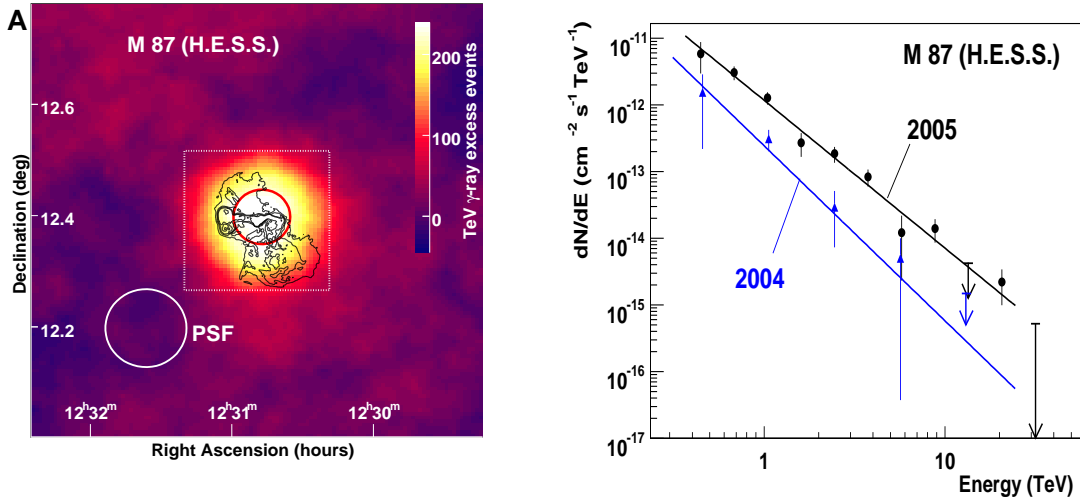
(a) The central region of M 87 in Gamma rays   **(b)** TeV gamma ray from M 87

Figure 1.10: GeV to TeV gamma ray observations of M 87 (figure taken from: Aharonian et al. (2006))
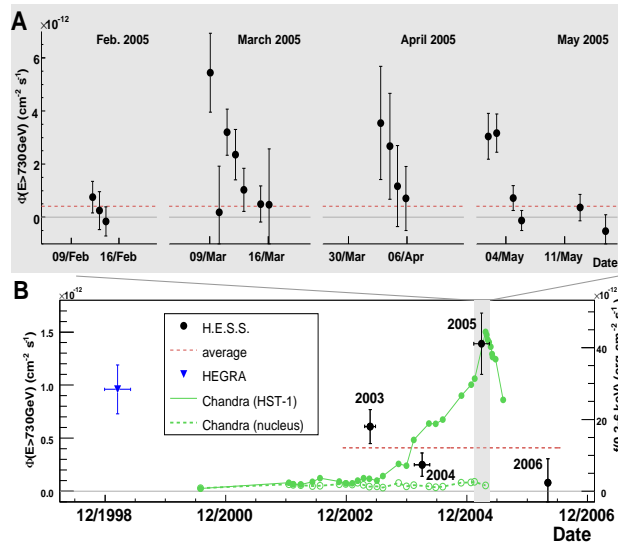
Figure 1.11: The TeV variability of M 87, limits the source region $5 \times R_s$. (figure taken from: Aharonian et al. (2006))

- *Gamma ray bursts:*

Gamma ray bursts (GRBs) were first discovered in 1967 by Vela satellite which was kept into space to check the nuclear test treaty between Soviet union and US, and the results of this discovery were later published by Klebesadel et al. (1973), where the emission was observed mainly in gamma rays. After this discovery, they were observed in X-ray emission by the Burst and Transient Source Experiment (BATSE) experiment on-board Compton Gamma Ray Observatory (CGRO) and by the gamma ray burst monitor (GRBM) on board the BeppoSAX satellite (Frontera et al., 2009). In these detections it has been found that the angular distribution of GRBs was isotropic in the sky and cosmological origin (Meegan et al., 1992; Metzger et al., 1997).

To understand these objects in multi-wavelength later in 2004 Swift gamma ray burst mission satellite with three instruments: the Burst Alert Telescope (BAT), the X-Ray Telescope (XRT) and the UV Optical Telescope (UVOT) started the detection of GRBs in the energy range of optical to MeV (Gehrels, 2004). Similarly, using EGRET instrument on CGRO, Hurley et al. (1994) reported one of the long duration GRB of lifetime of 90 minutes where they detected photons of energy 18 GeV. Later in 2008 the gamma burst monitor (GBM) in the Fermi-LAT satellite launched into space to detect transient sources mainly gamma ray bursts (McEnery & Fermi LAT Collaboration, 2010; Chiang & Racusin, 2011).

Gamma ray bursts (GRBs) are relativistically expanding fireballs (Rees & Meszaros, 1992, 1994) which can accelerate cosmic rays to energies upto 10^{20} eV and these are sources of gamma rays (Vietri, 1995; Böttcher & Dermer, 1998; Bhattacharjee & Gupta, 2004; Dermer & Atoyan, 2006). The GRBs have lifetime from millisecond to 10's of minutes and their number distribution w.r.t. life-time has a bimodal distribution. This distribution indicates that GRBs either emits short bursts of gamma rays of duration 30 millisecond or long bursts of duration 30 seconds (Gehrels et al., 2004a). The fast variability of these objects constrains the emission region within 100's of km. A pedagogical review on this subject discussed by Zhang & Mészáros (2004). These objects are most luminous in MeV gamma rays and the luminosity varies in the range of $10^{50} - 10^{54}$ erg/sec (Mészáros, 2006).

Mészáros & Rees (1997) studied the GRB afterglow in optical and radio wavelengths after their expansion into ISM. The detection of GRB 090423 by Swift and then the delayed infrared observation (2.15-μm) after 20 minutes by the United Kingdom Infrared Telescope (UKIRT), Hawaii established the red shift of this source at z $\sim$ 8.2

(Tanvir et al., 2009). The redshift of GRB 090429B was found to be 9.2 by photometric redshift calculations (Cucchiara et al., 2011). These red shifts of GRBs means that they are cosmological in origin and they are important to understand the conditions of early universe.

GRB physics is very promising; some of the open questions in GRBs like their classification, massive star collapse or neutron star-neutron star merger progenitor, central engine activity, ejecta composition and the particle acceleration and radiation processes etc are challenging (Zhang, 2011). The future Chinese-French GRB mission, SVOM (Space-based multi-band astronomical Variable Object Monitor) and its approach to solve these issues has been discussed by Zhang (2011).

1.2 Neutrino Astronomy

The idea of neutrino was put forward by Pauli in 1930 to conserve energy in the radioactive decay process where a proton converts into a neutron inside the nucleus. Neutrino was detected 25 years later by Cowan et al. (1956) in nuclear reactor experiments where they detected outer product (neutron and positron) of neutrino interaction with proton, $\bar{\nu}_e + p \rightarrow n + e^+$.

The neutrino astronomy started with the understanding of fusion process inside sun's core. The thermonuclear reaction ($4p \rightarrow {}^4He + 2e^+ + 2\nu_e$) inside the core of sun produces the solar energy and emits neutrino known as solar neutrino. Bahcall (1964) and Davis (1964) considered the possibility of the detection of the solar neutrino.

The detection of neutrinos from astrophysical sources would be a clear signature of either nuclear deexcitation or cosmic ray interactions. The confirmed astrophysical sources of neutrinos are the sun and the supernova SN 1987A.

In the cosmic ray interactions with the radiation field and the gas medium the secondary neutrinos are produced.

$$p_{cr} + (\gamma \text{ or } p_{atmosphere}) \rightarrow \pi^{\pm} \tag{1.1}$$

$$\pi^{\pm} \rightarrow \mu^{\pm} + \nu_{\mu}/\bar{\nu}_{\mu} \tag{1.2}$$

$$\mu^{\pm} \rightarrow e^{\pm} + \bar{\nu}_{\mu}/\nu_{\mu} + \nu_e/\bar{\nu}_e \tag{1.3}$$

In these interactions neutrinos which are produced in the atmosphere are known as atmospheric neutrinos while the Galatic and extragalactic neutrinos are called astrophysical neutrinos. The ratio of the neutrino fluxes of different flavors produced at the source is $\nu_e + \bar{\nu}_e : \nu_\mu + \bar{\nu}_\mu : \nu_\tau + \bar{\nu}_\tau = 1 : 2 : 0$. Due to the flavor mixing the fluxes of neutrinos of

each flavor are expected to be roughly equal on Earth $\nu_e + \bar{\nu}_e : \nu_\mu + \bar{\nu}_\mu : \nu_\tau + \bar{\nu}_\tau \simeq 1 : 1 : 1$ (Gaisser, 1991a; Choubey & Rodejohann, 2009). In these interactions two kind of neutrinos (electron type and muon type) are produced at the source. A detection of τ type of neutrino have a link with the oscillation behavior of neutrinos. The evidence for muon neutrino flavor oscillation to tau neutrino $\nu_\mu \leftrightarrow \nu_\tau$ were reported by Fukuda et al. (1998) (Super-Kamiokande Collaboration) after the analysis of 535 days of data, with a 90% confidence level.

Waxman & Bahcall (1998); Bahcall & Waxman (2001) calculated an upper bound on the neutrino flux from the astrophysical sources in which cosmic ray of energy greater than 1 EeV were produced. This upper limit of 2×10^{-8} GeV/(cm^2 sec sr) on neutrino flux was model independent and these authors explored it for AGN jets and GRBs where the source size was estimated larger than the p-p interaction mean free path. The connection of neutrinos to the cosmic rays have been discussed by (Berezinskii et al., 1990a; Mannheim, 1995; Engel et al., 2001; Halzen & Hooper, 2002; Waxman, 2005; Razzaque et al., 2005). This theoretical connection basically explores the astrophysical sources of neutrinos.

The atmospheric neutrino flux follows a power law behavior $E_\nu^{-3.7}$, which is much steeper than the cosmic or astrophysical neutrino flux E_ν^{-2} (Braun et al., 2008). Atmospheric neutrinos have the mean energy approximately 1 TeV (IceCube-Gen2 Collaboration et al., 2014). The best window to look for astrophysical neutrinos is around 100 TeV of neutrino energy where the atmospheric background is negligible, as shown in Figure 1.12.
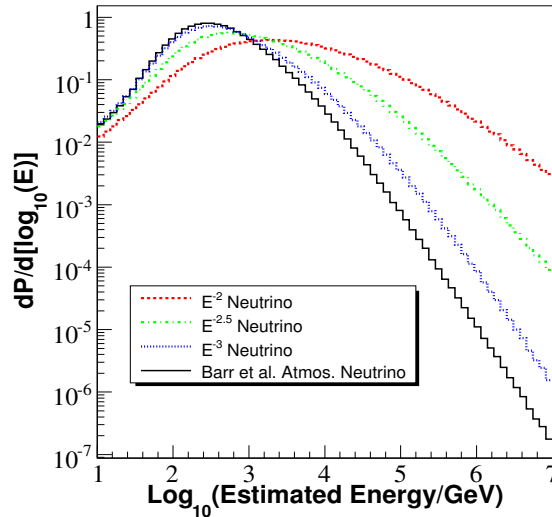
Figure 1.12: Atmospheric and astrophysical neutrino spectral energy distribution. (figure taken from: Braun et al. (2008))

The production of atmospheric neutrino resulted from the interaction of cosmic rays

with the atmosphere. In this interaction the ratio (R) = $\frac{\nu_\mu + \bar{\nu}_\mu}{\nu_e + \bar{\nu}_e}$ is approximately 2 in ideal conditions. At higher energy, the muon life time increases and they don't decay. In those cases this ratio may not be exactly equal to 2. In the neutrino detectors the detection of a neutrino occurs via the interaction of neutrino with target nucleus. The interaction of electron neutrino with target nucleus $\nu_e + N \rightarrow e^- + N'$ produces secondary electrons and the hadronic showers (Aartsen et al., 2014a). Similarly muonic (μ) and tau (τ) leptons and associated hadronic showers are produced from their parent muon and tau neutrino in their interaction with target nucleus.

The neutrino interaction cross section, has a very lower value (Formaggio & Zeller, 2012). This low cross section demands for huge target mass for their detection and due to this reason neutrino detectors are mainly established in deep underground regions, either in deep mines or in polar regions where clear ice selected as target mass.

Now we will discuss some of the neutrino experiments and their contribution to our understanding about neutrinos.

- *Homestake experiment (1968-94)*

  Homestake neutrino experiment was the first underground detector built in 1960's at the Homestake Gold Mine in Lead (US), South Dakota by the efforts of Bahcall (1964) and Davis (1964). This experiment detected the neutrinos from the solar core and led to the base for neutrino physics and astronomy. In this experiment the interaction of neutrinos with the chlorine atoms (which were available in a tank of liquid chlorine C_2Cl_4), i.e. $\nu_e + {}^{37}Cl \rightarrow e^- + {}^{37}Ar$. So the number of neutrinos detected were based on the production of Argon atoms. In this experiment, Davis (1964) found that the observed neutrinos were 0.33 times of the theoretical calculations of Bahcall (1964). This mismatch between the theory and observation was known as *solar neutrino problem*. This problem was the great contribution of this experiment to the future research in neutrino astronomy, and later solved by the combined effort of theoretical and observational results.

- *DUMAND (Deep Underwater Muon And Neutrino Detector Project)*

  The construction of this detector started in 1972, to detect Galactic and extragalactic point sources of neutrinos of energy greater than 50 GeV (Allkofer et al., 1990). Deep ocean water DUMAND optical sensors were at a separation of 0.5 km at a depth of 2 to 4 km for the detection of Cherenkov light produced by relativistic charged particles, mainly muons produced by neutrino interaction with water nuclei at DUMAND. This

detector detected some of the cosmic ray muons (Babson et al., 1990) and established the stable underwater neutrino detector techniques (Roberts, 1992).

- *Kamiokande and Super-Kamiokande (Kamioka Nucleon Decay Experiment)*

The Kamioka detector was a water tank detector in Japan, which used 1000's of tons of water for the interaction of neutrinos. This detector was built in 1982 and later it was upgraded to Kamiokande-II and successively to Super Kamiokande detector, which is currently active and uses 50000 ton's of water.

Kamiokande detected neutrinos from the solar core (Suzuki, 1995; Totsuka, 1991) and solar flares (Hirata et al., 1988b). Hirata et al. (1990) used the Kamiokande-II solar-neutrino data to understand the oscillation parameters of the neutrinos. This detector also detected the neutrinos from the supernova 1987 and it was the first neutrino source detected outside our solar system (Tozuka, 1988; Hirata et al., 1988a; Koshiba et al., 1988). The study of atmospheric neutrinos and their detection by Kamiokande detector was very important to understand the neutrino oscillations (Fukuda et al., 1998, 1999) .

- *ANTARES (Astronomy with a Neutrino Telescope and Abyss environmental RESearch project)*

The ANTARES is located inside Mediterranean sea at a depth of 2500 m, which has a detector area of 0.1 km^2 (ANTARES collaboration, 1997). This detector has a good view towards the galactic centre for the detection of neutrinos in the energy range 10 GeV to PeV from the direction of the southern sky (Aguilar et al., 2006; The ANTARES Collaboration et al., 2013).

The ANTARES data provides the upper limit on the neutrino flux from the cosmic point sources of neutrinos (Adrián-Martínez et al., 2012a). The ANTARES data has been used to explore the neutrinos from GRBs (ANTARES Collaboration, 2013), microquasars (Adrián-Martínez et al., 2014), gamma ray flaring blazars (Sánchez Losa & ANTARES Collaboration, 2013; Adrián-Martínez et al., 2012b), and from the Fermi bubble (ANTARES Collaboration et al., 2013).

- *AMANDA (Antarctic Muon And Neutrino Detector Array)*

The Antarctic Muon And Neutrino Detector Array (AMANDA) detector, operated in between 1996-2005 at the south pole, into the depth of 1.5 km to 2.0 km (Andres et al.,

2000). It has detected atmospheric muon neutrinos in the GeV to TeV energy range (Andrés et al., 2001; Wang, 2005). In the detection of neutrino flux it was very hard to surpass the atmospheric muon flux. AMANDA collaboration did not find any excess in the extraterrestrial diffuse neutrino flux (Ahrens et al., 2003) and no excess reported in the point sources of neutrinos (Ackermann et al., 2005; Abbasi et al., 2009). This detector later in 2005 was upgraded to the IceCube detector, which we have discussed below.

- *The IceCube detector*

The IceCube neutrino observatory is currently the most active neutrino detector at the South pole. This detector has built on a cubic kilometer ice at a depth of 1.45 km to 2.45 km, which reflects in its name (Halzen, 2006a; IceCube Collaboration et al., 2006). The IceCube detector at the south pole after its full operation in 2010 started detecting neutrino events. IceCube has detected the first set of 28 neutrino events in the energy range of TeV to PeV (IceCube Collaboration, 2013). The total number of neutrino events after the analysis of 3-years of data has been reached to 37 (Aartsen et al., 2014b). In these observations the maximum energy of the neutrino events were found to be 2 PeV. These observations are the first time detection of TeV to PeV neutrinos from any kind of terrestrial and extraterrestrial sources.

After the successfull detection of astrophysical neutrinos by the current IceCube detector, IceCube-Gen2 Collaboration et al. (2014) has proposed to extend the volume of the detector from 1 km^3 to 10 km^3. In future, it will be interesting to look if neutrino astronomy can be used to explore the presence of anti-neutrinos at 6.3 PeV in cosmic sources by resonance effects like Glashow effect (Glashow, 1960; Barger et al., 2014), to reveal the relic particles like magnetic monopoles and to look for indirect dark matter search (Chiarusi & Spurio, 2010). The GZK neutrino as discussed in section above is also one of the main goals for the IceCube Gen-2 neutrino observatory. There are high energy gamma ray sources detected by High Energy Stereoscopic System (HESS) observations, for example HESS J1841055 (Bartoli et al., 2013), but not detected in other wavelengths. If these sources can be detected by neutrino observations then it will reveal purely hadronic sources of cosmic rays.

These all neutrino detectors have helped the scientific community in understanding the bizzare properties of neutrinos like the flavor oscillation (or the mass of neutrinos) etc. The future neutrino observations have more opportunities to reveal the cosmic ray sources.

1.3   Antimatter from the astrophysical sources

Antimatter particles like antiproton, positron and antiparticles of heavy nuclei were detected in laboratory experiments (Anderson, 1933; Chamberlain et al., 1955; Antipov et al., 1971). These detections lead to look for the presence of antimatter in the universe. Antimatter in the form of antiprotons and positrons have been detected by the satellite experiments (Adriani et al., 2010a, 2013a) but there has been no success in the detection of the antiparticles of heavy nuclei like antihelium etc (Mayorov et al., 2011) from astrophysical sources.

Stephens & Golden (1987) has discussed the following mechanisms for the production of antiprotons in the astrophysical sources.

- Cosmic ray interaction and antiproton production

- Neutron oscillation process (antineutron production and their decay)

- Evaporation of mini black-holes and emission of nucleon/antinucleon pairs

- Decay of supersymmetric particles which are present in our galactic halo as a remnant of the big bang

- Antimatter galaxies in a symmetric universe

The first cosmic ray antiproton evidence in 1979 were reported by Golden et al. (1979). They used balloon-borne superconducting-magnet spectrometer for this detection. In their detection period of 3×10^4 sec they recorded total 46 antiprotons in rigidity range 5.6 to 12.5 GV/c. In these 46 events, 18 were from atmospheric and instrumental background. In similar balloon borne experiments with imaging calorimeter and a time-of-flight scintillator system more precise detection of antimatter particles like antiproton and positron have become possible. The balloon borne experiments have been detected antiproton flux in the kinetic energy range of 0.1 GeV to 50 GeV (Hof et al., 1996; Orito et al., 2000; Abe et al., 2012).

In the last decade, satellite experiments have been started for the detection of antimatter from cosmos. Alpha magneto spectrometer (AMS) satellite experiment at an altitude of 320 to 390 km has been mounted on the International Space Station. In this series, the prototype AMS-01 launched in 1998 and later in 2011 a full developed AMS-02 has been established into International Space Station. AMS-01 looked for the presence of antihelium and secondary antimatter particles from cosmos. In this search, for antihelium, no events were recorded, and an upper limit on antihelium to helium flux of value $< 1.1 \times 10^{-6}$ was reported by Alcaraz et al. (1999). The main aim of AMS-02 is to reveal antimatter and dark

matter in our universe. After its launch AMS-02 has been detected the positron flux in the energy range of 0.5 to 350 GeV (Aguilar et al., 2013).

The another satellite mission PAMELA (Payload for Antimatter Matter Exploration and Light-nuclei Astrophysics) has been launched into space in 2006 (Adriani et al., 2010b) and it orbits at an altitude of 350 to 610 km. PAMELA can detect charged particles mainly antiparticles (positron, antiproton) and some low charged nuclei in the energy range of 10's of MeV to 100's of GeV. PAMELA detector design and its performance efficiency has been discussed by Picozza et al. (2007). This detector can detect antiprotons from astrophysical sources and also from the geomagnetic field of the earth. The Van Allen radiation belt in the South Atlantic region penetrates towards earth's surface, and keeps a separation of 200 km w.r.t. surface of earth. This is called South Atlantic anomaly (SAA), where the flux of charged particles is higher compared to other positions at the same altitude. PAMELA satellite, when it crosses SAA region can detect antiprotons trapped in the geomagnetic field of the earth. Adriani et al. (2011b) reported the discovery of antiprotons from SAA region in the energy range of 60 to 750 MeV. They found that the antiproton flux from SAA region was three orders of magnitude higher than the antiproton flux from cosmic background at the time of solar minimum.

In the PAMELA observation of antiproton and positron from Galactic and extragalactic sources an excess of positron flux was seen but there was no excess seen in the antiproton flux. This positron excess may be due to dark matter annihilation. Supersymmetric dark matter decay origin had been discussed by Bergström et al. (2008) to explain the PAMELA data but still this can not be confirmed as pulsars are the main sources of positron flux (Hooper et al., 2009).

Antiproton flux from exotic physical processes like dark matter particle decay and from black hole evaporation process has cosmological implications which can help us in better understanding of dark matter presence around our Galactic halo (Stephens & Golden, 1987; MacGibbon & Webber, 1990; MacGibbon, 1991). These exotic physical processes produce maximum antiproton flux around 0.2 GeV (MacGibbon & Webber, 1990; MacGibbon, 1991) while the threshold energy for antiproton production via p-p interaction ($p + p \rightarrow 3p + \bar{p}$) has a value of approximately 7 GeV. After the detection of antiproton flux at kinetic energy less than 0.5 GeV by BESS experiments in 1993, Maki et al. (1996); Kiraly et al. (1981) calculated the spectrum of antiprotons from local interstellar primordial black holes.

Antiprotons can also come from dark matter annihilation processes. Silk & Srednicki (1984) hypothesized this possibility on first time, where they have taken a photino, super-symmetry partner of the photon, as a dark matter candidate particle. *In mixture models of antiproton production*, cosmic ray spallation (nuclear reactions of cosmic-ray nuclei on in-

terstellar matter) and dark matter annihilation were considered by Chardonnet et al. (1996).

Similarly, Chardonnet et al. (1996) used spherically symmetric neutralino density in our Galactic halo for the calculation of antiproton flux. They have used two zone diffusion model of antiproton propagation (since leaky box model had been ruled out due to cosmic ray gradient throughout the galactic disc). In the two zone model of diffusion, our Galaxy can be modelled by inner region of diffusion ($0 \leq r \leq R = 20$kpc, $|z| \leq h = 100$ pc) and an extended region of diffusion ($0 \leq r \leq R = 20$kpc, $|z| \leq L = 3$ kpc). They found that this two zone diffusion model was in good agreement with observational results below 300 MeV of antiproton energy.

Antiproton production solely from neutralino annihilation has been also discussed by Jungman & Kamionkowski (1994) and by Ellis et al. (1988). Recently, Fornengo et al. (2014) used the antiproton data detected by PAMELA for the calculation of dark matter annihilation cross section. Motivated from the cosmic ray observational results at earth, Blasi & Serpico (2009) calculated the contribution of Galactic old (2×10^4 years) supernova remnants to the fluxes of antiprotons at earth. In their calculation of antiproton to proton ratio $\frac{\bar{p}}{p}$ it has been considered that propagation effects for protons and antiprotons are similar.

The production of antiprotons via cosmic ray spallation and their propagation have been considered using two zone diffusion model by Donato et al. (2001). Recently, Kachelriess et al. (2015) have used the large hadron collider data to calculate the accurate value of cross section of antiproton production in p-p interactions which can be used to model the precise value of antiproton flux observed by PAMELA and AMS-02.

In our chapter 4 we have calculated antiproton flux from nearby supernova remnants and associated molecular clouds based on Fermi-LAT gamma ray observations.

Chapter 2

Testing hadronic models of gamma ray production at the core of Centaurus A

2.1 Introduction

Centaurus A (Cen A) is the closest extragalactic active galactic nucleus (AGN) (Marconi et al., 2000; Burns & Price, 1983). Based on radio classification, it is a FR-I type of radio galaxy. The classification of radio galaxies into FR-I and FR-II based on their surface brightness and radio luminosity studied by Fanaroff & Riley (1974). Fanaroff and Riley selected 199 extragalactic radio galaxies from 3C catalogue of Mackay (1971). In this study at 178 MHz, the galaxies with radio luminosity $2 \times 10^{25} \mathrm{W}/(\mathrm{Hz-sr})$ named as FR-I and above this luminosity the galaxies were named as FR-II.

The distance of Cen A from earth is 3.4 Mpc (Rejkuba, 2004). This galaxy has two giant radio lobes with $10°$ extension on the north-south direction in the sky (Feain et al., 2011). The substructures in Cen A, like inner lobes and jets have been studied in radio wavelength and X-ray band (Kraft et al., 2004) while the knot structures were revealed using optical observations (Brodie et al., 1983). The activity of black hole in Cen A has been studied by the dynamics of surrounding stars and gas medium (Neumayer, 2010).

Around 1970, the detection of gamma rays from this object indicated signatures of high energy radiative processes in Cen A (Grindlay et al., 1975; Hall et al., 1976; Sreekumar et al., 1999; Hartman et al., 1999). With the successful operation of Fermi-LAT (MeV to GeV gamma ray detector) and HESS (GeV to TeV gamma ray detector), this object has been detected extensively in the MeV to TeV gamma rays (Aharonian et al., 2009; Abdo et al., 2010b; Sahakyan et al., 2013). Fermi large area telescope (Fermi-LAT) is a gamma-ray satellite with 20 percent field of view of the sky, in the energy range of 20 MeV to 300 GeV (Atwood et al., 2009), similarly ground based high energy stereoscopic system (HESS) detects cosmic gamma rays in the energy range of 100 GeV to 10 TeV (Hofverberg & H.E.S.S. Collaboration, 2011).

The gamma rays from Cen A have been detected from its central few kpc regions which is defined as the core, kpc-scale inner jets and radio lobes (Abdo et al., 2010b). The HESS gamma ray observations or the excess of GeV to TeV gamma rays from Cen A coincide with the core. In a multi-wavelength campaign 2008-09, Cen A has been detected in the radio wavelength to TeV energy (Abdo et al., 2010b). Earlier to this, Cen A has been detected in radio wavelength (Ojha et al., 2010b,a) and the jets were detected in the X-rays (Gehrels et al., 2004b). During the multi-wavelength campaign 2008-09, this object emitted in MeV to GeV gamma rays (Abdo et al., 2010b) and a non-simultaneous GeV to TeV component (Aharonian et al., 2009).

The multi-wavelength data of Cen A can be explained by a single zone synchrotron self Compton (SSC) model (Abdo et al., 2010b) upto MeV energy, but this model cannot explain

the GeV to TeV component (Aharonian et al., 2009). In this model a relativistic population of electrons undergo synchrotron process in the magnetic field of the source and can explain the radio peak of the emission. The another peak of the emission around keV energy can be explained by the inverse Compton process for which the seed photons are the synchrotron photons produced by the same population of relativistic electrons, and due to this reason this model is known as SSC model (Jones et al., 1974).

The observation of very high energy gamma rays from Cen A may be because of negligible attenuation of these particles within the turbulent source medium which also refers to the relativistic outflows as found by Dondi & Ghisellini (1995) in gamma ray loud blazars. The features of active galactic nuclei (AGNs) have been discussed by Krawczynski & Treister (2013), which included the AGN jets, cores etc. In Figure 2.1 the morphology of Cen A has been shown.
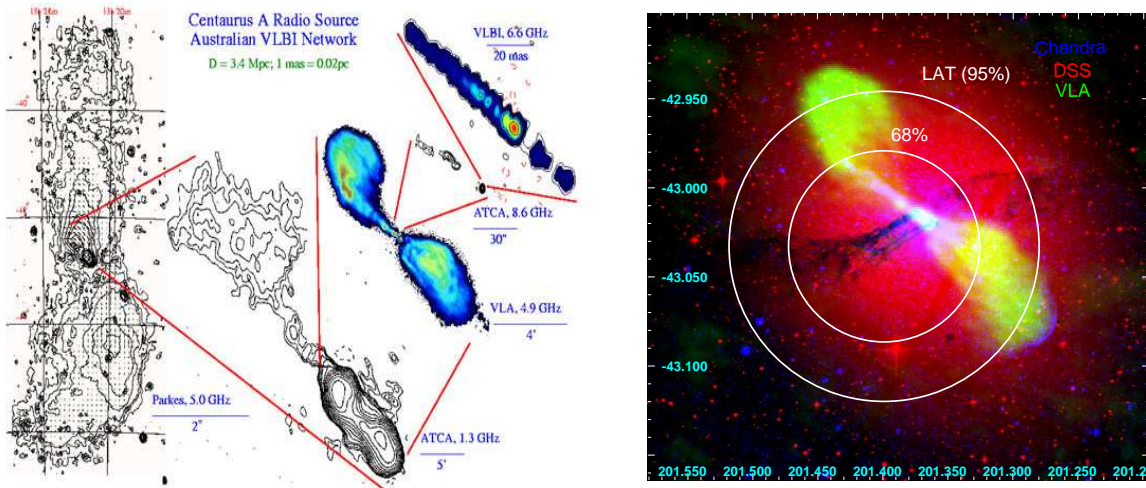
Figure 2.1: In left panel the radio imaging of Cen A,(figure taken from webpage of ATNF/CSIRO). In the right panel, Fermi Gamma ray observation of Cen A , with simultaneous radio, optical , X-ray observations. The LAT emission region is coincide with core, jets and radio lobes. We are interested in the core region (central few kpc region), (figure taken from Abdo et al. (2010b).

Other than gamma ray observations of Cen A, this object has been studied extensively in theoretical calculations as a potential source of UHECRs (Anchordoqui et al., 2001, 2011; Gopal-Krishna et al., 2010; Biermann & de Souza, 2012; Kachelrieß et al., 2009b). The directional correlation of ultrahigh energy cosmic rays (UHECRs) to the astrophysical sources studied with the cosmic ray observations from SUGAR (Winn et al., 1986), Fly's Eye (Bird et al., 1995), HiRes (Abu-Zayyad et al., 2001), AGASA (Takeda et al., 1998, 1999, 2003b), Haverah Park (Ave et al., 2003) and Pierre Auger observatory (Pierre Auger Collaboration et al., 2007, 2008). The results of correlation studies are highly dependent on the samples of data used from different experiments. The successful operation of Pierre Auger experiment

Table 2.1: SSC model parameters for the core emission of Cen A

Cen A parameter	Based on SSC model (Abdo et al., 2010b)
Bulk Lorentz factor (Γ)	7.0
Doppler factor (δ_D)	1.0
Jet angle (θ)	30°
Magnetic field (B)	6.2G
Comoving blob size (R)	3.0×10^{15} cm
Variability time scale (τ_v)	1.0×10^5 sec

and correlation of ultra high energy cosmic ray (UHECR) events above 55 EeV to the nearby sources may reveal cosmic accelerators (Pierre Auger Collaboration et al., 2007; Abreu et al., 2010). Due to the indirect detection of cosmic rays above PeV energy the composition remained uncertain. The photo-disintegration of cosmic ray heavy nuclei in the astrophysical sources can produce gamma rays and daughter nuclei (Stecker, 1969; Stecker & Salamon, 1999; Murase & Beacom, 2010; Anchordoqui et al., 2007b).

The observed diffuse UHECRs spectrum at earth may be a mixture of protons and heavy nuclei (Pierre Auger Collaboration et al., 2011). At higher energies greater than 5 EeV the cosmic ray composition detected by Abraham et al. (2010) is in favour of iron composition.

We have assumed that the two cosmic ray events observed from the direction of the core of Cen A are either protons or neutrons. Similar lines of thought were discussed by Sahu et al. (2012). In our case these UHECR protons and neutrons are produced after the photo-disintegration interaction. Cen A TeV gamma ray observation (Aharonian et al., 2009) has been related to the two extremely energetic cosmic ray events observed by Pierre Auger observatory from the direction of the core of Cen A within the hadronic model of $p - \gamma$ interactions by Sahu et al. (2012). In this scenario the luminosity of the cosmic ray protons of energy 13 TeV has to be close to the Eddington luminosity of the black hole ($L_{Edd} = 1.3 \times 10^{46}(M/10^8 M_{sun})$erg/sec). The two cosmic ray events correlated by Pierre Auger observatory towards Cen A in between 55 to 150 EeV can be explained with a lower luminosity budget of 9×10^{39}erg/sec (Anchordoqui et al., 2011).

In this chapter we will discuss the interaction of cosmic rays with the gas medium and the radiation field in the Cen A core. In our calculation we need the Cen source parameters ($\Gamma, \delta_D, \theta, B, R$) which are listed in Table 2.1 for the green fitted curve in Figure 2.2. drived by Abdo et al. (2010b) using the SSC model.
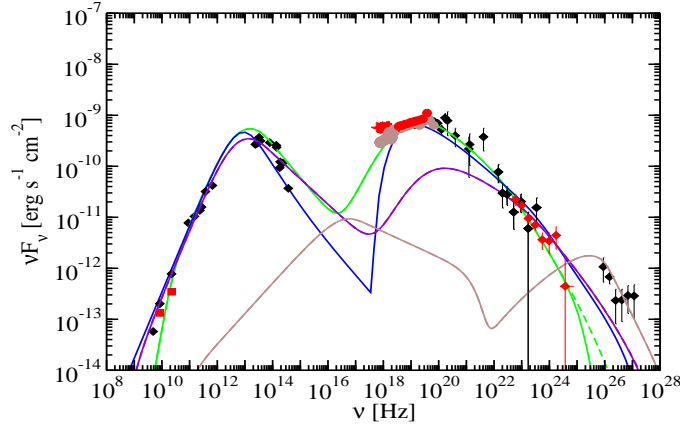
Figure 2.2: Centaurus A multi-wavelength observations and the SSC model fits. The green curve and the dashed green curves are the SSC model fit with and without $\gamma - \gamma$ attenuation. A SSC model fit with different parameters, as shown by violet curve can't explain the X-ray data and TeV emission while the brown curve can explain the TeV emission but in can't produce the other parts of SED. The decelerating jet model by Georganopoulos & Kazanas (2003), as shown by blue curve in the above figure, can't explain the TeV emission. The SSC model parameters for different curves can be found in Abdo et al. (2010b). The SSC model parameters for green curve are shown in Table 2.1 and are used in our calculation. Image Credit: Abdo et al. (2010b)

2.2   Hadronic models of gamma ray production

As we have discussed in the section above that the GeV to TeV emission from the central region of Cen A cannot be explained by a relativistic population of electrons in the core of Cen A. We have taken the case when cosmic rays are interacting in the core of Cen A and producing secondary particles. We have discussed the following hadronic processes in this chapter.

- *The interaction of cosmic rays with the gas medium.*

  The interaction of cosmic ray proton with the gas density at the source leads to production of secondary particles. These kind of interaction can be generalized to any composition of cosmic rays, for example any A-p kind of interactions, where A is the mass number of the atomic nuclei.

- *The interaction of cosmic rays with the radiation field.*

  In this scenario, the interaction of cosmic ray proton with the radiation field produces secondary particles.

- *The photo-disintegration of primary cosmic rays in the radiation field.*

The photo-disintegration of cosmic ray heavy nuclei followed by de-excitation of daughter nuclei, produces secondary particles.

To calculate the flux of secondary particles in the hadronic interactions, we need the spectrum of primary cosmic rays, seed photon spectrum and the information about the density of the gas medium at the source. We have choosen a power law cosmic ray spectrum with no breaks for the Cen A source from TeV to 100's of EeV energy of the cosmic rays. The normalization of the cosmic ray spectrum is constrained by the Pierre Auger observation while the index of the spectrum follows the GeV to TeV gamma ray spectral index.

The observed high energy gamma ray flux from Cen A can be used to reveal the hadronic processes inside this source (Gupta, 2012; Kachelrieß et al., 2009a). The GeV to TeV gamma rays observed from Cen A could be more useful to study this source as an UHECR accelerator (Aharonian et al., 2009). HESS experiment has detected gamma ray emission from the kpc scale central region whose morphology is basically the central black hole, the inner kpc jets and lobes (Aharonian et al., 2009). The gamma ray flux above energy 250 GeV is a single power law with index $2.73 \pm 0.45_{\mathrm{stat}} \pm 0.2_{\mathrm{sys}}$, denoted as $\frac{\mathrm{d}\phi_\gamma^{\mathrm{o}}(\mathrm{E}_\gamma^{\mathrm{o}})}{\mathrm{dE}_\gamma^{\mathrm{o}}\mathrm{dt^o dA}}$ in observer's frame on earth.

$$\frac{\mathrm{d}\phi_\gamma^{\mathrm{o}}(\mathrm{E}_\gamma^{\mathrm{o}})}{\mathrm{dE}_\gamma^{\mathrm{o}}\mathrm{dt^o dA}} = 2.45 \times 10^{-13} \Big(\frac{\mathrm{E}_\gamma^{\mathrm{o}}}{1\mathrm{TeV}}\Big)^{-2.73} \mathrm{cm}^{-2}\mathrm{sec}^{-1}\mathrm{TeV}^{-1} \tag{2.1}$$

The very high energy gamma ray emission observed by HESS is from the core (central region with inner jets and lobes) of Cen A.

The production of gamma rays at the core of Cen A depends on the efficiency of the hadronic interaction. We have first calculated the efficiency of the hadronic interactions at the core of Cen A. To calculate the rate of the hadronic interaction we need to convert the observed photon density at earth to a wind frame associated with the source. To do this we have defined two frame of references-

The first one is the wind rest frame, associated with the Cen A source jet and second frame of reference is the observer frame on earth. The wind rest frame is moving w.r.t. the observer frame on Earth.

We have calculated the very high energy gamma ray flux in the observer's frame on Earth to compare with HESS observations.

2.2.1   Pure Hadronic Interactions

In the pure hadronic interactions the cosmic rays which are accelerated to higher energies at the core of Cen A, interacts with the ambient neutral hydrogen density. These interaction

leads to the production of charged π^+, π^- and neutral pions π^0 with almost equal probabilities. The decay of neutral pions produces gamma rays and charged pions decay to neutrinos and antineutrinos.

In the first case as mentioned earlier we have assumed that the primary cosmic rays are only protons at the core of Cen A.

Based on SSC model parameters, (please see Table 2.1) the interaction region of cosmic rays at the Cen A source, in the wind rest frame is, $R = 3 \times 10^{15}$ cm. In the wind rest frame the optical depth for the pion production, in the pure hadronic interaction is decided by the density of gas medium. Each pion produced in $p - p$ interactions is assumed to carry 20% of the initial proton's energy. The optical depth for pion production in interactions with hydrogen density n_H/cm^3 in a blob of size of $R = 3 \times 10^{15}$ cm in the wind rest frame is $\tau_{pp} = R/l_{pp}$, where the mean free path is $l_{pp} = 3/n_H \times 10^{25}$cm for the p-p interaction cross-section of value approximately $\sigma_0 = 34.6$mb (Anchordoqui et al., 2007a).

In the wind rest frame the cosmic rays and gamma rays are emitted isotropically. These particles should undergo relativistic beaming effects in the observer's frame. Only those photons from Cen A are observed which are travelling along the line of sight of the observer. The observed emission at earth should be modified by the Doppler factor, which is defined as $\delta_D = \Gamma^{-1}(1 - \beta\cos\theta_{ob})^{-1}$. Where β is the dimensionless speed of the wind rest frame with respect to the observer on Earth and the angle between the observed photon and the wind's velocity is θ_{ob} as measured in observer's frame and Γ is the Lorentz boost factor of the wind rest frame.

The deflection of the cosmic ray protons of energy more than 56 EeV is negligible in extragalactic magnetic field (Pierre Auger Collaboration et al., 2007). The cosmic ray proton/neutron events detected above 55 EeV energy with directionality within $3°$ of the core of Cen A are travelling from the source to the observer with the same Doppler shift in energy as the gamma rays observed by HESS if they all have a common origin. The energies and times in the observer's frame and wind rest frame are related as $E_\gamma^o = \delta_D E_\gamma$ and $t^o = t/\delta_D$, we have neglected the redshift correction as redshift (z) of Cen A is much less than 1.

The gamma ray flux expected from decaying energetic pions produced in interactions of cosmic ray protons (expressed in number of protons per unit energy per unit time $\frac{dN_P}{dE_P dt}(E_P)$ in wind rest frame) with matter (Anchordoqui et al., 2007a) at the core region of Cen A is

$$\frac{d\phi_\gamma^o(E_\gamma^o)}{dE_\gamma^o dt^o dA} = \frac{2Y_\alpha}{4\pi D^2} \frac{R}{l_{pp}} \int_{E_{\pi^0,min}}^{E_{\pi^0,max}} \frac{dN_p(E_{\pi^0})}{dE_{\pi^0} dt} \frac{dE_{\pi^0}}{(E_{\pi^0}^2 - m_{\pi^0}^2)^{1/2}}. \qquad (2.2)$$

In the above equation the number of cosmic ray protons per unit energy at the core of Cen A $\frac{dN_P(E_{\pi^0})}{dE_{\pi^0} dt} = A_p E_{\pi^0}^{-\alpha}$, A_p is the normalisation constant and α is the spectral index. The distance

to the source is $D = 3.4\,\mathrm{Mpc}$. The minimum energy of pions is $E_{\pi^0,\min} = E_\gamma + m_{\pi^0}^2/(4E_\gamma)$ and the maximum energy is $E_{\pi^0,\max} = 0.2E_n^{\max}$ where $E_n^{\max}$ is the maximum energy of cosmic ray proton/nucleon, m_{π^0} is pion's rest mass and E_γ is the energy of gamma rays. The spectrum weighted moment Y_α has been calculated from Anchordoqui et al. (2007a).

$$Y_\alpha = \int_0^1 x^{\alpha-2} f_{\pi^0}(x)\,dx \tag{2.3}$$

The function $f_{\pi^0}(x) \simeq 8.18x^{1/2}\left(\frac{1-x^{1/2}}{1+1.33x^{1/2}(1-x^{1/2})}\right)^4\left(\frac{1}{1-x^{1/2}} + \frac{1.33(1-2x^{1/2})}{1+1.33x^{1/2}(1-x^{1/2})}\right)$. For $\alpha = 2.73$ we get $Y_\alpha = 0.03$. With eqn.(2.1), eqn.(2.2) and eqn.(2.3) we can find the normalisation constant of the UHECR proton spectrum A_p. UHECR neutrons produced in p-p interactions subsequently decay to protons, electrons and antineutrinos. We have also included the UHECR neutrons decaying to protons in calculating the expected UHECR event rate in Pierre Auger. The integrated exposure of the Pierre Auger detector is $(9000/\pi)\,\mathrm{km}^2$ and relative exposure for declination angle $(\delta = 47^\mathrm{o})$ is $\omega(\delta) \simeq 0.64$. The number of UHECR events expected in Pierre Auger detector can be calculated using the UHECR spectrum. The cosmic ray spectra in observer's frame and wind rest frame are related as,

$$\frac{dN_{p,n}^o(E_{p,n}^o)}{dE_{p,n}^o dt^o dA} = \frac{1}{4\pi D^2}\frac{dN_{p,n}(E_{p,n})}{dE_{p,n}dt} \tag{2.4}$$

Using the cosmic ray spectrum we can calculate the number of expected events in the Pierre Auger detector in the 15/4-years of duration,

$$N_{p,n}^o = \frac{15}{4} \times \frac{9000}{\pi}(\,\mathrm{km}^2)\omega(\delta)\int_{E_l^o}^{E_u^o}\frac{dN_{p,n}^o(E_{p,n}^o)}{dE_{p,n}^o dt^o dA}dE_{p,n}^o \tag{2.5}$$

We have used $E_{p,n}^o = \delta_D E_{p,n}$ as we have calculated the expected number of events in Pierre Auger which travelled in the direction θ_{ob}. Also, we have assumed $\delta_D = 1$ which corresponds to $\Gamma = 7$ and $\theta_{ob} = 30^\mathrm{o}$. In the above equation the lower and upper limits of the energy bin are $E_l^o = 55$ EeV and $E_u^o = 150$ EeV respectively. If we assume that the proton spectral index remains 2.73 upto the highest energy and they are not deflected by the intervening magnetic field then in 15/4 years 450 events are expected for $\tau_{pp} = 10^{-6}$, which corresponds to $n_H = 10^4\,\mathrm{cm}^{-3}$. For lower densities τ_{pp} will be smaller. In this case many more protons may escape from the source before interacting with the matter near the core region. The intervening magnetic field may deflect them away from us and some of them travelling towards us would trigger the detectors at the Pierre Auger observatory. As we are predicting a very large number of UHECR events in this case, the scenario of p-p interactions at the core is not favoured by the observational data from Pierre Auger. In the p-p

interaction scenario the luminosity of UHECRs in the energy bin of 55 EeV and 150 EeV is estimated as $L_{UHECR} \simeq 3 \times 10^{43} (\frac{1cm^{-3}}{n_H})$ erg/sec which is much less than the Eddington luminosity $L_{Edd} = 10^{46}$ erg/sec for Centaurus A.

In the second case we have calculated the interaction between the primary cosmic ray Fe nuclei and the ambient hydrogen density at the core region of Cen A. In this case the rate for Fe-p interactions is $R_{Fe-p} = n_H \sigma_{Fe} c$, where the cross-section for interaction of nuclei of mass number 56 is $\sigma_{Fe} = 34.6 \times 56^{3/4}$ mb. If UHECRs are Fe nuclei then pure hadron interactions may lead to the production of gamma rays. The cross-section of interactions are $A^{3/4}$ times higher in comparision to p-p interaction and hence the rate of A-p interactions is also higher by the same factor. If we consider there are only iron nuclei near the core region of Cen A, then the gamma ray flux expected on earth in pure hadron interactions Fe-p is

$$\frac{d\phi_\gamma^o(E_\gamma^o)}{dE_\gamma^o dt^o dA} = \frac{2Y_\alpha}{4\pi D^2} \frac{R}{l_{Fep}} \int_{E_{\pi^0,min}}^{E_{\pi^0,max}} \frac{dN_{Fe}(E_{\pi^0})}{dE_{\pi^0} dt} \frac{dE_{\pi^0}}{(E_{\pi^0}^2 - m_{\pi^0}^2)^{1/2}}. \tag{2.6}$$

The number of UHECR Fe nuclei per nucleon energy per unit time at the core region of Cen A is, $\frac{dN_{Fe}(E_p)}{dE_p dt} = 56 \frac{dN_{Fe}(E_{Fe})}{dE_{Fe} dt}$, with $E_{Fe} = 56 E_p$. We have expressed the number of Fe nuclei per unit energy of neutral pions per unit time as $\frac{dN_{Fe}(E_{\pi^0})}{dE_{\pi^0} dt}$. The mean free path of Fe-p interactions has been denoted by l_{Fep}, where $l_{Fep} = 0.048 l_{pp}$. Eqn.(2.6) can be expressed as

$$\frac{d\phi_\gamma^o(E_\gamma^o)}{dE_\gamma^o dt^o dA} = \frac{2Y_\alpha}{4\pi D^2} 56^{-\alpha+1} \frac{R}{l_{Fep}} \int_{E_{\pi^0,min}}^{E_{\pi^0,max}} \frac{dN_p(E_{\pi^0})}{dE_{\pi^0} dt} \frac{dE_{\pi^0}}{(E_{\pi^0}^2 - m_{\pi^0}^2)^{1/2}}. \tag{2.7}$$

In pure hadron interactions protons or neutrons will be produced with neutral or charged pions respectively. We calculate the flux of nucleons (protons and neutrons) produced in pure hadron interactions.

$$E_{p,n} \frac{dN_{p,n}(E_{p,n})}{dE_{p,n} dt} dE_{p,n} = 0.8 \frac{R}{l_{Fep}} E_{Fe} \frac{dN_{Fe}(E_{Fe})}{dE_{Fe} dt} dE_{Fe} \tag{2.8}$$

where, $E_{p,n} = 0.8 E_{Fe}/56$, assuming the secondary nucleon takes away 80% of the primary nucleon's energy. In this case the secondary nucleon flux produced in A-p interactions is very low and we expect no event in Pierre Auger detector in $15/4$ years.

Hence, we conclude that neither p-p nor Fe-p interaction scenario is consistent with the observational results from the core of Cen A.

2.2.2 Photo-hadronic Interactions

The dominant p-gamma interaction process is the delta resonance process which produces secondary gamma rays and neutrinos.

$$p + \gamma \to \Delta^+ \to \begin{cases} p + \pi^0 \to p + 2\gamma, & \text{fraction } 2/3 \\ n + \pi^+ \to n + e^+ + \nu_e + \nu_\mu + \bar{\nu}_\mu, & \text{fraction } 1/3 \end{cases}, \qquad (2.9)$$

We have used the p-γ interaction scenario as discussed by Waxman & Bahcall (1997), where the p-γ interaction rate is defined as,

$$R_{p-\gamma} = \frac{c}{\gamma_p^2} \int_{\epsilon_o}^{\infty} \xi\sigma(\epsilon)\epsilon d\epsilon \int_{\epsilon/(2\gamma_p)}^{\infty} \frac{dn(x)}{dx} \frac{dx}{x^2} \qquad (2.10)$$

In our calculations we have taken the peak value of the p-γ interaction cross section. Due to this approximation the above integration (2.10) reduces to,

$$R_{p-\gamma} = \frac{1}{\gamma_p^2} \xi\sigma_{\text{peak}}\epsilon_{\text{peak}}\Delta\epsilon \int_{\epsilon/(2\gamma_p)}^{\infty} \frac{dn(x)}{dx} \frac{dx}{x^2} \qquad (2.11)$$

where $\sigma(\epsilon_{\text{peak}}) = 0.5$ mb is the cross section at the resonance energy $\epsilon_{\text{peak}} = 0.3$ GeV in the proton rest frame. The full width of the resonance at half maxima is $\Delta\epsilon = 0.2$ GeV and $\xi = 0.2$ is the fractional energy going to a pion from a proton.

The threshold energy of pion production in proton rest frame is $\epsilon_o = 0.15$ GeV. $p - \gamma$ process has been discussed in detail by Sahu et al. (2012). They have shown that it can explain the observational results. In this model the luminosity of the cosmic ray protons at 13 TeV has to be 4×10^{45} erg/sec for production of 190 GeV gamma rays. The optical depth for $p - \gamma$ interactions for 13 TeV protons with 170 KeV photons is estimated to be 10^{-6} in Sahu et al. (2012). We get similar optical depth for $p - \gamma$ interactions at 13 TeV proton energy using our calculated rate of $p - \gamma$ interactions given in Figure 2.3.

2.2.3 Photo-Disintegration of Heavy Nuclei

If the primary cosmic rays are only Fe nuclei inside the core of Cen A then they may be photo-disintegrated by the low energy photons in that region. In the photo-disintegration of the primary nuclei, daughter nuclei and secondary nucleons (protons/neutrons) are produced.

$$A + \gamma \to A^\star \to (A - 1) + \gamma' + n \text{ or } p \qquad (2.12)$$

The daughter nuclei de-excite by emitting gamma rays. In the nuclear giant dipole resonance process (GDR) of photo-disintegration statistical emission of single nucleon dominates (Anchordoqui et al., 2007a). The particles escape from Cen A are basically high energy photons (after nuclear de-excitation) and nucleon (these are high energy cosmic rays particles) after the photo-disintegration. If the observed high energy gamma ray emission from Cen A is due to photo-disintegration process then we can calculate the expected nucleon (proton/neutron) flux from Cen A using the observed gamma ray flux. The ralation between these fluxes is discussed by Anchordoqui et al. (2007a). The rate of photo-disintegration process is calculated with eqn.(6) of Anchordoqui et al. (2007a)

$$R_{\text{phot−dis}} = \frac{c\pi\sigma_0\epsilon_0'\Delta}{4\gamma_p^2} \int_{\epsilon_0'/2\gamma_p}^{\infty} \frac{dn(x)}{dx} \frac{dx}{x^2}. \tag{2.13}$$

The value of the cross-section is $\sigma_0 = 1.45A$ mb, the central value of GDR $\epsilon_0' = 42.65A^{-0.21}$ MeV for $A > 4$ and width of the GDR is $\Delta = 8$ MeV. The Lorentz factor of each nucleon is $\gamma_p = E_{\text{Fe}}/(56m_p)$. We have used the photon spectral energy distribution observed on earth $\epsilon_\gamma^{o\,2} \frac{dN_\gamma^o(\epsilon_\gamma^o)}{d\epsilon_\gamma^o dt^o dA}$ (MeVcm^{-2}sec^{-1}) from the fit given in Abdo et al. (2010b), which is also shown with red solid curve in the Figure 2.4. The photon density per unit energy in the core region $\frac{dn(x)}{dx}$ is

$$4\pi R^2 c \frac{dn(x)}{dx} = 4\pi D^2 \delta_D^{-a} \frac{dN_\gamma^o(\epsilon_\gamma^o)}{d\epsilon_\gamma^o dt^o dA} \tag{2.14}$$

where, $a = b + \alpha + 1$ and $b = 2, 3$ for continuous and discrete jet respectively (Ghisellini et al., 1993). α is the spectral index of the SED taken from the SSC green fitted curve, $\epsilon_\gamma^{o\,2} \frac{dN_\gamma^o(\epsilon_\gamma^o)}{d\epsilon_\gamma^o dt^o dA} \propto \epsilon_\gamma^{o-\alpha}$. α takes different values in different energy regimes as discussed in the Appendix at the last section of this chapter.

We have denoted the energy of the low energy photons in the observer's frame by ϵ_γ^o and $\epsilon_\gamma^o = \delta_D x$. From the above equation it is noted that the photon density at the source depends on δ_D. In Abdo et al. (2010b) they have taken various values of Γ and δ_D, the SED fit of SSC model to Fermi data is given for $\Gamma = 7$ and $\delta_D = 1$ which corresponds to $\theta_{\text{ob}} = 30^o$. For smaller values of δ_D the photon density at the source would be much higher.

In photo-disintegration process protons and neutrons can be produced with equal probabilities. TeV gamma rays may be produced in this process from PeV UHECRs. Similar to eqn.(28) given in Anchordoqui et al. (2007a) we can relate the neutron, proton and gamma ray fluxes from photo-disintegration of nuclei of mass A.

$$\frac{dN_{n,p}^o(E_{n,p}^o)}{dE_{n,p}^o dt^o dA} = \frac{\bar{E}_{\gamma A}'}{m_n \bar{n}_A} \frac{d\phi_\gamma^o(E_\gamma^o)}{dE_\gamma^o dt^o dA} \tag{2.15}$$

where in the wind rest frame $E_\gamma = E_n \bar{E}'_{\gamma A}/m_n$.

We are interested to calculate the number of proton or neutron events in Pierre Auger above 55 EeV which maintain their directionality while travelling from the core of Cen A to the observer. They have the same Doppler shift in energy as the gamma rays observed by Aharonian et al. (2009) as they are produced in the same wind frame and travelling in the same direction from the source to the observer. If the gamma ray emission is monochromatic in the rest frame of the nucleus then its average has been denoted by $\bar{E}'_{\gamma A}$. $\bar{n}_A$ is the average multiplicity of gamma rays and m_n is rest mass of each nucleon. For Fe nuclei $\bar{E}'_{\gamma 56} = 2 - 4$ MeV and gamma ray multiplicity is $\bar{n}_{56} = 1 - 3$.

In the photo-disintegration the γ-ray flux produced from parent Fe-nuclei are connected by equation (2.16). If the rate of photo-disintegration is constant then parent nuclei spectrum will follow the spectrum of γ-ray flux. This approximation helps us to use GeV-TeV HESS observations to restrict spectral shape of the parent nuclei. Assuming the same spectral index of the neutron and proton spectrum from TeV to the highest energy we calculate the expected number of events in Pierre Auger detector in 15/4 years in the energy bin of 55 EeV to 150 EeV. We get two events for spectral index 2.45 with $\bar{E}'_{\gamma,56} = 4$ MeV and $\bar{n}_{56} = 2$ which agrees with the detection by Pierre Auger experiment from the direction of the core of Cen A. The power law spectrum which fits HESS data has spectral index $2.73 \pm 0.45_{\text{stat}} \pm 0.2_{\text{sys}}$ (Aharonian et al., 2009). The spectral index 2.45 used in our calculations is within the range of error in the spectral index obtained by Aharonian et al. (2009).

In this scenario variability of the source increasing the emission may yield more UHECR events from the direction of Cen A. Due to the low gamma ray flux from Cen A it was not possible by HESS experiment to detect variability in time scales shorter than days and with increments below a factor of 15-20 (Aharonian et al., 2009). If the size of the interaction region is $R = 3 \times 10^{15}$ cm (Abdo et al., 2010b), and the rate of the photo-disintegration process is $R_{\text{phot,dis}}$ then the high energy gamma ray emission can be related to the number of UHECR Fe nuclei per nucleon energy per unit time at the core of Cen A $\frac{dn_{\text{Fe}}}{dE_N dt}(E_N)$ as follows

$$\frac{d\phi^o_\gamma(E^o_\gamma)}{dE^o_\gamma dt^o dA} = \frac{1}{4\pi D^2} \frac{R}{\beta c} \frac{\bar{n}_{56} m_N}{2\bar{E}'_{\gamma,56}} \int_{\frac{m_N E_\gamma}{2\bar{E}'_{\gamma,56}}} \frac{dn_{\text{Fe}}(E_N)}{dE_N dt} R_{\text{phot,dis}} \frac{dE_N}{E_N} \qquad (2.16)$$

where $\beta = v/c \sim 1$ for UHECR nuclei.

We calculate the normalization constant of the UHECR Fe nuclei flux from eqn.(2.16). We have $\frac{dn_{\text{Fe}}(E_N)}{dE_N} = N_{\text{Fe}} E_N^{-\alpha}$. We use eqn.(2.16) to calculate $N_{\text{Fe}} = 2.65 \times 10^{-7}$. The normalization constant of the UHECR Fe nuclei can be calculated from the following relation, $A_{\text{Fe}} E_{\text{Fe}}^{-\alpha} = \frac{1}{56} N_{\text{Fe}} E_N^{-\alpha}$ (follow eqn (22) of Anchordoqui et al. (2007a)), and it comes out to

be $A_{Fe} = 9.08 \times 10^{-5} TeV^{-1} sec^{-1}$.

The HESS spectrum is measured above $E_\gamma^o = 250$ GeV. Gamma rays of energy 250 GeV are produced by Fe nuclei of per nucleon energy $E_N = E_\gamma m_N/(2\bar{E}'_{\gamma,56}) = 29$ TeV. In the Figure 2.3 we have plotted the rate of photo-disintegration of Fe nuclei with the energy per nucleon in the wind rest frame along x-axis. Between 1 TeV to 100 TeV nucleon energy in the wind rest frame the rate is almost constant and it is $2 \times 10^{-8} sec^{-1}$, for $\Gamma = 7$ and $\delta_D = 1$. At higher energy the rate increases but the cosmic ray nuclei flux decreases more rapidly as it follows a power law with spectral index -2.45. The luminosity of cosmic rays with known spectrum is defines as $L_{CR} = 4\pi D^2 \int_{ll}^{ul} A_{Fe} E_{Fe}^{-\alpha} E_{Fe} dE_{Fe} \frac{TeV}{sec}$. The luminosity of the UHECR Fe nuclei flux in the energy bin of 55×56 EeV and 150×56 EeV is $\sim 10^{42}$ erg/sec which is much below the Eddington's luminosity.

The 170 KeV photons at the second peak of SED in the Figure 2.4, photo-disintegrate Fe nuclei of energy $E_{Fe} = 2.8$ TeV. This result is obtained using the threshold energy condition $\epsilon'_0/2\gamma_p = 170$ keV, where γ_p is the Lorentz factor of each nucleon in wind rest frame and we have used $\delta_D = 1$ for the Doppler shift of the low energy photons. The gamma ray energy produced from photo-disintegration of 2.8 TeV Fe nuclei is calculated using the expression $E_\gamma = 2\bar{E}'_{\gamma,56} E_N/m_N$, where $\bar{E}'_{\gamma,56} = 4$ MeV and energy of each nucleon $E_N = 50$ GeV. We find the peak energy in the gamma ray spectrum from photo-disintegration of Fe nuclei by 170 keV photons is at 400 MeV. The spectrum of cosmic ray Fe nuclei has a break at 2.8 TeV due to the second peak in the SED at 170 KeV.

Above 2.8 TeV the spectral index -2.45 gives a good fit to the observational results. The total luminosity of the Fe cosmic rays in the energy range of 2.8 TeV-150 EeV has to be of the order of 10^{47} erg/sec, which is higher than the Eddington luminosity, (10^{46} erg/sec), of Cen A. We note that the luminosity required to accelerate cosmic rays above 10^{20} eV is higher than 10^{46} erg/sec (Dermer et al., 2009; Abdo et al., 2010b). In the scenario of Cen A, Dermer et al. (2009) has found that during high flaring emission the apparent isotropic luminosity of Cen A can easily exceed the Eddington limit. In the SED of Cen A, there are error bars on the observed photon flux and also there are no observational data points between the two peaks as shown in the Figure 2.4. The lower energy photons photo-disintegrate the higher energy Fe nuclei. The rate of photo-disintegration is directly proportional to the density of low energy target photons at the source. Higher density of low energy photons would lead to higher rate of photo-disintegration process. If the rate of photo-disintegration is higher then a lower luminosity of cosmic rays would be required to explain the observational results. The x-ray photon density is higher along the x-ray jet of Cen A, this would lead to more efficient production of high energy gamma rays and require lower UHECR luminosity.
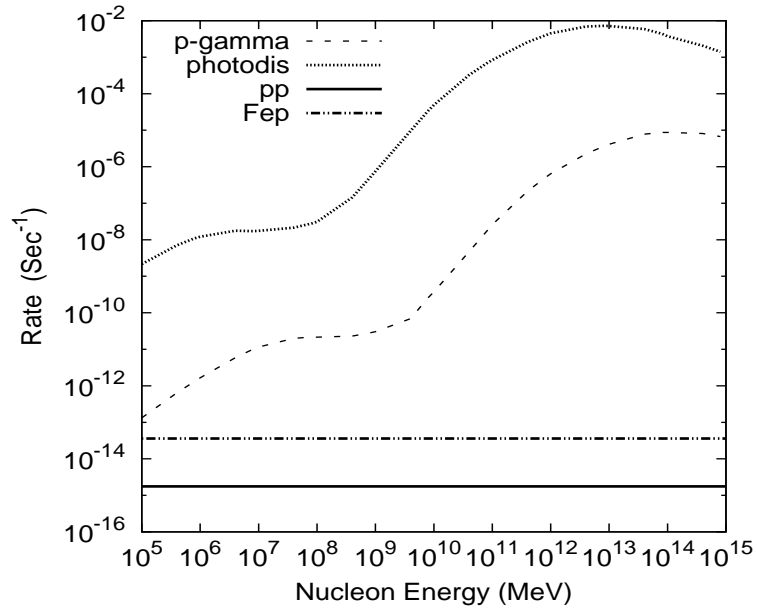
Figure 2.3: $p - p$ (solid line), $Fe - p$ (dash-dotted line) for $n_H = 1.7 cm^{-3}$ Kachelrieß et al. (2009a), $p - \gamma$ (dashed line), photo-disintegration rates of Fe nuclei (dotted line) calculated with the fit of SED Abdo et al. (2010b). X-axis represents energy per nucleon in the wind rest frame.

2.3 Discussion and Conclusion

Our calculated rates of the various processes of high energy gamma ray production are shown in Figure 2.3. We have used hydrogen density at the core of Cen A $n_H = 1.7$ cm^{-3} taken from Kachelrieß et al. (2009a) and the photon spectral energy distribution (SED) as given in Abdo et al. (2010b). The rate of photo-disintegration of Fe nuclei is the highest among all processes of high energy gamma ray production in Cen A core. The increase in the rates of photo-disintegration and pγ interactions near 10^{19} eV shown in Figure 2.3, is due to the first peak or the synchrotron peak in the photon SED as shown in Figure 2.2. The high energy gamma ray flux from photo-disintegration of Fe nuclei is shown with a black dashed line in Figure 2.4.

The γ ray spectrum 400 MeV-10 TeV (black dashed line), in Figure 2.4 is due to the
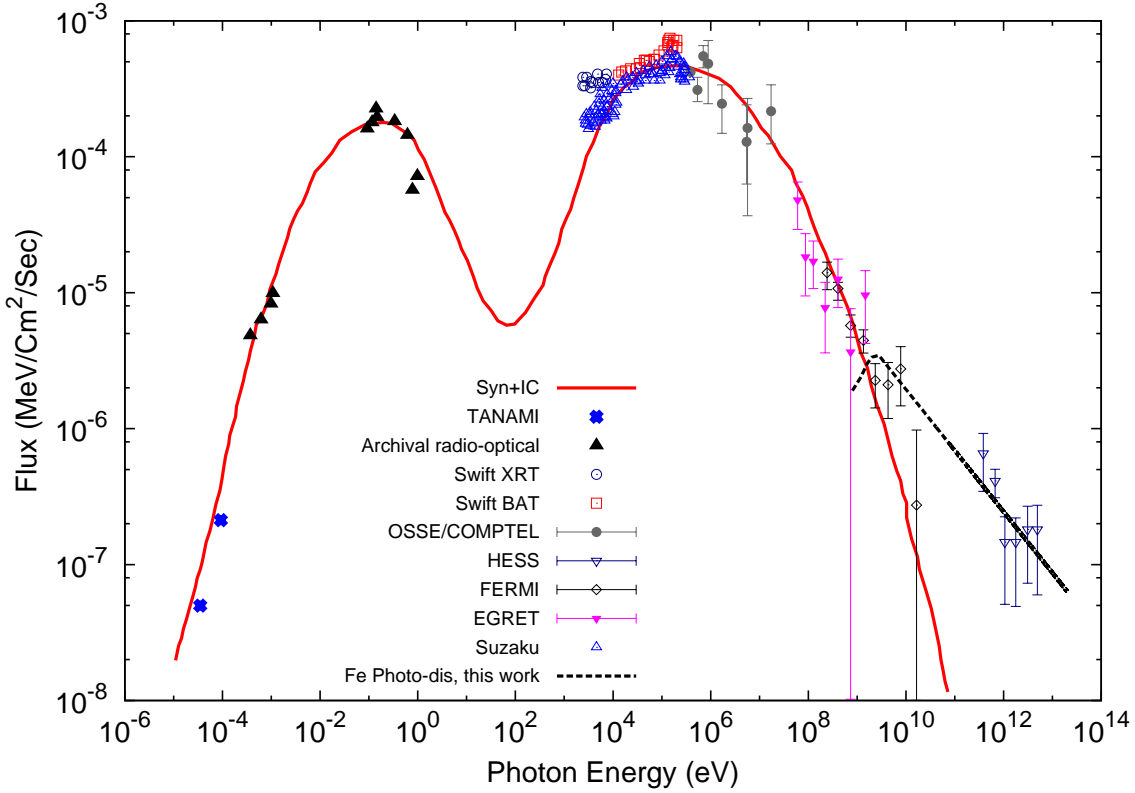
Figure 2.4: Spectral energy distribution (SED) $\epsilon_\gamma^{o\,2}\frac{dN_\gamma^o(\epsilon_\gamma^o)}{d\epsilon_\gamma^o}(\mathrm{MeVcm^{-2}sec^{-1}})$ from Cen A core, the solid red curve is the fit with synchrotron and SSC from Abdo et al. (2010b), high energy gamma ray spectrum from photo-disintegration of Fe nuclei shown with black dashed line.

photo-disintegration of cosmic rays is a power law. This spectrum is consistent with two UHECR events from Cen A.

$$\frac{d\phi_\gamma^o(E_\gamma^o)}{dE_\gamma^o dt^o dA} = 2.45 \times 10^{-13}\left(\frac{E_\gamma^o}{1\mathrm{TeV}}\right)^{-2.45}\mathrm{cm^{-2}sec^{-1}TeV^{-1}} \qquad (2.17)$$

Photo-disintegration of Fe nuclei followed by de-excitation of daughter nuclei is found to be consistent with the UHECR proton/neutron event rate observed by Pierre Auger between 55 EeV, 150 EeV and the high energy gamma ray flux measured by HESS.

In summary, we have found that the scenario of p-p interactions gives excess UHECR events from the core region of Cen A in the energy bin of 55 EeV and 150 EeV. If we consider there are only Fe nuclei as primary cosmic rays then in the case of pure hadronic interactions Fe-p the estimated UHECR event rate is very low. Sahu et al. (2012) have considered the production of 190 GeV gamma rays in interaction of 13 TeV protons with the 170 KeV photons in the second peak of the SED. In their model the luminosity of the 13 TeV protons has to be 4×10^{45} erg/sec.

In our case 29 TeV per nucleon energy of Fe nuclei is required to produce gamma rays of energy 250 GeV in photo-disintegration of Fe nuclei. In our model of photo-disintegration of Fe nuclei the total cosmic ray power has to be of the order of 10^{47} erg/sec. The required luminosity of the Fe cosmic ray nuclei is higher than the Eddington's luminosity of Cen A. However, we note that the requirement of luminosity depends on the photon density inside the source and size of the emitting region. The cosmic ray luminoity required in the photo-disintegration model would be lower if the density of the low energy photons is higher at the source or the size of the emitting region is smaller. Moreover, it has been discussed earlier that the isotropic luminosity in Cen A can easily exceed its Eddington's luminosity which is 10^{46} erg/sec during flaring states (Dermer et al., 2009). Dermer et al. (2009) also discussed that if the cosmic rays in Cen A are accelerated to approximately 100EeV, then the apparent isotropic cosmic ray luminosity in Cen A need to be more than the Eddington luminosity of the source.

After the publication of our work, the observations of Cen A are made by Fermi-LAT collaboration (Sahakyan et al., 2013). In their 4 years (2008-2012) of observations they found a new hard component in the gamma ray spectrum above 4 GeV, which can be explained by p-gamma interactions at the core of Cen A (Sahakyan et al., 2013). Similarly, Fraija (2014) explained the gamma ray emission of Cen A, above 4 GeV by photo-hadronic models. In their work they found that the emission upto 4 GeV can be explained by the SSC model and beyond 4 GeV the emission is due to the pion decay channel. In this pion decay channel they have considered the charged muon synchrotron cooling for the production of GeV emission.

Later, Kundu & Gupta (2014) explaind this new hard component and HESS observations using the photo-disintegration of cosmic ray nuclei. They found that the total luminosity in cosmic ray Fe-nuclei is 1.5 $\times 10^{43}$ erg/sec to explain the gamma ray flux above 1 GeV. In their calculations the total luminosity in cosmic ray nuclei is much lower than what we found in our work (Joshi & Gupta, 2013) to explain the HESS-observations (Aharonian et al., 2009). The main difference in these two models (Kundu & Gupta, 2014; Joshi & Gupta, 2013) is due to two different set of SSC parameter values $(\Gamma, \delta_{\mathrm{D}}, \theta, \mathrm{B}, \mathrm{R})$ used in their calculations.

2.4 Appendix

The spectral energy distribution from Abdo et al. Abdo et al. (2010b) shown by red solid curve in Figure 2.4, has been fitted in fourteen energy intervals with average error less than

10%. The parametrization used in our calculations are given below.

$$f(x) = -6.15 \times 10^{-9} + 2.21 \times 10^{3}x + 2.01 \times 10^{13}x^2; 1.00 \times 10^{-5} \leq \frac{x}{eV} \leq 7.7 \times 10^{-5}$$

$$f(x) = 1 \times 10^{-6} - 2.06 \times 10^{4}x + 1.502 \times 10^{14}x^2; 7.7 \times 10^{-5} \leq \frac{x}{eV} \leq 1.17 \times 10^{-4}$$

$$f(x) = -1.49 \times 10^{-7} + 5.23 \times 10^{3}x + 1.49 \times 10^{13}x^2; 1.17 \times 10^{-4} \leq \frac{x}{eV} \leq 4.32 \times 10^{-4}$$

$$f(x) = -1.55 \times 10^{-6} + 1.34 \times 10^{4}x - 4.63 \times 10^{11}x^2; 4.32 \times 10^{-4} \leq \frac{x}{eV} \leq 1.36 \times 10^{-2}$$

$$f(x) = 5.17 \times 10^{-5} + 3.77 \times 10^{3}x - 3.99 \times 10^{10}x^2 + 1.39 \times 10^{17}x^3;$$
$$1.36 \times 10^{-2} \leq \frac{x}{eV} \leq 1.34 \times 10^{-1}$$

$$f(x) = 1.96 \times 10^{-4} - 1.07 \times 10^{2}x + 2.63 \times 10^{7}x^2 - 2.33 \times 10^{12}x^3; 1.34 \times 10^{-1} \leq \frac{x}{eV} \leq 4.54$$

$$f(x) = 5.30 \times 10^{-5} - 5.77x + 2.65 \times 10^{5}x^2 - 4.14 \times 10^{9}x^3; 4.54 \leq \frac{x}{eV} \leq 28.3$$

$$f(x) = 3.57 \times 10^{-6} + 2.21 \times 10^{-2}x + 2.18x^2; 2.83 \times 10^{-2} \leq \frac{x}{keV} \leq 3.48$$

$$f(x) = 1.99 \times 10^{-5} + 2.62 \times 10^{-2}x - 5.74 \times 10^{-1}x^2; 3.48 \leq \frac{x}{keV} \leq 17.8$$

$$f(x) = 2.14 \times 10^{-4} + 6.44 \times 10^{-3}x - 5.75 \times 10^{-2}x^2 + 1.64 \times 10^{-1}x^3; 17.8 \leq \frac{x}{keV} \leq 185$$

$$f(x) = 4.77 \times 10^{-4} - 6.54 \times 10^{-5}x + 4.21 \times 10^{-6}x^2; 0.185 \leq \frac{x}{MeV} \leq 7.16$$

$$f(x) = 3.33 \times 10^{-4} - 1.95 \times 10^{-5}x + 5.55 \times 10^{-7}x^2 - 5.31 \times 10^{-9}x^3; 7.16 \leq \frac{x}{MeV} \leq 49$$

$$f(x) = 1.26 \times 10^{-4} - 1.16 \times 10^{-6}x + 4.35 \times 10^{-9}x^2 - 5.49 \times 10^{-12}x^3; 49 \leq \frac{x}{MeV} \leq 352$$

$$f(x) = 2.54 \times 10^{-5} - 3.3 \times 10^{-8}x + 1.29 \times 10^{-11}x^2; 0.352 \leq \frac{x}{GeV} \leq 1.44$$

$$f(x) = 2.73 \times 10^{-6} - 2.39 \times 10^{-10}x + 5.25 \times 10^{-15}x^2 - 3.26 \times 10^{-20}x^3; 1.44 \leq \frac{x}{GeV} \leq 90.94$$

Chapter 3

How many of the observed neutrino events can be described by cosmic ray interactions in the Milky Way?

3.1   Introduction

IceCube is a neutrino observatory at the south pole to detect neutrinos in the energy range of TeV to PeV (Halzen, 2006b; Halzen & Klein, 2010; IceCube Collaboration Hill, 2011; Kappes & IceCube Collaboration, 2013). In 2013, IceCube Collaboration (2013) reported the first results on the detection of neutrino events. It was the first detection of neutrinos in the energy range of TeV to PeV from any terrestrial and extraterrestrial sources. The origin of these neutrinos analyzed by Aartsen et al. (2013) and they concluded that these neutrino events are unlikely to be of atmospheric origin. IceCube Collaboration (2013) also indicated an evidence of extraterrestrial neutrino detection at the IceCube detector.

The astrophysical sources inject cosmic rays in the astrophysical medium. This medium is filled with radiation and gas density. The propagation of cosmic rays in our Galactic medium has been studied in the past several decades using many models and with increasing complexities to explain the observational results successfully (Gupta & Webber, 1989a; Berezinskii et al., 1990b; Letaw et al., 1993a; Dorman, 2006; Lee et al., 2007; Strong et al., 2007; Farahat et al., 2008; Blasi & Amato, 2012a,b). The transport equation written by Ginzburg & Syrovatskii (1964) contains various terms to include the possible gains and losses in the flux of cosmic rays.

In the Galactic and extragalactic magnetic field cosmic rays undergo random motions and interact with matter and background radiations. This interaction leads to many interesting physical phenomena like spallation of heavier nuclei to lighter nuclei, (Silberberg & Tsao, 1990; Ramaty & Lingenfelter, 1999a,b; Combet et al., 2005), secondary gamma rays and neutrinos will be produced by their interactions with background radiation and matter (Evoli et al., 2007; Gupta, 2012; Stecker, 2013) and their diffusion in momentum space lead to reacceleration (Heinbach & Simon, 1995; Simon & Heinbach, 1996). The cosmic ray propagation models with energy dependent diffusion coefficient D(E) and re-acceleration were subsequently introduced to explain the observational results (Gupta & Webber, 1989b; Berezinskii et al., 1990c; Gaisser, 1991b; Letaw et al., 1993b).

The observations of cosmic ray induced air shower have an enormous impact on our understanding of the high energy phenomena in the universe (Chou et al., 2005; Risse et al., 2005; Abbasi et al., 2010; Apel et al., 2013; Knurenko & Sabourov, 2013; The Pierre Auger Collaboration et al., 2013). The compilation of cosmic ray data from various air-shower experiments show a knee region near 3 PeV and ankle region near 10^4 PeV in the all particle cosmic ray spectrum (Gaisser et al., 2013).

Anchordoqui et al. (2013) used IceCube neutrino observations (IceCube Collaboration, 2013) to understand the knee and ankle features of the cosmic ray spectrum assuming that

these neutrino events could be of Galactic origin. Cosmic ray interactions in the inner Galaxy have been considered as the possible origin of some of the IceCube detected events and Fermi/LAT observed gamma rays (Neronov et al., 2013). The five shower-like neutrino events correlated with the Galactic centre region by Razzaque (2013) could have originated from cosmic ray acceleration in SNRs (supernova remnants).

The correlation of the gamma ray and the neutrino fluxes and the Galactic origin of the IceCube events have been studied by Ahlers & Murase (2013). They pointed out that within wide angular uncertainties off the Galactic plane, it is plausible that about 10 events are of Galactic origin. Recently the sub-PeV and PeV neutrinos have been correlated with the cosmic rays above the second knee in the very high energy cosmic ray spectrum. In this connection Murase et al. (2013) considered the hadronic interaction in cosmic ray sources and Liu et al. (2013) considered hypernova remnants as possible candidate sources.

The neutrino events detected by the IceCube detector could also have originated from magnetic energy dominated gamma-ray bursts (Winter, 2013), from low power gamma ray bursts (Murase & Ioka, 2013), and from cores of active galactic nuclei (Stecker, 2013).
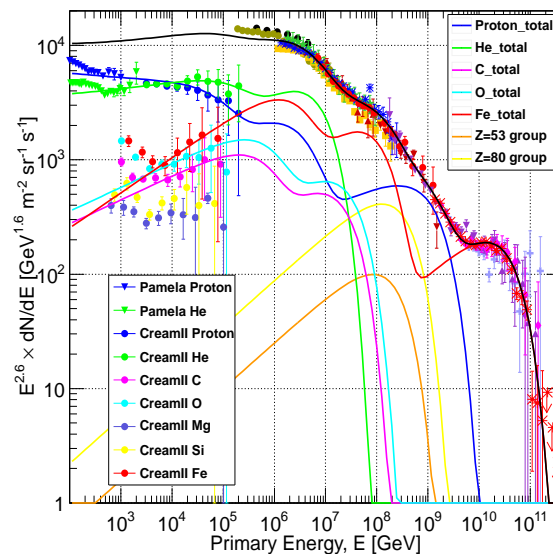
Figure 3.1: Cosmic ray spectrum observed at earth. All compositions are shown. (figure taken from Gaisser et al. (2013))

In the present work we consider the observed steady state flux of cosmic rays (Gaisser et al., 2013) for the calculation of the diffuse neutrino flux produced in cosmic ray interactions. Thus our results neither depend on the unknown injection spectrum, nor on the escape time of very high energy cosmic rays. In the neutrino flux calculation we have used recent cosmic ray observational data, also shown in Figure 3.1.

3.2 Proton Interactions and Target Geometry

Very High Energy Cosmic Rays (VHECRs) interaction with Galactic matter produces charged and neutral pions. The charged pions decay to muons and muon type neutrinos ($\pi^\pm \rightarrow \mu^\pm + \nu_\mu(\bar{\nu}_\mu)$). The muons subsequently decay to electrons, electron type neutrinos and muon type neutrinos ($\mu^\pm \rightarrow e^\pm + \nu_e(\bar{\nu}_e) + \bar{\nu}_\mu(\nu_\mu)$). The ratio of the neutrino fluxes of different flavors produced in this way is $\nu_e + \bar{\nu}_e : \nu_\mu + \bar{\nu}_\mu : \nu_\tau + \bar{\nu}_\tau = 1 : 2 : 0$.

The fluxes of neutrinos of each flavor are expected to be roughly equal on Earth after flavor mixing $\nu_e + \bar{\nu}_e : \nu_\mu + \bar{\nu}_\mu : \nu_\tau + \bar{\nu}_\tau \simeq 1 : 1 : 1$ (Gaisser, 1991a). For the numerical calculations, however, we compute the flavor mixing precisely using the current best-fit values Gonzalez-Garcia et al. (2012) (first octant solution).

For the description of the p-p interactions, we follow the formalism discussed by Kelner et al. (2006a). The p-p interaction time is given by $t_{pp}(E_p) = 1/(n_H\,\sigma_{pp}(E_p)\,c)$, where n_H is the mean hydrogen number density of Galactic matter and the cross section of the interaction is $\sigma_{pp}(E_p) = 34.3 + 1.88\ln(E_p/1\text{TeV}) + 0.25(\ln(E_p/1\text{TeV}))^2$ mb. The average (over different experiments) cosmic ray spectrum above 100 TeV (Gaisser et al., 2013) has been approximated with power laws with several breaks for our calculation; the spectrum has been linearly interpolated among $(5, 0)$, $(6.5, 0)$, $(8.5, -0.85)$, $(9.7, -1.7)$, $(10.5, -1.7)$, $(11, -2.3)$ on a double log scale in $\log_{10}E[\text{GeV}]$, $\log_{10}E^{2.6}J[\text{GeV}^{1.6}\text{cm}^{-2}\text{s}^{-1}\text{sr}^{-1}]$.

The neutrino injection spectra $Q_\nu[\text{cm}^{-3}\text{s}^{-1}\text{GeV}^{-1}]$ are given by

$$Q_\nu(E_\nu) = cn_H \int_0^1 \sigma_{pp}(\frac{E_\nu}{x})N_p(\frac{E_\nu}{x})f(x, \frac{E_\nu}{x})\frac{dx}{x} \qquad (3.1)$$

for the appropriate flavor-dependent parametrizations of the distribution functions given in Eqs. (62) and (66) of Kelner et al. (2006a), which include the proper pion multiplicities. The integration over $x \equiv E_\nu/E_p$ is carried out to include the contributions from all protons having energy equal to or higher than E_ν. However, on the average 5% of a proton's energy goes to a secondary neutrino, which means that the maximum contribution to the neutrino flux at energy E_ν comes from the protons of energy twenty times E_ν. Note that the neutrino injection is computed from the proper density $n_H[\text{cm}^{-3}]$ and the steady state density $N_p[\text{cm}^{-3}\,\text{GeV}^{-1}]$ obtained from solving the cosmic ray transport equation. If we assume that the cosmic ray density is the same everywhere in the galaxy (or hydrogen halo), we can directly use the observed cosmic ray flux to compute $N_p = 4\pi J_p/c$, where the fluxes are given in units $[\text{cm}^{-2}\text{s}^{-1}\text{sr}^{-1}\text{GeV}^{-1}]$. That is, the neutrino production neither relies on the

cosmic ray injection, nor on the cosmic ray escape time. The observed neutrino flux can be computed by

$$J_\nu = \frac{1}{4\pi} \int dV \frac{Q_\nu}{4\pi r^2} \tag{3.2}$$

where r is the distance between Earth and production region. For a (hypothetical) spherical hydrogen halo with radius R centred at Earth and a homogeneous target density, we have $J_\nu = Q_\nu R/(4\pi)$. For an arbitrary halo shape, we can re-write Eq. (3.1) as

$$J_\nu(E_\nu) = R_{\mathrm{eff}} n_{\mathrm{H}} \int_0^1 \sigma_{\mathrm{pp}}(\frac{E_\nu}{x}) J_{\mathrm{p}}(\frac{E_\nu}{x}) f(x, \frac{E_\nu}{x}) \frac{dx}{x}, \tag{3.3}$$

Here the effective radius $R_{\mathrm{eff}} \equiv \int dV/(4\pi r^2)$ for a homogeneous halo, integrated over the appropriate production region; for a halo centered at Earth, one recovers $R = R_{\mathrm{eff}}$. If the hydrogen density or cosmic ray density depends on the location, this effect can be also expressed in terms of the effective radius R_{eff} in a more complicated scheme; for a detailed study of the spatial distribution of hydrogen and cosmic rays, see Evoli et al. (2007) .

In some models, (Evoli et al., 2007) the average atomic hydrogen density in the Galaxy modelled with radii 10's of kpc and height 100's of pc calculated to be ~ 0.5 cm^{-3}. The density of ionized, neutral and molecular hydrogen as a function of the height from the Galactic plane relative to the Earth's location and the radial distance from the Galactic centre have been calculated by Feldmann et al. (2013) using the gamma ray data observed by Fermi gamma ray space telescope. Relative to the Earth's location the density of atomic and molecular hydrogen gas drops from 1cm^{-3} to 0.1cm^{-3} within a distance of 1-1.5 kpc above the Galactic plane. The density of ionized hydrogen gas steeply falls from 0.3cm^{-3} to 0.001cm^{-3} within the same distance. The hydrogen densities of 1cm^{-3} are unlikely for the $10's$ kpc of spherical halo as discussed by Dickey & Lockman (1990), Kalberla & Kerp (2009), and Blitz & Robishaw (2000).

We completely independently derive the average hydrogen density from the neutrino observations, assuming that the observed events come from interactions between cosmic rays and hydrogen within the halo. We consider different shapes of the hydrogen halo. The effective radii from Eq. (3.3) for the different geometries and the Earth 8.33 kpc off the Galactic centre are listed in Table 3.1, where we denote the radius of the spherical region around the Galactic centre by R_{GC}.

In the following, we use $R_{\mathrm{eff}} = 10$kpc or $R_{\mathrm{eff}} = 1$kpc for different extreme models, but our results can be easily re-scaled with Table 3.1. While for the spherical halo around the Galactic center and extending beyond Earth $R_{\mathrm{eff}} \sim 7 - 13$kpc seems plausible, smaller val-

Shape	$R_{GC,kpc}$	h_{kpc}	$R_{eff,kpc}$
Spherical	10.		7.2
Spherical	15.		13.3
Cylindrical	10.	0.5	1.7
Cylindrical	10.	0.25	1.0
Cylindrical	15.	0.5	2.1
Cylindrical	15.	0.1	0.58

Table 3.1: The effective halo radius R_{eff}, calculated for different halo shapes and parameters. Here R_{GC} refers to the radius around the Galactic centre, and $\pm h_{kpc}$ to the extension of the cylinder beyond the Galactic plane for the cylindrical shape.

ues are obtained for the cylindrical halos: For realistic scale heights $h \lesssim 250\,\mathrm{pc}$, $R_{eff} \simeq 1\,\mathrm{kpc}$.

3.3 Effect of Cosmic Ray Composition

The observed cosmic ray flux contains protons, helium, carbon, oxygen, iron and heavier nuclei. In Gaisser et al. (2013), the helium nuclei flux exceeds the proton flux above 10 TeV and at 1 PeV helium and iron nuclei fluxes are comparable (shown with curves of different colors in Figure 4 of Gaisser et al. (2013)). At 100 PeV the cosmic ray flux contains mostly iron nuclei and at 1 EeV protons dominate over iron nuclei. Each nucleon in the nucleus interact with a Galactic hydrogen atom and pions are produced which subsequently decay to neutrinos and gamma rays. In the case of composite nucleus, the (observed) cosmic ray flux of nuclei with mass number A is $J_A(E_A) = dN_A(E_A)/dE_A$.

We tested two different approaches to compute the neutrino flux for heavier compositions. One is essentially the superposition model: we assume that the nucleus with mass number A and energy E_A behaves as A nucleons with energy E_A/A. As a consequence, we can use Eq. (3.3) to compute the neutrino flux by replacing $J_p(E_p) = dN_p(E_p)/dE_p \rightarrow A^2 J_A(AE_p) = A^2 dN_A(AE_p)/dE_A$. For a simple power law with spectral index α, one has $J_p(E_p) = A^{2-\alpha}E_p^{-\alpha}$, and as a consequence, the result is identical to protons for $\alpha = 2$. As another approach, we rather follow Anchordoqui et al. (2007a) and take into account that the cross section σ_{A-p} is higher by a factor of $A^{3/4}$ than σ_{p-p}. In this case, we can re-write Eq. (3.3) as

$$J_\nu(E_\nu) = R_{eff} n_H \int_0^1 \sigma_{Ap}\left(\frac{E_\nu}{x_A}\right) J_A\left(\frac{E_\nu}{x_A}\right)$$
$$\times A f\left(A x_A, \frac{E_\nu}{A x_A}\right) \frac{dx_A}{x_A}, \tag{3.4}$$

where $x_A = x/A$ is the fraction of the nucleus energy going into the neutrino. For a simple power law, this yields a neutrino flux $\propto A^{1.75-\alpha}$, which is about a factor of $A^{0.25}$ smaller than the one of the superposition model, with some compensation by the slightly higher cross section. The reason is, roughly speaking, that the cross section of the nucleus is somewhat smaller than that of A nucleons, because of the surface area/volume ratio $\sim A^{2/3}$. Note that these differences are very small (at the level of 20%), and we use the (more realistic) model in Eq. (3.4) in the following, which allows us to implement variable compositions easily.
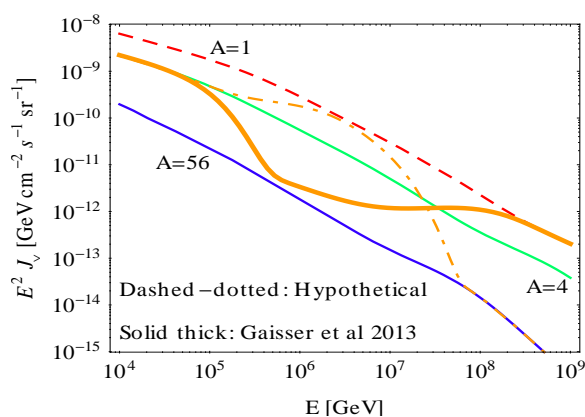
Figure 3.2: Predicted neutrino flux for different cosmic ray compositions, $n_H = 1 cm^{-3}$, and $R_{eff} = 1 kpc$, corresponding to emission from a cylindrical halo with radius 10 kpc and half height 250 pc ($\nu_\mu + \bar{\nu}_\mu$ flux including flavor mixing) The solid and dotted-dashed yellow curve follows the total neutrino spectrum due to the variation of cosmic ray abundance with energy

.

The neutrino flux roughly scales as $A^{1.75-\alpha}$, it is clear that the pure proton composition gives the highest flux and the pure iron composition the lowest (As cosmic ray index α, takes vales greater than 1.75). We have used the cosmic ray composition model by Gaisser et al. (2013) to calculate the neutrino spectrum. The neutrino spectrum from this model is shown in Figure 3.2 by solid thick lines. This neutrino spectrum has a dip at PeV energies which disfavours the IceCube neutrino observations, where at PeV energies an abundance of neutrinos has been seen (IceCube Collaboration, 2013). We have tried to model this abundance by tuning the composition of comic ray spectrum (Hypothetical model). For the "hypothetical model", a helium composition between 5×10^4 GeV and 4×10^6 GeV has been chosen, then proton between 10^7 and 10^8 GeV, and then iron at 10^9 GeV (and higher), linearly interpolated among these values. This hypothetical model is supported by a better statistics, as shown in Figure 3.3. In the Figure 3.3 the left panel shows the neutrino prediction based on Gaisser et al. (2013) model and the right panel is our hypothetical model. In this modelling the neutrino events detected by the IceCube detector are binned in four energy intervals 30-200 TeV, 0.2-1 PeV, 1-2 PeV and 2-100 PeV. The validity of our hypothetical model can be
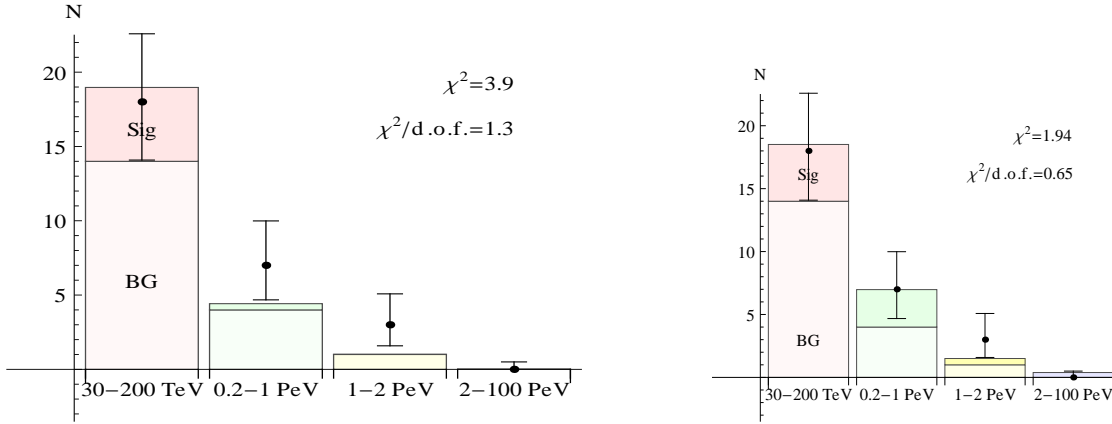
Figure 3.3: Observed (dots) and fitted (bars) event rates in the different energy bins for the Gaisser et al. (2013) and hypothetical models in the left and right panels, respectively. Here the model with directional information has been used. The required hydrogen densities are tabulated in Table 2.

checked by the future observation of cosmic rays and their secondary particles. Note that all cases with a composition heavier than hydrogen at 100 TeV lead to a predicted neutrino flux about one order of magnitude below the flux required to describe the IceCube observation (IceCube Collaboration, 2013).

3.4   Results for the target density

The fluxes in Figure 3.2 depend on the product $R_{eff} \times n_H$. Here we fit the computed neutrino spectra to the data in order to see what values can reproduce that, and what can be said about the fraction of neutrinos from cosmic ray interactions. We follow the method described by Winter (2013) updated by IceCube Collaboration (2013). The neutrino events detected by the IceCube detector are binned in four energy intervals 30-200 TeV, 0.2-1 PeV, 1-2 PeV and 2-100 PeV. We use two different approaches: (1) Ignoring direction, we assume that all non-atmospheric events needs to be described by the interactions with hydrogen, computing the atmospheric background with the method discussed by Winter (2013); model "**All sky**". (2) We choose the events from the skymap IceCube Collaboration (2013) which may potentially come from the cosmic ray interactions with the hydrogen halo within the directional uncertainties, and we correct for fraction of isotropically distributed events which may fall into the Galactic plane; model "**Directional inf.**".* The rest of the events is treated as (extragalactic and atmospheric) isotropic background. In addition, we assume that the neutrino directions are correlated with the diffuse gamma ray emission from the Galactic

---

*We remove the events at the lowest energies, as expected for the atmospheric background, in the ratio 2:1 showers to tracks. The selected events are 2, 3, 4, 13, 14, 15, 22, 25, 27 (IceCube Collaboration, 2013).

Composition	All sky $R_{eff} = 10 kpc$		Directional inf. $R_{eff} = 1 kpc$	
	n_H $[cm^{-3}]$	χ^2 /d.o.f.	n_H $[cm^{-3}]$	χ^2 /d.o.f.
Hydrogen ($A = 1$)	$1.6^{+0.3}_{-0.5}$	1.9	$6.2^{+4.2}_{-3.7}$	0.8
Helium ($A = 4$)	$5.9^{+1.7}_{-1.5}$	2.1	24^{+17}_{-15}	0.8
Iron ($A = 56$)	130^{+38}_{-34}	2.5	530^{+370}_{-330}	0.9
Gaisser et al. (2013)	$9.3^{+3.2}_{-2.8}$	5.1	32^{+30}_{-26}	1.3
Hypothetical	$4.5^{+1.3}_{-1.2}$	1.4	20^{+13}_{-11}	0.7

Table 3.2: Best-fit hydrogen density for different cosmic ray compositions (first column) and two different composition and halo models. Here also the 1σ errors from the fit to neutrino data are given, as well as the χ^2 per degree of freedom for the fit. The errors are non-Gaussian because of Poissonian statistics.

plane, which is limited to a Galactic latitude below $5°$, see the paper by Ackermann et al. (2012). This reduces the IceCube exposure to that flux by about a factor of ten because of the reduced solid angle.

We present our main results in Table 3.2, where the best-fit target densities and the χ^2/d.o.f. are shown for different composition models (rows), and two different extreme models for the directional information and halo sizes (columns). Note that $R_{eff} = 10 kpc$ has been chosen for the "all sky" model, and $R_{eff} = 1 kpc$ for the directional model; for different values, the results can be easily re-scaled using Table 3.1. From the all sky model, only the pure hydrogen composition produces realistic values for n_H, at the expense of a huge halo size.

For the model "directional information", the flux per solid angle in Eq. (2) has to be divided by the solid angle assumed for the Galaxy ($0.087 \times 4\pi$) instead of 4π. Consequently, Figure 3.2 represents the solid angle-averaged flux. For the directional model, it is to be increased by the factor $1/0.087$ within the Galactic plane, and zero otherwise (c.f., Figure 3.5, where the gamma-ray flux in the directional model is higher than in the all sky case). As a consequence, n_H in Table 3.2 has to be lowered by this factor in the directional case.

Note that the statistics are good enough to derive lower bounds for the hydrogen density in the all sky case. In the directional model, the statistics are much poorer and the error bars therefore much larger. Because of the small solid angle coverage of the signal, the required target densities are extremely large, which is unlikely. However, the event rates in IceCube from the direction of the Galactic plane can be well reproduced, see Figure 3.3. For the Gaisser et al. (2013) cosmic ray composition (left panel), we obtain a relatively poor fit because of the dip at PeV (middle bins), exactly where the neutrino data require a peak (compare to Figure 3.2). A better fit of the shape is, as expected, obtained for our hypothetical

cosmic ray composition model, see right panel. Although this model is incompatible with cosmic ray composition data, it may serve as a proof of principle that one can produce a peak at PeV with composition changes only. Note again that there is no direct dependence on the cosmic ray injection and escape time in our calculation. The propagation of ultra high energy gamma rays from source to us influenced by the radio background as calculated by Protheroe & Biermann (1996). This is also shown in Figure 3.4.
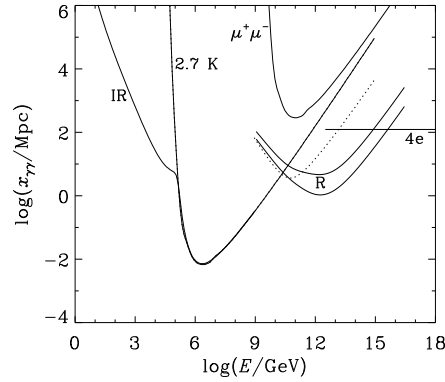
Figure 3.4: Mean free path variation with gamma ray energy, (figure taken from Protheroe & Biermann (1996))

In the total 28 set of neutrino events only 9, events are correlated to the Galactic plane. The width of this plane is limited in the range of $-5°$ to $5°$. The physical mechanism of neutrino production also produces gamma rays, whose flux is very much similar to the neutrino flux. We calculate the flux of gamma rays from the Galactic plane by this multi-messenger connection. In the energy range of 100 GeV to 10^8 GeV this flux comes out to be 100 times higher than the corresponding observed flux from the Galactic plane (Ackermann et al., 2012). The gamma-ray observation also concludes that the neutrino events from the Galactic plane are can not be greater than 0.09. For illustration, we have shown shown this multi-messenger connection in our Figure 3.5. The curves for the gamma ray fluxes are also corrected for absorption due to the background radiation with the mean free paths calculated in Protheroe & Biermann (1996) for $d = 10\text{kpc}$. The upper limits on the diffuse gamma ray flux from various experiments are compared with our results. One strong constraint comes from the KASCADE and CASAMIA limits at a few hundred TeV. On the other hand, the Fermi-LAT observation at 100 GeV Ackermann et al. (2012) does not impose a problem for the A=1 "All sky" model, whereas the directional model clearly exceeds the bound. The data above a few hundred TeV can be circumvented away by the attenuation of the gamma rays over long distances.
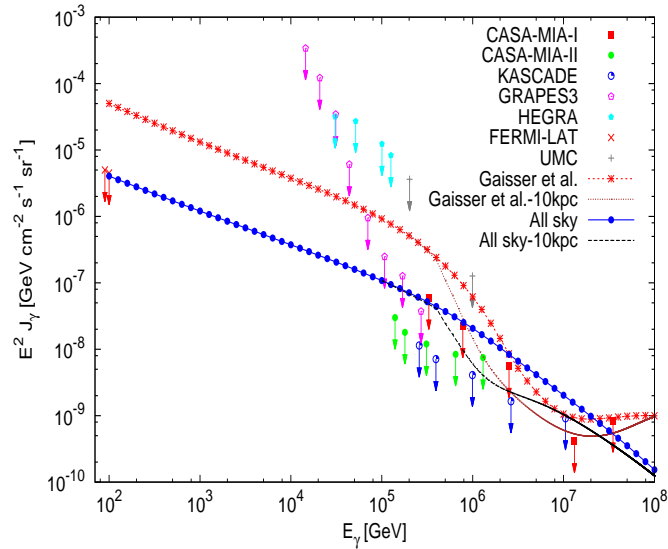
Figure 3.5: Unattenuated gamma ray flux for two different models (A=1, All sky versus Gaisser et al. (2013) composition, directional information) compared with the limits from CASA-MIA-I Chantell et al. (1997), KASCADE Schatz et al. (2003), HEGRA Karle et al. (1995), GRAPES-3 GRAPES-3 Collaboration (2009) and UMC Matthews et al. (1991). In addition, bounds from the Fermi-LAT Galactic plane diffuse emission Ackermann et al. (2012) (Figure 17) and CASA-MIA Borione et al. (1998) are shown (CASA-MIA-II). The "10 kpc" curves show the effect of absorption due to the background radiation for a distance of 10 kpc Protheroe & Biermann (1996). The required hydrogen densities are tabulated in Table 2.

3.5   Discussion and Conclusion

Taking into account the spectral shape of the observed neutrino spectrum, we have tested if it is plausible to describe the observed neutrino flux in the TeV to PeV range by interactions between cosmic rays and matter in the interstellar medium. We have discussed several composition models for the cosmic rays and several geometries for the target matter halo. For the directional information on the neutrino events, we have chosen two possibilities: either all events above the atmospheric backgrounds are to be described by the matter interactions, or only the events compatible with the directions from the Galactic plane whereas the rest forms an isotropic (atmospheric and extragalactic) background. In the latter case, we have also taken into account a probable correlation with the diffuse gamma ray emission from the Galactic plane.

We have demonstrated that strong constraints arise from a) the expected target densities obtained from cosmic ray propagation models, b) bounds on the diffuse gamma ray emission from the Galactic plane, c) the measured cosmic ray composition contradicting the flux shape observed in IceCube, and d) the directional correlation with the diffuse gamma ray emission from the Galactic plane, limiting the expected solid angle of the signal flux. In the most plausible scenario (directional information used, cosmic ray composition model by Gaisser

et al. (2013)), the required target density is about a factor of 100 above current expectations to describe the neutrino events from the direction of the Galactic plane. In the Gaisser et al. (2013) composition model nine signal events are obtained for the best-fit $n_H = 32 \; \text{cm}^{-3}$. In the directional case the average n_H is $\sim 1 \; \text{cm}^{-3}$, about $9/32 \simeq 0.3$ events may come from cosmic ray interactions in the Milky Way. Ignoring the directional information, a larger contribution $\simeq 1$ event is possible, taking into account the cosmic ray composition data, plausible halo sizes, and the gamma ray constraints. However, this scenario requires unrealistically large target densities. In conclusion, we have demonstrated that, taking into account the known constraints, only a small fraction of the observed neutrino events may originate from the Galactic plane or from the Galactic halo.

Chapter 4

Cosmic Ray Antiprotons from Nearby Cosmic Accelerators

Based on :

4.1 Introduction

The observations of gamma rays from the SNRs which are associated with dense molecular clouds can be very useful to understand their contribution to antimatter particles. The Fermi-LAT gamma ray observations of the SNRs has been very important to understand their contribution to secondary positron fluxes (Ahlers et al., 2009). Similarly, the PAMELA (Payload for Antimatter Matter Exploration and Light-nuclei Astrophysics) observations of positrons and antiprotons can be used to understand the propagation of cosmic rays from the Galactic sources towards the detector on Earth (Shibata & Futo, 2008; Ahlers et al., 2009).

The cross section for antiproton production in p-p collisions based on accelerator data in the laboratory system with the projectile proton energy range of 10 to 1000 GeV has been discussed by (Shibata & Futo, 2008). The expermental data on cosmic antiprotons can be used to calculate the neutral hydrogen gas density (n_H) of the ISM, source density (Q) of cosmic rays and the diffusion coefficient (D) of the cosmic rays (Shibata et al., 2008). All these parameters provides us the better insight to understand the propagation of cosmic rays in our Galaxy.

The secondary antiproton flux produces mainly in the cosmic ray interactions with the background radiation and matter ($p\,p \rightarrow p\,\bar{p}\,p\,p$). Similarly, gamma rays are also produced in the same interactions ($p\,p \rightarrow \pi^0 \rightarrow \gamma\,\gamma$). The main different in these two processes is their production cross section and threshold energy of production (Shibata et al., 2008). The Fermi-LAT observation of gamma rays and PAMELA observations of antiprotons are very important to investigate the secondary origin of antiprotons.

The production of antiprotons in supernova remnants and the calculation of antiproton to proton ratio ($\frac{\bar{p}}{p}$) due to secondary interaction processes have been modelled by Blasi & Serpico (2009), Fujita et al. (2009) and by Berezhko & Ksenofontov (2014). Antiprotons are also produced by the interaction of diffused cosmic rays in the ISM with the hydrogen density. The antiproton flux from the ISM during the propagation of cosmic rays have been modelled by Donato et al. (2001), Shibata et al. (2008) and by Shibata & Futo (2008).

In this paper we discuss that the gamma ray emission from hadronic accelerators close to us (SNRs plus associated molecular clouds) can be used to find out the contributions of these sources to the diffuse cosmic ray antiproton flux measured near the earth. The observations of antiprotons by PAMELA satellite in the energy range of 60 MeV to 180 GeV has been reported by Adriani et al. (2010a).

We have considered some nearby SNRs observed in gamma rays by Fermi LAT, many of them are associated with molecular clouds. The gamma ray fluxes observed from these sources are most likely produced in hadronic interactions of cosmic ray protons. The hadronic

models of gamma ray production from SNRs were reported by Tanaka et al. (2011) in Vela Jr., by Abdo et al. (2010e,a,d) and Ackermann et al. (2013b) in IC443, W44 and W28, by Castro & Slane (2010) in W30 and by Giordano et al. (2012) in Tycho supernova remnant.

The antiprotons may annihilate and interact with the cold protons inside the sources and some of them will escape to the interstellar medium. Due to the low density of hydrogen or cold protons in the interstellar medium diffusion loss of cosmic ray antiprotons is more important than the loss due to interactions. We have used the cross-sections of production of antiprotons from Shibata et al. (2008). The simple formalism discussed in this paper can be applied to any hadronic cosmic ray source from which the gamma ray flux has been measured. Ahlers & Murase (2013) considered the production of electrons and positrons in SNRs in hadronic interactions. In case of hadronic interactions the observed gamma ray flux produced in neutral pion decay can be used to normalize the primary cosmic ray flux and to obtain the fluxes of other secondary particles.

4.2 Antiprotons and Gamma Rays from Nearby SNRs

The cosmic ray density of the protons inside the sources is expressed by a power law with spectral index α, $\frac{dQ_p(E_p)}{dE_p dV dt} = C_p E_p^{-\alpha}$. These cosmic rays interact with the ambient cold protons in the molecular clouds producing charged and neutral pions. The charged pions decay to neutrinos/antineutrinos and electrons/positrons. The neutral pions decay to gamma rays. Antiprotons are also produced in the interactions of cosmic ray protons with the cold protons but with a different cross-section of interaction. The antiproton flux injected from cosmic ray interactions is

$$\frac{dQ_{\bar{p}}^{inj}(E)}{dEdVdt} = 2\, t_{esc}^{inner}\, \rho_s\, c \int_E^\infty \sigma_{pp \to \bar{p}X}(E, E_p) \frac{dQ_p(E_p)}{dE_p dV dt} \frac{dE_p}{E_p}. \tag{4.1}$$

The factor of 2 accounts for the contribution from antineutrons equally produced in p-p interactions. The speed of the relativistic cosmic rays is close to the speed of light c. The average time of escape for the cosmic rays from the SNR-molecular cloud region is t_{esc}^{inner} sec, average number density of cold protons in the inetracting medium is ρ_s cm^{-3}.

We used the cross section of antiproton production discussed by Shibata et al. (2008) for high energy antiprotons. The Eqn.(4.1) reduces to

$$\frac{dQ_{\bar{p}}^{inj}(E)}{dEdVdt} = 2t_{esc}^{inner} \rho_s\, c\, \bar{\sigma}_\alpha(E)\, C_p\, E^{-\alpha} \tag{4.2}$$

The values of $\bar{\sigma}_\alpha(E)$ are given in Fig.4. of Shibata et al. (2008) for a power law spectrum

of cosmic rays with spectral index $\alpha = 2.6$ to 2.8. We have used the cross-sections corresponding to spectral index 2.6 in our calculations. The diffusion of cosmic rays (Ginzburg & Syrovatskii, 1964) for a spherically symmetric geometry can be used to obtain the propagated or observed cosmic ray antiproton flux.

The diffusion coefficient $D(E) = D_0 \left(E/E_0 \right)^{\delta}$ is assumed to be only energy dependent with $\delta = 0.33$ above the break at $E_0 = 4$ GeV and $D(E) = D_0 \sim 10^{28}$ cm^2/sec below $E_0 = 4$ GeV. The cosmic ray antiprotons interact with the cold protons inside the source and in the interstellar medium. The annihilation cross-section of antiprotons with protons steeply falls off above 1 GeV while the $\bar{p} - p$ inelastic cross-section rises at the same energy. The total $\bar{p} - p$ interaction cross-section is nearly constant at high energy.
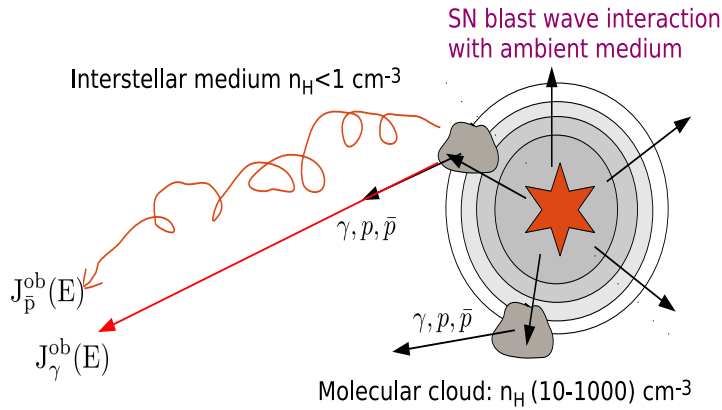
Figure 4.1: Schematic view of the charged and neutral particle propagation from nearby astrphysical sources. n_H denotes the density of hydrogen gas, $J_{\bar{p}}^{ob}(E)$ and $J_{\gamma}^{ob}(E)$ are the fluxes of antiprotons and gamma rays from the individual supernova remnant which are associated with the molecular clouds and detected by the Fermi-LAT γ-ray observations.

The formalism discussed in this work uses spherical symmetry around the source. If the source is located close to us and it is well inside the galactic halo the effect of the boundaries of galactic halo may be neglected. Near the Earth the observed cosmic ray flux is in steady state. The source is emitting continuously. The spherical volume containing the cosmic rays is expanding as a result cosmic ray density is falling inside this volume. At the same time

new cosmic rays are arriving from the source. If the loss and gain are compensated then a steady state cosmic ray flux is maintained at a distance R from the source.

The propagation of antiprotons and protons in the ISM undergoes diffusive motion. The solution of cosmic ray propagation in the diffusive approximation, in a spherically symmetric case, can be followed from Aharonian & Atoyan (1996) or from the standard text of Ginzburg & Syrovatskii (1964). In general the cosmic rays undergo ionization and nuclear energy losses in the ISM. If the kinetic energy of cosmic rays is greater than 1 GeV then, the nuclear losses are more important Aharonian & Atoyan (1996). We have considered the nuclear losses in out calculations, which are justified as the energies under calculation are greater than 1 GeV.

The propagation of antiprotons and protons in the interstellar magnetic field can be calculated under the diffusive approximation. Eqn.(9) of Aharonian & Atoyan (1996), provides the maximum antiproton flux at a distance R is

$$J_{\bar{p}}^{ob}(E) = c \frac{dQ_{\bar{p}}^{inj}(E)}{dEdVdt} \frac{V_{source}}{(4\pi)^2 \, D(E) \, R} \tag{4.3}$$

This flux is isotropic with dimension $GeV^{-1}cm^{-2}sec^{-1}sr^{-1}$. Where V_{source} is the volume of the source and $D(E)$ is the energy dependent diffusion coefficient and R is the distance to the source. The gamma ray flux density produced inside a source in cosmic ray interactions is

$$\frac{dQ_{\gamma}^{inj}(E)}{dEdVdt} = 2t_{esc}^{inner} \frac{\rho_s \, c}{K_\pi} \int_{E_{min}}^{\infty} \sigma_{pp\to\gamma\gamma}\left(m_p + \frac{E_\pi}{K_\pi}\right) \frac{dQ_p(m_p + E_\pi/K_\pi)}{dE_p dVdt} \frac{dE_\pi}{\sqrt{E_\pi^2 - m_\pi^2}} \tag{4.4}$$

from eqn.(78) of Kelner et al. (2006b, 2009), where $E_p = m_p + E_\pi/K_\pi$. The minimum energy of the pions $E_{min} = E + m_\pi^2/4E$ and $K_\pi = 0.17$ gives the fraction of the proton's energy going to the pion. The gamma ray flux received on earth is $J_{\gamma}^{ob}(E) \, GeV^{-1}cm^{-2}sec^{-1}$.

$$J_{\gamma}^{ob}(E) = \frac{dQ_{\gamma}^{inj}(E)}{dEdVdt} \frac{V_{source}}{4\pi R^2} \tag{4.5}$$

The cross-section of p-p interactions for the production of neutral pions is

$$\sigma_{pp\to\gamma\gamma}(E_p) = 34.3 + 1.88\ln(E_p/1TeV) + 0.25\ln(E_p/1TeV)^2\left[1 - \left(\frac{E_{th}}{E_p}\right)^4\right]^2 mb. \tag{4.6}$$

where $E_{th} = m_p + 2m_\pi + m_\pi^2/2m_p = 1.22GeV$. In our calculation this cross section is constant ~ 30 mb in the energy range of 10 GeV-1000 GeV. Using eqn.(4.3) and eqn.(4.5)

the ratio of the observed fluxes of antiprotons and gamma rays is

$$\text{Ratio(E)} = \frac{J_{\bar{p}}^{ob}(E)}{J_{\gamma}^{ob}(E)} = \frac{c\,R\,\frac{dQ_{\bar{p}}^{inj}(E)}{dEdVdt}}{4\pi\,D(E)\,\frac{dQ_{\gamma}^{inj}(E)}{dEdVdt}}. \tag{4.7}$$

With eqn.(4.2) to eqn.(4.6) we simplify eqn.(4.7) to

$$\text{Ratio(E)} = \frac{J_{\bar{p}}^{ob}(E)}{J_{\gamma}^{ob}(E)} = \frac{c\,R\,K_{\pi}\,\alpha}{4\,\pi\,D(E)} \times \frac{\bar{\sigma}_{\alpha}(E)}{\sigma_{pp\to\gamma\gamma}} \tag{4.8}$$

The observed gamma ray fluxes from the individual sources considered in this work are multiplied with the ratio given in eqn.(4.8) to obtain the cosmic ray antiproton fluxes from each of them. Our calculated antiproton fluxes are shown in Fig.1. and compared with the antiproton flux observed by PAMELA (Adriani et al., 2010a). In our case α is varying in the range of 1.85 to 3.02 as shown in Table-I.
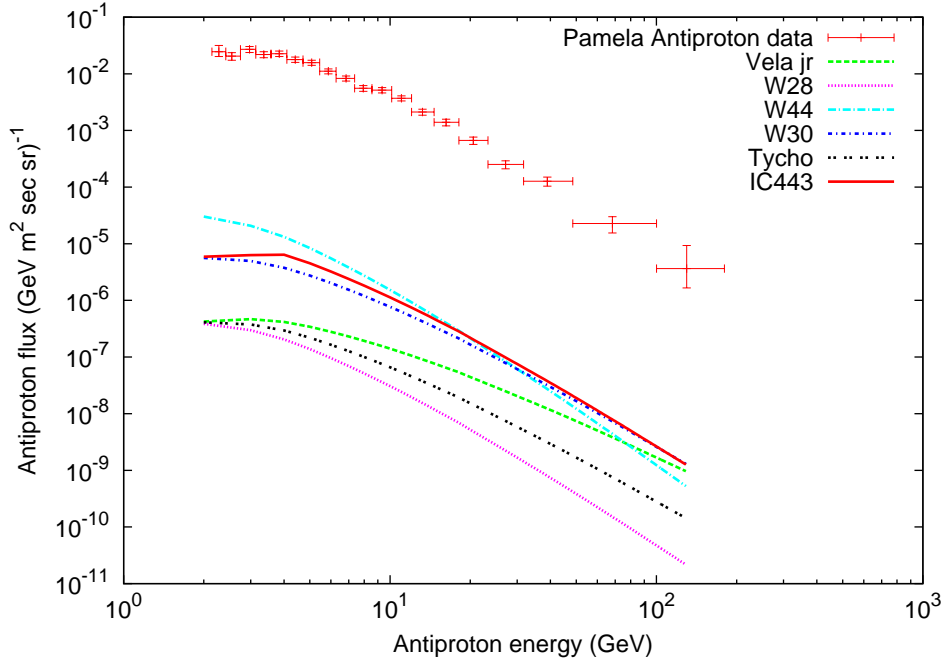
Figure 4.2: Antiproton fluxes from hadronic cosmic accelerators close to us compared with the total flux observed by PAMELA (Adriani et al., 2010a)

The proton fluxes calculated for the SNRs associated with molecular clouds are shown in Fig.2. assuming their escape time from the molecular clouds $t_{esc}^{inner} = 1000$ years. The density of the molecular clouds is assumed to be $\rho_s = 100\ cm^{-3}$ which corresponds to p-p interaction time $t_{pp} = 6 \times 10^5$ years (Gabici et al., 2009). In this case the escape time is much smaller than the p-p interaction time so the proton spectra are not attenuated significantly.

TABLE-I

Nearby SNRs considered in the present work

SNR	R kpc	Energy range GeV	Gamma ray flux $\mathrm{GeV^{-1}cm^{-2}sec^{-1}}$	Ref
Vela Jr	0.75	1-300	$8.65 \times 10^{-9} E^{-1.85}$	Tanaka et al. (2011)
IC443	1.5	0.2-3.25	$6.12 \times 10^{-8} E^{-1.93}$	Abdo et al. (2010e)
		Above 3.25	$1.29 \times 10^{-7} E^{-2.56}$	Ackermann et al. (2013b)
W28	2	0.4-1	$4.66 \times 10^{-8} E^{-2.09}$	Abdo et al. (2010a)
		Above 1	$4.66 \times 10^{-8} E^{-2.74}$	
W44	3	0.1-1.9	$1.15 \times 10^{-7} E^{-2.06}$	Abdo et al. (2010d)
		Above 1.9	$2.13 \times 10^{-7} E^{-3.02}$	Ackermann et al. (2013b)
W30	4.5	0.1-100	$2.16 \times 10^{-8} E^{-2.4}$	Castro & Slane (2010)
Tycho	1.7-5	0.4-100	$1.38 \times 10^{-9} E^{-2.3}$	Giordano et al. (2012)
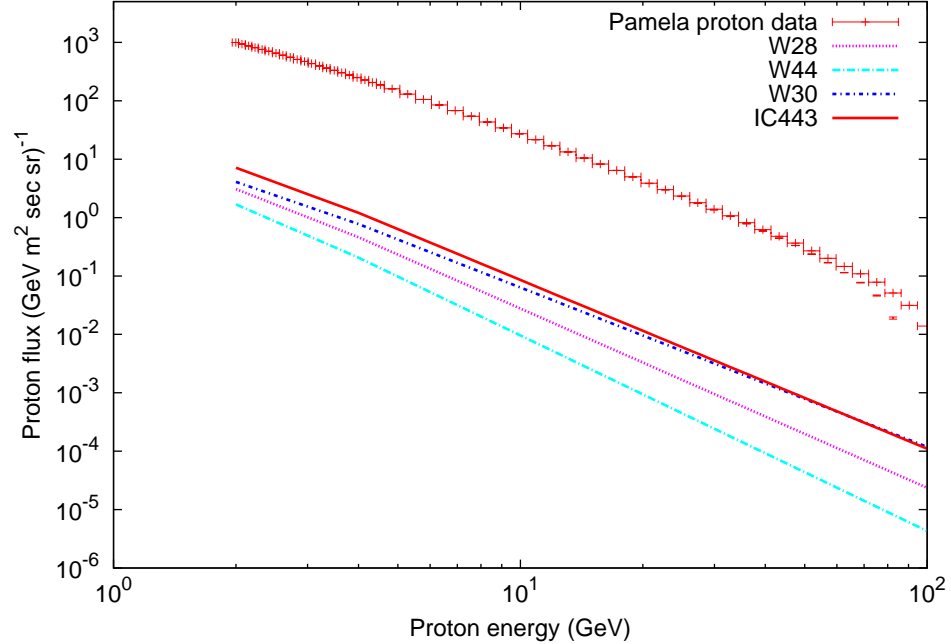
Figure 4.3: Proton fluxes from the molecular clouds associated with SNRs compared with the total flux observed by PAMELA (Adriani et al., 2011a, 2013b) for the following values of parameters $\mathrm{t_{esc}^{inner}} = 1000$ years, $\rho_{\mathrm{s}} = 100 \, \mathrm{cm^{-3}}$.

4.3 Summary and Conclusion

A large number of gamma ray point sources have been detected by Fermi LAT and other gamma ray detectors. In some of these sources hadronic interaction of cosmic rays is the underlying mechanism of gamma ray production. We have discussed a simple formalism to find the antiproton fluxes produced inside SNRs and molecular clouds in cosmic ray interactions p-p using the gamma ray fluxes from these sources produced in hadronic interactions p-p through the decay of neutral pions. The cosmic ray antiproton fluxes originating in p-p interactions from nearby cosmic accelerators are found to be much less compared to the flux observed by PAMELA (Adriani et al., 2010a). We have assumed energy independent escape of the cosmic ray antiprotons from the sources. Our calculated spectra have energy dependence qualitatively similar to the observed antiproton and proton spectra shown in Fig.1. and Fig.2.. Thus this assumption does not contradict the observational results. We have shown the spectra above 2 GeV as above which the effect of solar modulation are not important.

Chapter 5

Summary and Conclusion

Gamma rays, neutrinos and antiprotons are secondary products of the cosmic ray interactions. In this thesis, we have used the observational data from the Fermi-LAT, HESS, Ice-Cube and PAMELA experiments to understand some of the theoretical aspects of cosmic ray interactions. We have mainly discussed the hadronic interactions for the production of gamma rays, neutrinos and antiprotons.

Hadronic models of gamma ray production at the core of Centaurus A

Centaurus A (Cen A) has been observed in the energy range of 10^{-5} eV to TeV. The SED of Cen A has two peaks at 4×10^{-2} eV and 170 keV respectively (Abdo et al., 2010b). Abdo et al. (2010b) found that the multi-wavelength emission of Cen A in the energy range of 10^{-5} eV to 10 times GeV can be explained by the Synchrotron Self Compton (SSC) model. In this model, the SED peak at 4×10^{-2} eV can be explained by the synchrotron emission of the relativistic electrons and the peak at 170 keV can be explained by the inverse Compton of synchrotron photons with the relativistic electrons.

In the SSC model, the combined variation of bulk Lorentz factor (Γ), Doppler factor (δ_D), the angle between the jet axis and the observer's line of sight (θ), the magnetic field in the source region (B) and the size of the emission region (R) can explain the multi-wavelength data. Abdo et al. (2010b) tried different sets of SSC parameters to explain the multi-wavelength data of Cen A. They found that the HESS detected GeV to TeV component (which we refer to as TeV component) was a new component and it can't be explained within the SSC framework.

The HESS gamma-ray excess of TeV component from Cen A coincides with the core of

Cen A (core of Cen A is the central kpc-scale region which includes the black hole, inner jets and the inner radio lobes). Sahu et al. (2012) suggested that $p - \gamma$ interaction in the core of Cen A can explain this TeV component. So the combined spectral energy distribution (SED) of Cen A can be explained by the SSC emission upto 10 times GeV and the GeV to TeV component can be explained by the photo-hadronic (p-γ) interactions.

In our work, we have considered some other possibilities of hadronic interactions at the core of Cen A. We have used the results of HESS GeV to TeV gamma ray detection from Cen A (Aharonian et al., 2009) and the Pierre Auger correlation of UHECRs to Cen A (Pierre Auger Collaboration et al., 2007) to reach a conclusion. We have considered the following scenarios,

- The primary cosmic rays at the core of Cen A are protons and the high energy gamma rays are produced in p-p interactions.

- The primary cosmic rays are Fe nuclei and the high energy gamma rays are produced in Fe-p interactions.

- The primary cosmic rays are Fe nuclei and they are photo-disintegrated at the core. In this interaction the unstable daughter nuclei are produced and gamma rays are produced after their de-excitation.

The gamma ray flux from these processes are compared with the flux observed by HESS experiment to calculate the normalization factor of the primary cosmic rays at the core of Cen A. We calculated the expected number of cosmic ray nucleon events between 55 EeV and 150 EeV in each of these cases to ensure that the scenarios are consistent with the observations by Pierre Auger experiment.

We have taken the cosmic ray proton spectral index to be approximately 2.73, based on the HESS gamma ray observations. The p-p interaction in the Cen A core produces 450 cosmic ray events in the energy range of 55 EeV to 150 EeV, which is very large compared to the Pierre Auger correlated cosmic ray events towards Cen A. So p-p interaction gamma ray production mechanism is not consistent to explain the HESS TeV component from Cen A core. Similarly in the Fe-p interaction at the core of Cen A, the flux of cosmic ray events is 100 times lower than the correlated events towards Cen A. So we conclude that pure hadronic interaction scenario for the production of gamma rays at the core of Cen A is not consistent with the Pierre Auger UHECR observations.

Further in our calculations of interaction at the core of Cen A, we found that the photo-disintegration of iron nuclei is most efficient. The interaction rate for this process was 100

times higher compared to the p-γ interaction rate. We know that p-γ process is already a plausible mechanism for the production of gamma rays at the core of Cen A (Sahu et al., 2012).

Motivated from these results, we calculated the gamma ray production at the core of Cen A due to iron photo-disintegration. The photo-disintegration process is known as the giant dipole resonance (GDR) by which the disintegration of a nuclei takes place. The statistical emission of a single nucleon is dominant in the nuclear giant dipole resonance process (Anchordoqui et al., 2007a). This interaction takes place at a resonance energy $\epsilon'_0 = 42.65A^{-0.21}$ MeV for $A > 4$, where A is the mass number for the heavy nuclei (Anchordoqui et al., 2007a).

We have explained the TeV component from Cen A using the photo-disintegration process in the Cen A source. The SSC set of parameters used in our calculations are ($\Gamma = 7$, $\delta_D = 1.0$, $\theta = 30°$, B = 6.2 G, $R = 3.0 \times 10^{15}$cm). In this process, the low energy photons trigger the photo-disintegration of iron nuclei above threshold energy of 10 to 30 MeV in their rest frame. In the photo-disintegration process, MeV photons are produced after the de-excitation of the unstable nuclei in their rest frame. We calculated the normalization of cosmic ray flux by comparing the HESS gamma ray flux to the photo-disintegrated gamma ray flux. We have done this calculation in the energy range of 1 TeV to 100 TeV per nucleon, when the interaction rate is approximately constant to 2×10^{-8}sec^{-1}.

These de-excited MeV gamma rays are observed in the GeV to TeV energy range in the observer's frame due to the Lorentz factor of the boosted nucleus. We first consider the two peak interactions with the cosmic ray nuclei. The peak photons at 4×10^{-2} eV will interact with the cosmic ray nuclei with Lorentz boost factor of order 10^9 and the observed gamma rays will be of energy approximately $10^9 \times 10^7$ or 10^{16} eV. Hence, these kind of interactions can not be compared with the observations.

In the current picture of Cen A, the interaction of second peak at 170 keV with the cosmic ray Fe nuclei is very important. These photons will interact with the cosmic ray iron nuclei at energy 2.8 TeV and the energy of the observed photons will have a corresponding peak at 400 MeV. To explain the TeV component, the total cosmic ray power has to be of the order of 10^{47}erg/sec. The luminosity of the cosmic ray Fe nuclei required to explain the HESS and Pierre Auger observations depends on the density of low energy photons at the source along with the size of the emitting region. This means that the luminosity of cosmic rays needed in photo-disintegration process is a function of parameters used in the SSC models. We did not explore a new set of SSC parameters to lower the luminosity as it was known that the isotropic luminosity of Cen A source can exceed its Eddington luminosity of 10^{46}erg/sec during flaring states (Dermer et al., 2009).

Cen A is continuously monitored in gamma rays by current gamma ray instruments. After publication of our work, Fermi-LAT published 4 years (2008-2012) of gamma ray observation data of Cen A in the energy range of 100 MeV to 50 GeV(Sahakyan et al., 2013), where they detected an unusual hardening in the gamma ray spectrum above 4 GeV. In their analysis of this data, they expected this hardening is possible due to the presence of a hard component in the parent cosmic ray spectrum and the observed gamma ray spectrum can be explained by $\mathrm{p} - \gamma$ interaction. Similarly, Fraija (2014) explained the gamma ray emission of Cen A, above 4 GeV by photo-hadronic models. In their work they found that the emission upto 4 GeV can be explained by the SSC model and beyond 4 GeV the emission is due to the pion decay channel. In this pion decay channel they have considered the charged muon synchrotron cooling for the production of GeV emission.

Later, Kundu & Gupta (2014) explained this hard component and HESS data using the photo-disintegration model. They used a different set of SSC model parameters ($\Gamma = 7$, $\delta_D = 0.25$, $\theta = 65°$, $\mathrm{B} = 33.0\,\mathrm{G}$, $\mathrm{R} = 5.8 \times 10^{15}\mathrm{cm}$). They found that the total luminosity in cosmic ray Fe-nuclei is $1.5 \times 10^{43}\mathrm{erg/sec}$ to explain the gamma ray flux above 1 GeV, and it is due to a different SED of SSC model parameters used in their calculation. The charged muons are produced in the photo-hadronic (p-γ) interactions, which emit synchrotron radiation. All these results indicate that the high energy gamma ray emission in the energy range of GeV to TeV from the core of Cen A has a hadronic origin.

TeV to PeV neutrinos from the cosmic ray interactions in the Milky Way Galaxy

In the cosmic ray induced origin, neutrinos are mainly produced in hadronic interactions. The Ice cube neutrino detector at the South Pole has detected neutrino events in the energy range of TeV to PeV. In the 2 years (2011-13) of observations, 28 TeV to PeV neutrino events of extraterrestrial origin have been detected (IceCube Collaboration, 2013) and has accumulated to 37 neutrino events after 3 years (2011-13) of observations (Aartsen et al., 2014b).

In the Galactic infrared background the photo-hadronic or p-γ interactions are not dominant (Gupta, 2012) compared to p-p interactions. Charged and neutral pions are produced in the interaction of cosmic rays with the hydrogen nuclei in the interstellar medium. The charged pions decay to muons and muon type neutrinos ($\pi^\pm \to \mu^\pm + \nu_\mu(\bar{\nu}_\mu)$). The muons subsequently decay to electrons, electron type neutrinos and muon type neutrinos ($\mu^\pm \to e^\pm + \nu_e(\bar{\nu}_e) + \bar{\nu}_\mu(\nu_\mu)$). The ratio of the neutrino fluxes of different flavors produced in this

way is $\nu_e + \bar{\nu}_e : \nu_\mu + \bar{\nu}_\mu : \nu_\tau + \bar{\nu}_\tau = 1 : 2 : 0$. The fluxes of neutrinos of each flavor are expected to be roughly equal on Earth after flavor mixing $\nu_e + \bar{\nu}_e : \nu_\mu + \bar{\nu}_\mu : \nu_\tau + \bar{\nu}_\tau \simeq 1 : 1 : 1$ (Gaisser, 1991a).

The neutrino flux varies with atomic mass number A, as $A^{2-\alpha}$, here $\alpha > 2$ is the spectral index of the cosmic ray spectrum. As a result the pure proton composition will produce the maximum neutrino flux while the pure iron composition the lowest. We have used the observed cosmic ray spectrum from the cosmic ray model by Gaisser et al. (2013). In their model, the iron composition dominates at 10^8 GeV, and this gives a dip in the neutrino flux at PeV energies, if we calculate the neutrino flux from the interaction of cosmic rays with the density of neutral hydrogen in the Galactic plane.

In our calculations, the aim is to understand the origin of the IceCube detected neutrino events. These neutrino events can have an atmospheric, Galactic or extragalactic origin. In this work we have tested if it is plausible to describe the observed neutrino flux in the TeV to PeV range by interactions between cosmic rays and matter in the interstellar medium of our Galaxy. We have calculated the atmospheric neutrino events and the Galactic diffuse neutrino signal in the energy range of the IceCube observations.

In the atmospheric scenario, we know that the neutrino flux is mainly distributed into the electron-type and muon-type neutrinos. The atmospheric scale height is not sufficient for the production of tau-type neutrinos due to flavor oscillations. We have computed the atmospheric neutrino background with the method discussed by Winter (2013) and found that 9 events are coming from the atmospheric contribution which is very near to the IceCube estimation $10^{+4.5}_{-3.9}$.

In our discussion of the Galactic contribution, we have taken two type of cases: (1) Ignoring direction; when the neutrinos are coming from all the possible directions "**All sky model**" where we take 19 neutrino events into our sample, as we subtracted the atmospheric events from the total events.

(2) When the neutrino events are selected from the Galactic plane; we call it "**Directional inf.**", where we take the neutrino sample 9, which is the contribution from the Galactic disc after we subtract the low energy atmospheric events. In addition, we assume that the neutrino directions are correlated with the diffuse gamma ray emission from the Galactic plane, which is limited to a Galactic latitude below $5°$ (Ackermann et al., 2012).

The neutrino events detected by the IceCube detector are binned into four energy intervals 30-200 TeV, 0.2-1 PeV, 1-2 PeV and 2-100 PeV. We have used the diffuse gamma ray bound by Fermi-LAT (Ackermann et al., 2012), the current cosmic ray model by Gaisser et al. (2013), and the known density of neutral hydrogen in our Galactic plane to restrict the number of neutrino events from our Galaxy. We have found that in both scenarios "**All sky**

model", "**Directional inf.**" approximately none of the neutrino events are produced due to the interaction of cosmic rays with the neutral hydrogen in the Galactic medium.

In theoretical studies, these neutrino origin have been correlated to Fermi bubble by Lunardini et al. (2014) where they showed that 6 - 7 of the 37 events may come from the Fermi bubble. Similar theoretical calculations of the IceCube neutrino events can be correlated to the extragalactic objects (Ahlers & Halzen, 2014) and to the cluster of galaxies Zandanel et al. (2015). In future more neutrino data from the IceCube detector and other neutrino detectors may resolve the astrophysical sources of neutrinos.

Cosmic ray proton and antiproton fluxes from the nearby cosmic ray sources in the energy range of 2 to 100 GeV

PAMELA (Payload for Antimatter Matter Exploration and Light-nuclei Astrophysics) collaboration has detected cosmic ray proton and antiproton fluxes in the energy range of 1 GeV to 100's of GeV (Adriani et al., 2011a, 2010a). Supernova blast wave can accelerate cosmic rays easily upto PeV energies (Drury, 1983; Blandford & Eichler, 1987; Jones & Ellison, 1991). If the cosmic ray protons escaping from these accelerators enter into a molecular cloud target of hydrogen density 10 to $1000/\mathrm{cm}^3$ then secondary particles are produced effectively.

We have calculated the diffuse antiproton and proton fluxes from the nearby supernova remnants Vela jr, W28, W44, W30, Tycho and IC443 whose association with molecular clouds are known and are detected by Fermi-LAT in gamma rays. The secondary gamma rays ($\mathrm{p\,p} \rightarrow \pi^0 \rightarrow \gamma\,\gamma$) and secondary antiprotons ($\mathrm{p\,p} \rightarrow \mathrm{p\,\bar{p}\,p\,p}$) are produced in these interactions.

In the p-p interactions the cross section of interaction remains approximately constant and due to this the proton flux at the source follows the spectral index very much similar to the observed Fermi-LAT gamma ray observations. This helps a lot in our calculations because the unknown parameters like the escape time of cosmic rays inside the molecular cloud $\mathrm{t}_{\mathrm{esc}}^{\mathrm{inner}}$, the cloud density ρ_{s} etc gets cancelled out.

We have found that the cosmic ray antiproton fluxes expected from the individual nearby cosmic accelerators are 1000 times less than the total antiproton flux observed by the PAMELA experiment. We have also calculated the diffuse cosmic ray proton flux from these SNRs which is 100 times lower than the PAMELA flux.

Bibliography

Aartsen, M. G., Abbasi, R., Abdou, Y., et al. 2013, Physical Review Letters, 111, 021103

Aartsen, M. G., Abbasi, R., Ackermann, M., et al. 2014a, Journal of Instrumentation, 9, 3009P

Aartsen, M. G., Ackermann, M., Adams, J., et al. 2014b, Physical Review Letters, 113, 101101

Abbasi, R., Ackermann, M., Adams, J., et al. 2009, Phys. Rev. D, 79, 062001

Abbasi, R. U., Abu-Zayyad, T., Allen, M., et al. 2008, Physical Review Letters, 100, 101101

—. 2010, ApJ, 713, L64

Abdo, A. A., Ackermann, M., Ajello, M., et al. 2010a, ApJ, 718, 348

—. 2010b, ApJ, 719, 1433

—. 2010c, ApJ, 710, L92

—. 2010d, Science, 327, 1103

—. 2010e, ApJ, 712, 459

Abe, K., Fuke, H., Haino, S., et al. 2012, Physical Review Letters, 108, 051102

Abraham, J., Abreu, P., Aglietta, M., et al. 2008, Physical Review Letters, 101, 061101

—. 2010, Physical Review Letters, 104, 091101

Abreu, P., Aglietta, M., Ahn, E. J., et al. 2010, Astroparticle Physics, 34, 314

Abu-Zayyad, T., Belov, K., Bird, D. J., et al. 2001, ApJ, 557, 686

Acciari, V. A., Aliu, E., Arlen, T., et al. 2010, ApJ, 714, 163

Ackermann, M., Ahrens, J., Bai, X., et al. 2005, Phys. Rev. D, 71, 077102

Ackermann, M., et al. 2012, Astrophys.J., 750, 3

Ackermann, M., Ajello, M., Allafort, A., et al. 2013a, Science, 339, 807

—. 2013b, Science, 339, 807

Adrián-Martínez, S., Samarai, I. A., Albert, A., et al. 2012a, ApJ, 760, 53

Adrián-Martínez, S., Al Samarai, I., Albert, A., et al. 2012b, Astroparticle Physics, 36, 204

Adrián-Martínez, S., Albert, A., André, M., et al. 2014, Journal of High Energy Astrophysics, 3, 9

Adriani, O., Barbarino, G. C., Bazilevskaya, G. A., et al. 2010a, Physical Review Letters, 105, 121101

Adriani, O., Barbarino, G. C., Bazilevskaja, G. A., et al. 2010b, in American Institute of Physics Conference Series, Vol. 1223, American Institute of Physics Conference Series, ed. C. Cecchi, S. Ciprini, P. Lubrano, & G. Tosti, 33–42

—. 2011a, Science, 332, 69

—. 2011b, ApJ, 737, L29

—. 2013a, Physical Review Letters, 111, 081102

—. 2013b, ApJ, 765, 91

Aguilar, J. A., Albert, A., Ameli, F., et al. 2006, Astroparticle Physics, 26, 314

Aguilar, M., Alberti, G., Alpat, B., et al. 2013, Physical Review Letters, 110, 141102

Aharonian, F., Akhperjanian, A., Barrio, J., et al. 2001, A&A, 370, 112

Aharonian, F., Akhperjanian, A. G., Aye, K.-M., et al. 2005a, A&A, 442, 1

—. 2005b, Science, 309, 746

Aharonian, F., Akhperjanian, A. G., Bazer-Bachi, A. R., et al. 2006, Science, 314, 1424

Aharonian, F., Akhperjanian, A. G., Anton, G., et al. 2009, ApJ, 695, L40

Aharonian, F. A. 2004, Very high energy cosmic gamma radiation : a crucial window on the extreme Universe

Aharonian, F. A., & Atoyan, A. M. 1996, A&A, 309, 917

Aharonian, F. A., & Bogovalov, S. V. 2003, New A, 8, 85

Ahlers, M., & Halzen, F. 2014, Phys. Rev. D, 90, 043005

Ahlers, M., Mertsch, P., & Sarkar, S. 2009, Phys. Rev. D, 80, 123017

Ahlers, M., & Murase, K. 2013, ArXiv e-prints, arXiv:1309.4077

Ahrens, J., Bai, X., Barwick, S. W., et al. 2003, Physical Review Letters, 90, 251101

Albert, J., Aliu, E., Anderhub, H., et al. 2007, A&A, 474, 937

—. 2009, ApJ, 693, 303

Alcaraz, J., Alvisi, D., Alpat, B., et al. 1999, Physics Letters B, 461, 387

Allen, G. E., Keohane, J. W., Gotthelf, E. V., et al. 1997, ApJ, 487, L97

Allkofer, C. O., Babson, J., Barish, B., et al. 1990, International Cosmic Ray Conference, 4, 357

Anchordoqui, L. A., Beacom, J. F., Goldberg, H., Palomares-Ruiz, S., & Weiler, T. J. 2007a, Phys. Rev. D, 75, 063001

—. 2007b, Physical Review Letters, 98, 121101

Anchordoqui, L. A., Goldberg, H., Lynch, M. H., et al. 2013, ArXiv e-prints 1306.5021v3, arXiv:1306.5021

Anchordoqui, L. A., Goldberg, H., & Weiler, T. J. 2001, Physical Review Letters, 87, 081101

—. 2011, Phys. Rev. D, 84, 067301

Anderson, C. D. 1933, Phys. Rev., 43, 491

Anderson, M. C., Keohane, J. W., & Rudnick, L. 1995, ApJ, 441, 300

Andres, E., Askebjer, P., Barwick, S. W., et al. 2000, Astroparticle Physics, 13, 1

Andrés, E., Askebjer, P., Bai, X., et al. 2001, Nature, 410, 441

ANTARES collaboration. 1997, ArXiv Astrophysics e-prints, astro-ph/9707136

ANTARES Collaboration. 2013, J. Cosmology Astropart. Phys., 3, 6

ANTARES Collaboration, Adrián-Martínez, S., Albert, A., et al. 2013, ArXiv e-prints, arXiv:1308.5260

Antipov, Y., Denisov, S., Donskov, S., et al. 1971, Nuclear Physics B, 31, 235

Apel, W. D., Arteaga-Velázquez, J. C., Bekk, K., et al. 2013, Astroparticle Physics, 47, 54

Atwood, W. B., Abdo, A. A., Ackermann, M., et al. 2009, ApJ, 697, 1071

Auger, P., Ehrenfest, P., Maze, R., Daudin, J., & Fréon, R. A. 1939, Reviews of Modern Physics, 11, 288

Ave, M., Knapp, J., Lloyd-Evans, J., Marchesini, M., & Watson, A. A. 2003, Astroparticle Physics, 19, 47

Axford, W. I., Leer, E., & Skadron, G. 1977, International Cosmic Ray Conference, 11, 132

Baars, J. W. M., Genzel, R., Pauliny-Toth, I. I. K., & Witzel, A. 1977, A&A, 61, 99

Babson, J., Barish, B., Becker-Szendy, R., et al. 1990, Phys. Rev. D, 42, 3613

Bahcall, J., & Waxman, E. 2001, Phys. Rev. D, 64, 023002

Bahcall, J. N. 1964, Phys. Rev. Lett., 12, 300

Barger, V., Fu, L., Learned, J. G., et al. 2014, Phys. Rev. D, 90, 121301

Baring, M. G. 2004, Advances in Space Research, 33, 552

Bartoli, B., Bernardini, P., Bi, X. J., et al. 2013, ApJ, 767, 99

Bell, A. R. 1978a, MNRAS, 182, 147

—. 1978b, MNRAS, 182, 443

—. 1992, MNRAS, 257, 493

—. 2015, MNRAS, 447, 2224

Bell, A. R., & Lucek, S. G. 1996, MNRAS, 283, 1083

Bennett, K., Bignami, G. F., Buccheri, R., et al. 1977a, in ESA Special Publication, Vol. 124, Recent Advances in Gamma-Ray Astronomy, ed. R. D. Wills & B. Battrick, 83–93

Bennett, K., Bignami, G. F., Boella, G., et al. 1977b, A&A, 61, 279

Berezhko, E. G., & Ksenofontov, L. T. 2014, ApJ, 791, L22

Berezinskii, V. S., Bulanov, S. V., Dogiel, V. A., & Ptuskin, V. S. 1990a, Astrophysics of cosmic rays

—. 1990b, Astrophysics of cosmic rays

—. 1990c, Astrophysics of cosmic rays

Bergström, L., Bringmann, T., & Edsjö, J. 2008, Phys. Rev. D, 78, 103520

Bhattacharjee, P., & Gupta, N. 2004, Pramana, 62, 789

Biermann, P. L., & de Souza, V. 2012, ApJ, 746, 72

Bird, D. J., Corbato, S. C., Dai, H. Y., et al. 1995, ApJ, 441, 144

Blandford, R., & Eichler, D. 1987, Phys. Rep., 154, 1

Blandford, R. D., & Ostriker, J. P. 1978a, ApJ, 221, L29

—. 1978b, ApJ, 221, L29

Blasi, P., & Amato, E. 2012a, J. Cosmology Astropart. Phys., 1, 010

—. 2012b, jcap, 1, 011

Blasi, P., & Serpico, P. D. 2009, Physical Review Letters, 103, 081103

Blitz, L., & Robishaw, T. 2000, ApJ, 541, 675

Bongiorno, S. D., Falcone, A. D., Stroh, M., et al. 2011, ApJ, 737, L11

Borione, A., Catanese, M. A., Chantell, M. C., et al. 1998, ApJ, 493, 175

Böttcher, M., & Dermer, C. D. 1998, ApJ, 499, L131

Braun, J., Dumm, J., De Palma, F., et al. 2008, Astroparticle Physics, 29, 299

Brodie, J., Koenigl, A., & Bowyer, S. 1983, ApJ, 273, 154

Burns, J. O., & Price, R. M. 1983, Scientific American, 249, 56

Caprioli, D., Blasi, P., & Amato, E. 2011, Astroparticle Physics, 34, 447

Casandjian, J.-M., & Grenier, I. A. 2008, A&A, 489, 849

Castro, D., & Slane, P. 2010, ApJ, 717, 372

Chakraborti, S., Ray, A., Soderberg, A. M., Loeb, A., & Chandra, P. 2011, Nature Communications, 2, arXiv:1012.0850

Chamberlain, O., Segrè, E., Wiegand, C., & Ypsilantis, T. 1955, Phys. Rev., 100, 947

Chantell, M. C., Covault, C. E., Cronin, J. W., et al. 1997, Physical Review Letters, 79, 1805

Chardonnet, P., Mignola, G., Salati, P., & Taillet, R. 1996, Physics Letters B, 384, 161

Charlesworth, M., & Spencer, R. E. 1982, MNRAS, 200, 933

Chiang, J., & Racusin, J. L. 2011, in American Institute of Physics Conference Series, Vol. 1358, American Institute of Physics Conference Series, ed. J. E. McEnery, J. L. Racusin, & N. Gehrels, 205–208

Chiang, J., & Romani, R. W. 1994, ApJ, 436, 754

Chiarusi, T., & Spurio, M. 2010, European Physical Journal C, 65, 649

Chou, A. S., Arisaka, K., Pernas, M. D. A., et al. 2005, 29th ICRC, 2005, Pune, India, 7, 319

Choubey, S., & Rodejohann, W. 2009, Phys. Rev. D, 80, 113006

Chupp, E. L., Forrest, D. J., Higbie, P. R., et al. 1973a, Nature, 241, 333

Chupp, E. L., Forrest, D. J., & Suri, A. N. 1973b, NASA Special Publication, 342, 285

Clark, G. W., Garmire, G. P., & Kraushaar, W. L. 1968, ApJ, 153, L203

Combet, C., Maurin, D., Donnelly, J., O'C. Drury, L., & Vangioni-Flam, E. 2005, aap, 435, 151

Cowan, C. L., Reines, F., Harrison, F. B., Kruse, H. W., & McGuire, A. D. 1956, Science, 124, 103

Cucchiara, A., Levan, A. J., Fox, D. B., et al. 2011, ApJ, 736, 7

Davis, L. 1956, Physical Review, 101, 351

Davis, R. 1964, Phys. Rev. Lett., 12, 303

Dermer, C. D., & Atoyan, A. 2006, New Journal of Physics, 8, 122

Dermer, C. D., Razzaque, S., Finke, J. D., & Atoyan, A. 2009, New Journal of Physics, 11, 065016

Dickey, J. M., & Lockman, F. J. 1990, ARA&A, 28, 215

Donato, F., Maurin, D., Salati, P., et al. 2001, ApJ, 563, 172

Dondi, L., & Ghisellini, G. 1995, MNRAS, 273, 583

Dorman, L., ed. 2006, Astrophysics and Space Science Library, Vol. 339, Cosmic Ray Inter-
    actions, Propagation, and Acceleration in Space Plasmas

Drury, L. O. 1983, Reports on Progress in Physics, 46, 973

—. 2012, MNRAS, 422, 2474

Dubus, G. 2013, A&A Rev., 21, 64

Ebisuzaki, T., & Tajima, T. 2014, Astroparticle Physics, 56, 9

Ebisuzaki, T.; Tajima, T. 2014, The European Physical Journal Special Topics, 223,
    doi:10.1140/epjst/e2014-02162-6

Ellis, J., Flores, R. A., Freese, K., et al. 1988, Physics Letters B, 214, 403

Ellison, D. C. 1983, International Cosmic Ray Conference, 10, 108

Ellison, D. C., & Ramaty, R. 1984, Advances in Space Research, 4, 137

Ellison, D. C., Reynolds, S. P., & Jones, F. C. 1990, ApJ, 360, 702

Engel, R., Seckel, D., & Stanev, T. 2001, Phys. Rev. D, 64, 093010

Evoli, C., Grasso, D., & Maccione, L. 2007, J. Cosmology Astropart. Phys., 6, 3

F. Hess, V. 1912, Physikalische Zeitschrift, 13, 1084

Fanaroff, B. L., & Riley, J. M. 1974, MNRAS, 167, 31P

Farahat, A., Zhang, M., Rassoul, H., & Connell, J. J. 2008, ApJ, 681, 1334

Feain, I. J., Cornwell, T. J., Ekers, R. D., et al. 2011, ApJ, 740, 17

Feldmann, R., Hooper, D., & Gnedin, N. Y. 2013, ApJ, 763, 21

Fermi, E. 1949, Physical Review, 75, 1169

Fermi LAT Collaboration, Ackermann, M., Ajello, M., et al. 2012, Science, 335, 189

Fichtel, C. E., Hartman, R. C., Kniffen, D. A., et al. 1975, ApJ, 198, 163

Fichtel, C. E., Kniffen, D. A., Hartman, R. C., et al. 1977, in ESA Special Publication, Vol. 124, Recent Advances in Gamma-Ray Astronomy, ed. R. D. Wills & B. Battrick, 191–200

Formaggio, J. A., & Zeller, G. P. 2012, Reviews of Modern Physics, 84, 1307

Fornengo, N., Maccione, L., & Vittino, A. 2014, J. Cosmology Astropart. Phys., 4, 3

Forrest, D. J., Chupp, E. L., Suri, A. N., & Reppin, C. 1973, NASA Special Publication, 339, 165

Fraija, N. 2014, MNRAS, 441, 1209

Fraschetti, F., & Melia, F. 2008, MNRAS, 391, 1100

Frontera, F., Guidorzi, C., Montanari, E., et al. 2009, ApJS, 180, 192

Fujita, Y., Kohri, K., Yamazaki, R., & Ioka, K. 2009, Phys. Rev. D, 80, 063003

Fukuda, Y., Hayakawa, T., Ichihara, E., et al. 1998, Physical Review Letters, 81, 1562

Fukuda, Y., Hayakawa, T., Ichihara, E., et al. 1998, Phys. Rev. Lett., 81, 1562

—. 1999, Phys. Rev. Lett., 82, 1810

Gabici, S., Aharonian, F. A., & Casanova, S. 2009, MNRAS, 396, 1629

Gaensler, B. M., & Slane, P. O. 2006a, ARA&A, 44, 17

—. 2006b, ARA&A, 44, 17

Gaggero, D. 2012, Cosmic Ray Diffusion in the Galaxy and Diffuse Gamma Emission

Gaisser, T. K. 1991a, S&T, 82, 46

—. 1991b, S&T, 82, 46

Gaisser, T. K., Stanev, T., & Tilav, S. 2013, Frontiers of Physics, ArXiv e-prints 1303.3565, arXiv:1303.3565

Gehrels, N. 2004, in Astronomical Society of the Pacific Conference Series, Vol. 312, Gamma-Ray Bursts in the Afterglow Era, ed. M. Feroci, F. Frontera, N. Masetti, & L. Piro, 495

Gehrels, N., Chincarini, G., Giommi, P., et al. 2004a, ApJ, 611, 1005

—. 2004b, ApJ, 611, 1005

Georganopoulos, M., & Kazanas, D. 2003, ApJ, 594, L27

Ghisellini, G., Padovani, P., Celotti, A., & Maraschi, L. 1993, ApJ, 407, 65

Ginzburg, V. L., & Syrovatskii, S. I. 1964, The Origin of Cosmic Rays

Giordano, F., Naumann-Godo, M., Ballet, J., et al. 2012, ApJ, 744, L2

Glashow, S. L. 1960, Phys. Rev., 118, 316

Golden, R. L., Horan, S., Mauger, B. G., et al. 1979, Physical Review Letters, 43, 1196

Gombosi, T. I., Lorencz, K., & Jokipii, J. R. 1989, J. Geophys. Res., 94, 15011

Gonzalez-Garcia, M. C., Maltoni, M., Salvado, J., & Schwetz, T. 2012, Journal of High Energy Physics, 12, 123

Gopal-Krishna, Biermann, P. L., de Souza, V., & Wiita, P. J. 2010, ApJ, 720, L155

GRAPES-3 Collaboration. 2009, Proceedings of the 31st ICRC,Lodz,Poland

Greisen, K. 1966, Phys. Rev. Lett., 16, 748

Grindlay, J. E., Helmken, H. F., Brown, R. H., Davis, J., & Allen, L. R. 1975, ApJ, 197, L9

Grupen, C. 2005, Astroparticle Physics, doi:10.1007/3-540-27670-X

Gunn, J. E., & Ostriker, J. P. 1969, Phys. Rev. Lett., 22, 728

Gupta, M., & Webber, W. R. 1989a, ApJ, 340, 1124

—. 1989b, ApJ, 340, 1124

Gupta, N. 2012, Astroparticle Physics, 35, 503

H. E. S. S. Collaboration, Abramowski, A., Aharonian, F., et al. 2015, A&A, 577, A131

Hall, R. D., Walraven, G. D., Djuth, F. T., Haymes, R. C., & Meegan, C. A. 1976, ApJ, 210, 631

Halzen, F. 2006a, European Physical Journal C, 46, 669

—. 2006b, European Physical Journal C, 46, 669

Halzen, F., & Hooper, D. 2002, Reports on Progress in Physics, 65, 1025

Halzen, F., & Klein, S. R. 2010, Review of Scientific Instruments, 81, 081101

Hartman, R. C., Bertsch, D. L., Bloom, S. D., et al. 1999, ApJS, 123, 79

Heinbach, U., & Simon, M. 1995, ApJ, 441, 209

Helder, E. A., & Vink, J. 2008, ApJ, 686, 1094

Helmboldt, J. F., & Kassim, N. E. 2009, AJ, 138, 838

Hermsen, W., Swanenburg, B. N., Bignami, G. F., et al. 1977, Nature, 269, 494

Hillas, A. M. 1984, ARA&A, 22, 425

—. 2013, Astroparticle Physics, 43, 19

Hirata, K., Kajita, T., Koshiba, M., et al. 1988a, International Cosmic Ray Conference, 9, 53

Hirata, K. S., Inoue, K., Kajita, T., Kifune, T., & Kihara, K. 1990, Physical Review Letters, 65, 1301

Hirata, K. S., Kajita, T., Kifune, T., Kihara, K., & Nakahata, M. 1988b, Physical Review Letters, 61, 2653

Hof, M., Menn, W., Pfeifer, C., et al. 1996, ApJ, 467, L33

Hofverberg, P., & H.E.S.S. Collaboration. 2011, Nuclear Instruments and Methods in Physics Research A, 639, 23

Hooper, D., Blasi, P., & Dario Serpico, P. 2009, J. Cosmology Astropart. Phys., 1, 25

Horan, D., & Wakely, S. 2008, in AAS/High Energy Astrophysics Division, Vol. 10, AAS/High Energy Astrophysics Division 10, 41.06

Hurley, K., Dingus, B. L., Mukherjee, R., et al. 1994, Nature, 372, 652

Hwang, U., Laming, J. M., Badenes, C., et al. 2004, ApJ, 615, L117

IceCube Collaboration. 2013, Science, 342, 1

IceCube Collaboration, Achterberg, A., Ackermann, M., et al. 2006, Astroparticle Physics, 26, 155

IceCube Collaboration Hill, G. C. 2011, Nuclear Physics B Proceedings Supplements, 221, 103

IceCube-Gen2 Collaboration, :, Aartsen, M. G., et al. 2014, ArXiv e-prints, arXiv:1412.5106

Jones, F. C., & Ellison, D. C. 1991, Space Sci. Rev., 58, 259

Jones, T. W., O'dell, S. L., & Stein, W. A. 1974, ApJ, 188, 353

Joshi, J. C., & Gupta, N. 2013, Phys. Rev. D, 87, 023002

Jungman, G., & Kamionkowski, M. 1994, Phys. Rev. D, 49, 2316

Kachelriess, M., Moskalenko, I. V., & Ostapchenko, S. S. 2015, ApJ, 803, 54

Kachelrieß, M., Ostapchenko, S., & Tomàs, R. 2009a, New Journal of Physics, 11, 065017

—. 2009b, New Journal of Physics, 11, 065017

Kalberla, P. M. W., & Kerp, J. 2009, ARA&A, 47, 27

Kanbach, G., Bennett, K., Bignami, G. F., et al. 1977, in ESA Special Publication, Vol. 124, Recent Advances in Gamma-Ray Astronomy, ed. R. D. Wills & B. Battrick, 21–32

Kanbach, G., Bertsch, D. L., Dingus, B. L., et al. 1996, A&AS, 120, C461

Kappes, A., & IceCube Collaboration. 2013, Journal of Physics Conference Series, 409, 012014

Karle, A., Martinez, S., Plaga, R., et al. 1995, Physics Letters B, 347, 161

Kato, T. N., & Takahara, F. 2001, MNRAS, 321, 642

Kelner, S. R., & Aharonian, F. A. 2008, prd, 78, 034013

Kelner, S. R., Aharonian, F. A., & Bugayov, V. V. 2006a, Phys. Rev. D, 74, 034018

—. 2006b, Phys. Rev. D, 74, 034018

—. 2009, Phys. Rev. D, 79, 039901

Kiraly, P., Szabelski, J., Wdowczyk, J., & Wolfendale, A. W. 1981, Nature, 293, 120

Klebesadel, R. W., Strong, I. B., & Olson, R. A. 1973, ApJ, 182, L85

Kniffen, D. A., Fichtel, C. E., Hartman, R. C., Lamb, R. C., & Thompson, D. J. 1977, in ESA Special Publication, Vol. 124, Recent Advances in Gamma-Ray Astronomy, ed. R. D. Wills & B. Battrick, 45–53

Knurenko, S. P., & Sabourov, A. 2013, in European Physical Journal Web of Conferences, Vol. 53, European Physical Journal Web of Conferences, 4004

Koshiba, M., Hirata, K., Kajita, T., et al. 1988, Nuclear Physics B Proceedings Supplements, 3, 441

Kotera, K., & Olinto, A. V. 2011a, ARA&A, 49, 119

—. 2011b, ARA&A, 49, 119

Kraft, R. P., Forman, W. R., Hardcastle, M. J., et al. 2004, in Bulletin of the American Astronomical Society, Vol. 36, AAS/High Energy Astrophysics Division #8, 910

Kraushaar, W. L., Clark, G. W., Garmire, G. P., et al. 1972, ApJ, 177, 341

Krawczynski, H., & Treister, E. 2013, Frontiers of Physics, 8, 609

Kruells, W. M. 1992, A&A, 260, 49

Kundu, E., & Gupta, N. 2014, jcap, 4, 30

Lee, S. H., Kamae, T., & Ellison, D. C. 2007, in American Institute of Physics Conference Series, Vol. 921, The First GLAST Symposium, ed. S. Ritz, P. Michelson, & C. A. Meegan, 401–402

Letaw, J. R., Silberberg, R., & Tsao, C. H. 1993a, ApJ, 414, 601

—. 1993b, ApJ, 414, 601

Levinson, A. 2000, Physical Review Letters, 85, 912

Linsley, J. 1963, Phys. Rev. Lett., 10, 146

Liu, R.-Y., Wang, X.-Y., Inoue, S., Crocker, R., & Aharonian, F. 2013, ArXiv e-prints 1310.1263, arXiv:1310.1263

Lunardini, C., Razzaque, S., & Yang, L. 2014, ArXiv e-prints, arXiv:1412.6240

Lyutikov, M., & Ouyed, R. 2007, Astroparticle Physics, 27, 473

MacGibbon, J. H. 1991, Phys. Rev. D, 44, 376

MacGibbon, J. H., & Webber, B. R. 1990, Phys. Rev. D, 41, 3052

Mackay, C. D. 1971, MNRAS, 154, 209

Maeda, Y., Uchiyama, Y., Bamba, A., et al. 2009, PASJ, 61, 1217

Maki, K., Mitsui, T., & Orito, S. 1996, Phys. Rev. Lett., 76, 3474

Malkov, M. A., & Drury, L. O. 2001, Reports on Progress in Physics, 64, 429

Mannheim, K. 1995, Astroparticle Physics, 3, 295

Marconi, A., Schreier, E. J., Koekemoer, A., et al. 2000, ApJ, 528, 276

Matthews, J., Ciampa, D., Green, K. D., et al. 1991, ApJ, 375, 202

Mayorov, A. G., Galper, A. M., Adriani, O., et al. 2011, Soviet Journal of Experimental and Theoretical Physics Letters, 93, 628

McEnery, J. E., & Fermi LAT Collaboration. 2010, in Bulletin of the American Astronomical Society, Vol. 42, AAS/High Energy Astrophysics Division #11, 675

Meegan, C. A., Fishman, G. J., Wilson, R. B., et al. 1992, Nature, 355, 143

Mészáros, P. 2006, Reports on Progress in Physics, 69, 2259

Mészáros, P., & Rees, M. J. 1997, ApJ, 476, 232

Metzger, M. R., Djorgovski, S. G., Kulkarni, S. R., et al. 1997, Nature, 387, 878

Miller, J. A., Guessoum, N., & Ramaty, R. 1990, ApJ, 361, 701

Millikan, R. A. 1925, Nature, 116, 823

—. 1926, Proceedings of the National Academy of Science, 12, 48

Murase, K., Ahlers, M., & Lacki, B. C. 2013, Phys. Rev. D, 88, 121301

Murase, K., & Beacom, J. F. 2010, Phys. Rev. D, 82, 043008

Murase, K., & Ioka, K. 2013, Physical Review Letters, 111, 121102

Neronov, A., Semikoz, D. V., & Tchernin, C. 2013, ArXiv e-prints 1307.2158, arXiv:1307.2158

Neronov, A. Y., Semikoz, D. V., & Tkachev, I. I. 2009, New Journal of Physics, 11, 065015

Neumayer, N. 2010, PASA, 27, 449

Ojha, R., Kadler, M., Böck, M., et al. 2010a, ArXiv e-prints, arXiv:1001.0059

—. 2010b, A&A, 519, A45

Orito, S., Maeno, T., Matsunaga, H., et al. 2000, Phys. Rev. Lett., 84, 1078

O'Sullivan, S., Reville, B., & Taylor, A. M. 2009, MNRAS, 400, 248

Parker, E. N., & Tidman, D. A. 1958, Physical Review, 111, 1206

Penzias, A. A., & Wilson, R. W. 1965, ApJ, 142, 419

Picozza, P., Galper, A. M., Castellini, G., et al. 2007, Astroparticle Physics, 27, 296

Pierre Auger Collaboration. 2014, ArXiv e-prints, arXiv:1411.6111

Pierre Auger Collaboration, Abraham, J., Abreu, P., et al. 2007, Science, 318, 938

—. 2008, Astroparticle Physics, 29, 188

Pierre Auger Collaboration, Abreu, P., Aglietta, M., et al. 2011, J. Cosmology Astropart. Phys., 6, 22

Protheroe, R. J., & Biermann, P. L. 1996, Astroparticle Physics, 6, 45

Ramana Murthy, P. V., & Wolfendale, A. W. 1993, Gamma-ray Astronomy

Ramaty, R., & Lingenfelter, R. E. 1999a, in Bulletin of the American Astronomical Society, Vol. 31, American Astronomical Society Meeting Abstracts #194, 865

Ramaty, R., & Lingenfelter, R. E. 1999b, in Astronomical Society of the Pacific Conference Series, Vol. 171, LiBeB Cosmic Rays, and Related X- and Gamma-Rays, ed. R. Ramaty, E. Vangioni-Flam, M. Cassé, & K. Olive, 104

Razzaque, S. 2013, ArXiv e-prints 1309.2756, arXiv:1309.2756

Razzaque, S., Mészáros, P., & Waxman, E. 2005, International Journal of Modern Physics A, 20, 3099

Reed, J. E., Hester, J. J., Fabian, A. C., & Winkler, P. F. 1995, ApJ, 440, 706

Rees, M. J., & Meszaros, P. 1992, MNRAS, 258, 41P

—. 1994, ApJ, 430, L93

Rejkuba, M. 2004, A&A, 413, 903

Risse, M., Homola, P., Engel, R., et al. 2005, Physical Review Letters, 95, 171102

Roberts, A. 1992, Reviews of Modern Physics, 64, 259

Rudak, B., & Dyks, J. 1999, MNRAS, 303, 477

Saha, L., Ergin, T., Majumdar, P., Bozkurt, M., & Ercan, E. N. 2014, A&A, 563, A88

Sahakyan, N., Yang, R., Aharonian, F. A., & Rieger, F. M. 2013, ApJ, 770, L6

Sahu, S., Zhang, B., & Fraija, N. 2012, Phys. Rev. D, 85, 043012

Sánchez Losa, A., & ANTARES Collaboration. 2013, Nuclear Instruments and Methods in Physics Research A, 725, 60

Schatz, G., Feßler, F., Antoni, T., et al. 2003, in International Cosmic Ray Conference, Vol. 4, International Cosmic Ray Conference, 2293

Shibata, T., & Futo, Y. 2008, Astroparticle Physics, 29, 30

Shibata, T., Futo, Y., & Sekiguchi, S. 2008, ApJ, 678, 907

Silberberg, R., & Tsao, C. H. 1990, Phys. Rep., 191, 351

Silk, J., & Srednicki, M. 1984, Phys. Rev. Lett., 53, 624

Simon, M., & Heinbach, U. 1996, apj, 456, 519

Sreekumar, P., Bertsch, D. L., Hartman, R. C., Nolan, P. L., & Thompson, D. J. 1999, Astroparticle Physics, 11, 221

Stawarz, L., & for the H.E.S.S.Collaboration. 2013, ArXiv e-prints, arXiv:1307.4823

Stecker, F. W. 1969, Physical Review, 180, 1264

—. 1971, NASA Special Publication, 249

—. 2013, Phys. Rev. D, 88, 047301

Stecker, F. W., & Salamon, M. H. 1999, ApJ, 512, 521

Stephens, S. A., & Golden, R. L. 1987, Space Sci. Rev., 46, 31

Strong, A. W., Moskalenko, I. V., & Ptuskin, V. S. 2007, Annual Review of Nuclear and Particle Science, 57, 285

Suzuki, Y. 1995, Nuclear Physics B Proceedings Supplements, 38, 54

Takeda, M., Hayashida, N., Honda, K., et al. 1998, Physical Review Letters, 81, 1163

—. 1999, ApJ, 522, 225

Takeda, M., Sakaki, N., Honda, K., et al. 2003a, Astroparticle Physics, 19, 447

—. 2003b, Astroparticle Physics, 19, 447

Tam, P. H. T., Huang, R. H. H., Takata, J., et al. 2011, ApJ, 736, L10

Tanaka, T., Allafort, A., Ballet, J., et al. 2011, ApJ, 740, L51

Tanvir, N. R., Fox, D. B., Levan, A. J., et al. 2009, Nature, 461, 1254

The ANTARES Collaboration, Adrián-Martínez, S., Albert, A., et al. 2013, ArXiv e-prints, arXiv:1308.1599

The Pierre Auger Collaboration, Aab, A., Abreu, P., et al. 2013, ArXiv e-prints 1307.5059, arXiv:1307.5059

Thompson, D. J., Fichtel, C. E., Hartman, R. C., Kniffen, D. A., & Lamb, R. C. 1977a, ApJ, 213, 252

Thompson, D. J., Fichtel, C. E., Hartman, R. C., et al. 1977b, in NASA Conference Publication, Vol. 2, NASA Conference Publication, ed. C. E. Fichtel & F. W. Stecker, 3–14

Tinyakov, P. 2014, Nuclear Instruments and Methods in Physics Research Section A: Accelerators, Spectrometers, Detectors and Associated Equipment, 742, doi:10.1016/j.nima.2013.10.067

Torres, D. F., & Anchordoqui, L. A. 2004, Reports on Progress in Physics, 67, 1663

Totsuka, Y. 1991, Nuclear Physics B Proceedings Supplements, 19, 69

Tozuka, Y. 1988, Astronomical Herald, 81, 4

Trombka, J., Fichtel, C., Grindlay, J., & Hofstadter, R. 1978, Science, 202, 933

Tueller, J., Mushotzky, R. F., Barthelmy, S., et al. 2008, ApJ, 681, 113

Vietri, M. 1995, ApJ, 453, 883

Vinyaikin, E. N. 2007, Astronomy Reports, 51, 87

Walker, R. C., Beilicke, M., Cheung, C., et al. 2012, in American Astronomical Society Meeting Abstracts, Vol. 219, American Astronomical Society Meeting Abstracts, 154.31

Wang, Y.-R. 2005, PhD thesis, The University of Wisconsin - Madison

Waxman, E. 2005, Physica Scripta Volume T, 121, 147

Waxman, E., & Bahcall, J. 1997, Physical Review Letters, 78, 2292

Waxman, E., & Bahcall, J. 1998, Phys. Rev. D, 59, 023002

Webb, G. M. 1983, ApJ, 270, 319

Weekes, T. C., Cawley, M. F., Fegan, D. J., et al. 1989, ApJ, 342, 379

Winn, M. M., Ulrichs, J., Peak, L. S., McCusker, C. B. A., & Horton, L. 1986, Journal of Physics G Nuclear Physics, 12, 653

Winter, W. 2013, Phys. Rev. D, 88, 083007

Yuki, S., & Shibata, S. 2012, PASJ, 64, 43

Zandanel, F., Tamborra, I., Gabici, S., & Ando, S. 2015, A&A, 578, A32

Zatsepin, G. T., & Kuz'min, V. A. 1966, Soviet Journal of Experimental and Theoretical Physics Letters, 4, 78

Zhang, B. 2011, Comptes Rendus Physique, 12, 206

Zhang, B., & Mészáros, P. 2004, International Journal of Modern Physics A, 19, 2385